Supplemental Materials for:

Cenozoic incision history of the Little Colorado River: its role in carving Grand Canyon and onset of rapid incision in the last ~2 Ma in the Colorado River System

Karl E. Karlstrom[1], Laura J. Crossey[1], Eileen Embid[1], Ryan Crow[2], Matthew Heizler[3], Richard Hereford[2], L. Sue Beard[2], Jason Ricketts[4], Steve Cather[3], Shari Kelley[3]

Geosphere, 2016, DOI:10.1130/GES01304.1

LIST OF DATA REPOSITORY (DR) ITEMS

SECTION DR-1. Bedrock Incision Rate Data …….…….1
- Figure DR-1.1 Thermal history model and paleodepth of sample 01GC103 (Lee et al., 2013)
- Figure DR-1.2 Incision rate for the 1.993 Ma Blue Mesa tuff relative to the Moenkopi Wash
- Figure DR-1.3 Image of northern San Francisco volcanic field showing 0.89 Ma Black Point flow
- Figure DR-1.4 E-W cross section from Haines and Bowles (1976) showing drill hole RB No. 5
- Figures DR-1.5, 1.6, 1.7 Photographs of incision points from travertine dated gravels
- Figure DR-1.8 Incision rates calculated from U-series ages of travertines
- Figure DR-1.9. Profiles of eastern tributaries to the LCR (above Holbrook Arizona)

SECTION DR-2. Thermochronology …….....18
- Section DR-2 Thermochronology modeling
- Table DR-2.1 Table of key thermochronology samples
- Figure DR-2.2 Age-elevation and eU-age data from LCR-region
- Figure DR-2.3 Youngest age –elevation plot for LCR samples
- Section DR-2.4 Geologic constraint boxes imposed on HeFTy models
- Section DR-2.5 Sample by sample modeling details for samples A through N
- Figure DR-2.6 Comparison of models with and without the Rim Gravel constraint box
- Figure DR-2.7 Comparison of models with and without the Bidahochi constraint box

SECTION DR-3- 40AR/39AR METHODS AND DATA …….....41
- Table DR-3.1. Analytical methods
- Table DR-3.2. 40Ar/39Ar basalt data
- Table DR-3.3. 40Ar/39Ar Sanidine analytical data

SECTION DR-4. U-series data from travertines from the Springerville area ……..44

SECTION DR-1. BEDROCK INCISION RATE DATA

The last regional study of the Little Colorado River drainage was Cooley et al. (1969). Since then advances in geochronology and geomorphology, as well as intense interest in the incision history of the Colorado River and age of Grand Canyon (e.g. Crow et al., 2014; Karlstrom et al., 2014) provide motivation for this newer synthesis. The purpose of this drainage-basin-scale incision study is to present new data as well as older data in as unified a context as possible. This data repository should be used in conjunction with Table 1 of the paper to help the reader understand the reasoning used to interpret the variable quality incision point data. Incision rates in this study are bedrock incision rates; our goal is to resolve spatial and temporal variation in bedrock incision and erosion across the LCR drainage basin. Bedrock incision rates are averages over a given time interval that do not consider shorter term aggradation and incision cycles for that location. Bedrock incision can be positive (net erosion) or negative (net aggradation) at a given spot and over a given time interval. The steps used in estimating reported incision rates in Table 1 of this paper are described below; each has uncertainties. The magnitude of uncertainty includes geologic as well as geochronologic uncertainty and is not readily quantifiable for most data points. Based on other regional studies (e.g. Aslan et al., 2010; Karlstrom et al., 2011), our estimate is that uncertainties may be in the range of 10-20 %.

1) We first identify a river terrace bedrock strath or, more distant from a river, an interpreted incisional surface such as a pediment that may have been graded to a river terrace. Uncertainties in which surfaces represent incisional surfaces is a potential problem for the "surfaces" mapped by Cooley et al. (1969) in an era when "peneplains" were considered incisional surfaces of wide extent. But these surfaces may alternatively be bedrock benches, and/or most represent diachronous landscape features rather than a single episode of erosion. Nevertheless, Cooley et al.'s (1969) regional surface/terrace mapping is the best available and our compilation shows that, where dated, higher surfaces and basalt inverted topography yield progressively older ages than lower surfaces and basalts. We therefore interpret the general pattern of surfaces as a record of progressive incision of the valley with recognition that additional study is needed for better characterization, correlation, and dating of terraces and surfaces.

2) The height of the terrace strath or bedrock incisional surface is measured relative to the nearest river location (projected approximately orthogonally) and/or any nearer largest major tributary. Height is measured as the elevation of the strath relative to the elevation of the river (or river bed for dry washes) and does not, in this study, consider water depth or thickness of gravel above bedrock (c.f. Karlstrom et al., 2007) as these are generally unknown for the LCR. Heights for some river terraces were measured directly via laser range finder or Jacob staff. Heights in the Springerville area were derived from GIS-based projection of basalt and gravel heights relative to the modern river profile (Embid, 2009). Height estimates for samples distant from the river are from Google Earth or topographic maps. Incision points farthest from the trunk river or nearest tributary have higher uncertainties due to projection ambiguities. Tributaries can incise at different rates than their trunk river, so mainstem (LCR) incision rates are distinguished from tributary (trib) incision rates in Table 1. Control points on interpreted incisional surfaces distant from the mainstem and from major tributaries are considered landscape denudation rates in Table 1.

3) The presence of river gravels above a strath allows the point to be designated as a river or tributary incision rate. Basalt capped surfaces (inverted topography) often do not have identified sub-basalt gravels and in these cases, the basalt is interpreted to reflect local base level (lowest place in the local landscape) and the estimated denudation rates are considered maxima because the basalt flow may not have reached a significant river tributary. When basalt plateaus have "run-out" geometries (thin flows that form sinuous river-like map patterns) such as near Springerville, they are considered as recording paleo-tributaries and reported as river or tributary incision rates.

4) The age of the strath is usually estimated by dating material above the strath such that most incision age estimates are technically minima and incision rates maxima for that strath. However, as in many incision rate studies, if gravels are present at the strath, the age of the overlying dated material is likely a close proxy for the age of the gravels in the active thalwag. In some cases, dated material (e.g. a basalt flow) may overlie an (unrecognized) older perched terrace rather than the thalwag gravels; this

could make the age significantly younger than the strath and would produce a maximum incision rate. Detrital grain dating provides a maximum depositional age for a fluvial deposit hence a minimum incision rate. Geochronology used in this study is of variable vintage and reliability. Newer ^{40}Ar-^{39}Ar dates are preferred where available to older K-Ar dates on basalt, but both are reported. Detrital zircon (U-Pb) and sanidine (^{40}Ar-^{39}Ar) dates are reported for the White Mesa alluvium. New ^{40}Ar-^{39}Ar dates are presented for ash in alluvial deposits that overlie the Moenkopi and Blue Canyon surfaces. New U-Series dates are reported for travertine-cemented gravels in the Springerville area.

5) Thermochronology data points are used to provide landscape denudation estimates over longer time scales. Hefty is used to generate time-temperature paths that best predict the observed data according to the RDAMM model (Flowers et al., 2009). The weighted mean path of the good solutions as well as individual best-fit T-t path are both reported and shown in the main text and DR. The weighted mean path is used to compare samples but it may not predict the observed data as well as the individual best fit path, so we use the latter for denudation estimates. Paired rim and river level samples are only available for samples 1-5 in Grand Canyon (Lee et al., 2013).

Point-by-point discussion of incision rate data points reported in Table 1 and Figures 14 and 16 of main paper.

LOWER REACH- COLORADO RIVER CONFLUENCE TO THE CAMERON AREA

#1A. Thermochronologic constraints on the elevation of the confluence between the Colorado River and the Little Colorado River paleovalley at the time of integration of the Colorado River through Grand Canyon at 6 Ma depends on the depth of the postulated 25-15 Ma East Kaibab paleocanyon. The 1830 m elevation of Cape Solitude (Scarborough, 2001) is a reasonable maximum LCR elevation at ~ 6 Ma. But instead we use thermochronologic data from sample 01GC103 from the Dox Formation located 4.3 miles downstream from the CR-LCR confluence (Lee et al., 2013) that suggests that this sample was 20-30 °C and hence buried 400-800 m at 10-6 Ma (assuming a surface temperature of 10 °C and geothermal gradient of 25 °C/km -- Lee et al., 2013, their Fig 9E and DR Fig. 1 below). This 1200-1600 m range of elevations of the 6 Ma LCR paleovalley is shown visually in Figure 3, and the 1600 m elevation is used for paleoprofile reconstruction in Figure 14A. However, the lowest temperature parts of the cooling history are near the limit of what is resolvable using AHe modeling. If we use the modeled cooling through 40 °C at ~ 20 Ma, this would predict 1.2 km depth of burial and an LCR paleovalley bottom elevation at ~ 2 km, near or just above the present rim of the LCR-CR confluence area at 20 Ma, as proposed by Scarborough (2001). Further, different mean annual surface temperature and geothermal gradient assumptions result in different temperature to depth "conversions" such that the thermochronological constraints on paleosurfaces (as shown in Figure 6) should be viewed as having large error bars.

#1B. Direct constraints on 2-6 Ma paleoprofiles of the LCR-CR confluence region are sparse. A U-Pb speleothem age of 2.68 Ma was obtained from a "very small cave" in the Kwagunt Creek drainage near CR river mile 57, about 5 river miles upstream of the CR-LCR confluence and 2.6 km up the tributary from the river. Elevations and locations are approximate in the Polyak et al. (2008) paper, but they infer an incision rate relative to the Colorado River of 166 m/Ma assuming that this age records the time that a mammillary speleothem formed on the roof of the cave when a horizontal water table dropped through the cave due to incision of the CR. Based on its reported elevation and distance from the river, we estimated the cave to be about 260 m above the floor of Kwagunt Creek which would give a tributary incision rate of about 100 m/Ma. Karlstrom et al. (2008) questioned the assumption of a flat water table, Crow et al. (2014) interpreted it to be a maximum river incision rate, and we also interpret this incision point to be a maximum tributary incision rate.

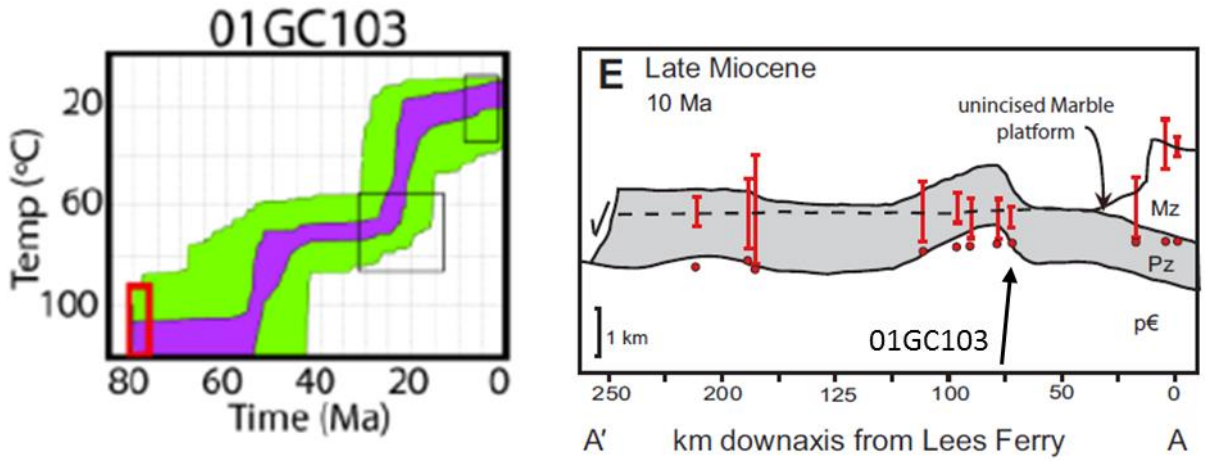

Figure DR-1.1 Thermal history model and paleodepth of sample 01GC103 (Lee et al., 2013). Elevation of the base of the East Kaibab Paleocanyon near the CR-LCR confluence at ca. 6 Ma is loosely constrained by thermochronology sample 01GC-103 located 3 miles downstream from the confluence. Left is thermal history model (from Lee et al., 2013, their Appendix B); right is their Fig. 9E with arrow pointing to sample. Temperature-to-depth conversion uses modeled temperature range of 20-30 °C at 6 Ma and assumes a surface temperature of 10 °C and a geothermal gradient of 25 °C/km. Resulting depths of burial would be 400 to 800 m placing the valley bottom between 1200 and 1600 m elevation for this sample which is from ~800 m elevation. These low modeled temperatures and resulting estimated palaeodepths are likely at or beyond the limit of resolution of the AHe data. Using modeled cooling through 40 °C at ~ 20 Ma would predict 1.2 km depth of burial and an LCR valley bottom at elevation ~ 2 km and near the present rim of the GC at 20 Ma.

1C. Colorado River strath terraces are well preserved between CR river miles 57 (Kwagunt Creek) and RM 65 (Palisades Creek). Bedrock straths are well defined and travertine coats mainstem river gravels. U-series dates were reported by Crow et al. (2014) who dated both detrital travertine clasts in river gravels and infilling travertines around clasts to get the best estimates for age of gravel deposition on bedrock straths. Regressions of all data show a semi-steady bedrock incision rate of 160 m/Ma over the last 625 ka for this reach of eastern Grand Canyon. Thus, the elevation of the CR-LCR confluence was also about 925 m at 625 ka which can be interpolated to 985 m at ~ 1 Ma if one assumes steady incision over the last 1 Ma, as shown in Figures 3 and 14A.

2A. The White Mesa Alluvium (Hereford et al., 2016) in the Crooked Ridge paleoriver model of Lucchitta et (2011; 2013) was considered to be early Miocene. New detrital sanidine data (Hereford et al., 2016; and this paper) now shows single grain ages that range from 2.02 ±0.02 to 1.84 ± 0.05 within the White Mesa alluvium from both Crooked Ridge and White Mesa. This provides a maximum depositional age of 1.84-2.02 Ma for the alluvium. The location and height of the Crooked Ridge deposits are shown in Figures 1, 3, and 14A. The sediments are exposed in Crooked Ridge, an inverted topography example where the < 2 Ma gravels are more resistant than the surrounding Triassic bedrock. This ridge and paleoriver system are headed directly for the Gap, a "windgap" (bedrock paleochannel?) in the resistant Navajo Sandstone of the Echo Cliffs monocline. The elevation of the base of the alluvium near The Gap is ~ 1700 m but it is not straight forward to infer an incision rate from this point relative to the LCR because of uncertainty regarding the path this paleoriver may have taken between the Gap and the LCR. Figure 14A shows a possible shortest path that follows Big Creek, an "underfit" tributary to the LCR that intersects the modern LCR at 900 m elevation and may have intersected the paleo-LCR- CR confluence ~1200m (Fig. 14A). Alternatively, it may have intersected near the confluence of Moenkopi Wash (now

at 1250 m). A 1200-1250 m confluence of the LCR and CR at 2 Ma would suggest a (poorly constrained) maximum incision rate of ~ 188- 213 m/Ma.

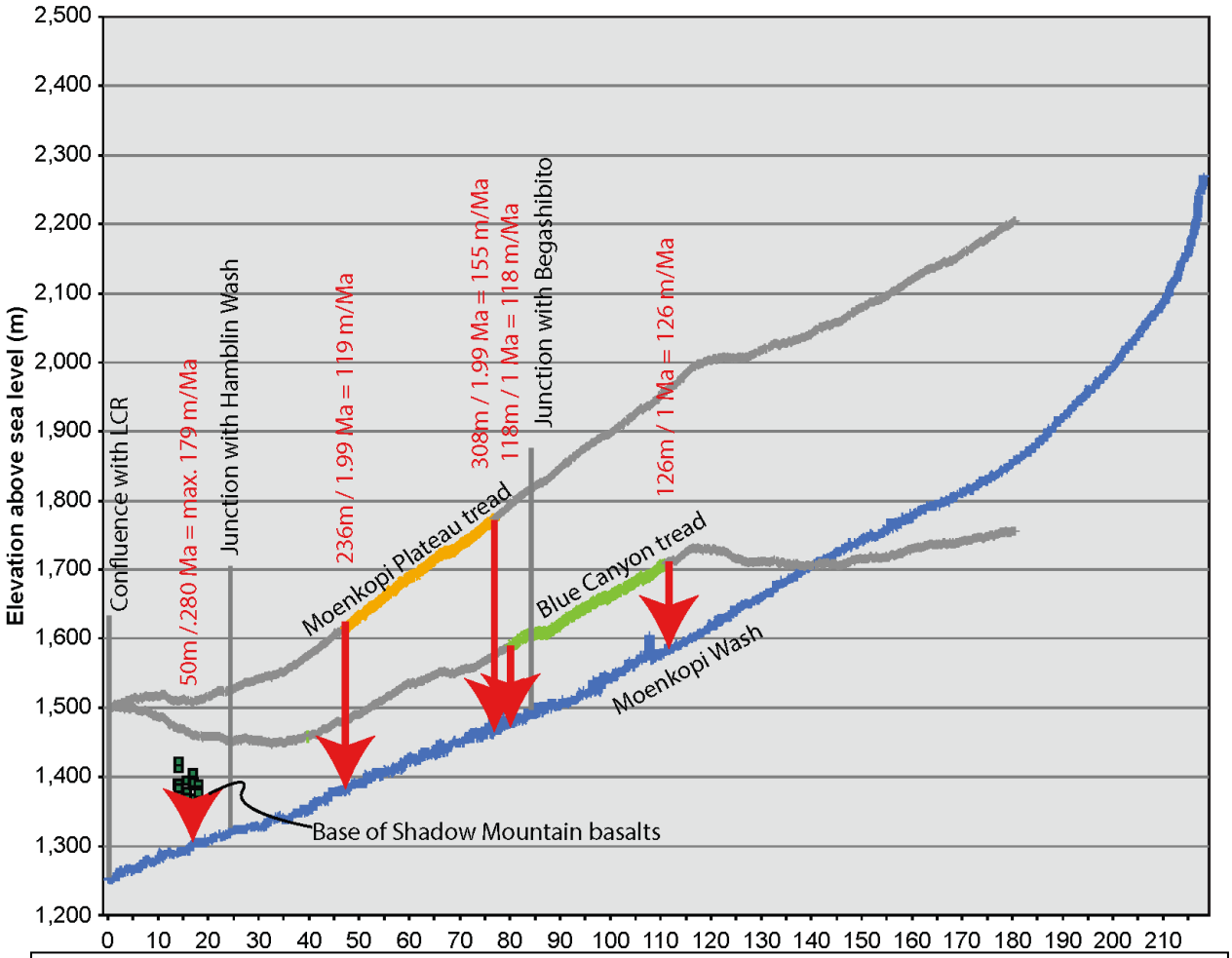

Figure DR-1.2. Incision rate for the 1.993 Ma Blue Mesa tuff relative to Moenkopi Wash tributary was calculated by projecting the 2 Ma ash (incision point #3) on the Moenkopi Plateau surface down slope to the nearest LCR tributary-Moenkopi Wash. Projected heights ranged from 236-308 m (mean of 272 m) which gives incision rates of 119-155 m/Ma (mean of 137 m/Ma over the last 2 Ma). A similar projection of point #4, the Blue Canyon tread with the 1 Ma Bishop Tuff, gives 118-126 m and incision rates of 118-126 m over the last 1 Ma. The mean values are reported in Table 1. This plot also shows the heights of bases of the 275 ka basalt flow at Shadow Mountain relative to Moenkopi Wash.

2B. Lacustrine units in the White Mesa alluvium are described by Hereford et al. (2016); these constrain the gradient of the White Mesa paleovalley on Figure 14A and Figure DR-2 and show it to be similar to modern Moenkopi Wash tributary.

3. An ash fall tuff named Blue Point tuff (Hereford et al., 2016) is interbedded with alluvial deposits on Moenkopi Plateau that are correlated with White Mesa Alluvium. It yields an $^{40}Ar/^{39}Ar$ sanidine age of 1.99 ± 0.002 Ma. The SW-dipping tread of Moenkopi Plateau is projected to Moenkopi Wash and yields heights of 236-308 m and tributary incision rates of 119-155 m/Ma or a mean of 137 m/Ma (Fig. DR-2).

4. Blue Canyon Plateau ash fall tuff is interbedded with gravels that are inset into Moenkopi Plateau on Blue Canyon plateau. This ash is correlated using tephrochronology with the 1.2- 0.8 Ma Bishop- Glass Mountain Tuff (Hereford et al., 2016). The ash is within 2 km of Moenkopi Wash and is on a tread of an incisional surface that is projected to Moenkopi Wash in Figure DR-2 and yields heights of 118-126 m /Ma and incision rates of 118-126 m/Ma (mean of 122 m/Ma). The similar tributary incision rates of the projected 2 and 1 Ma surfaces relative to Moenkopi Wash supports an interpretation that these are incisional surfaces, likely pediments, that were graded to paleo-channel positions during progressive incision.

5. Black Point basalt flow originated in San Francisco Peaks volcanic field and flowed ~30 km to the LCR paleovalley (Fig. DR-4). The edge of the flow is just west of the modern river; the flow entered the LCR channel (as evidenced by sub-basalt river gravels) and caused the river to shift to the east. The eastern edge of the flow is involved in numerous landslide toreva blocks and LCR gravels can be found at the base of slumped segments. A sample was collected for dating within 1 m of the flow top at an elevation of 1489 m. At the location where the sample was obtained, mass failure at the margins of the flow partially obscured a cross sectional view through the flow. However, Lower Colorado River gravels were found at an elevation of ~1466 m and also at a Moenkopi bedrock bench at an elevation of ~1374 m. Figure DR-4 (from Haines and Bowles, 1976) shows results of drilling through the flow. In drill hole RB5 the flow was found to be 18 m (60') thick with the upper 1.8 m (6') being vesicular. Below that was 22.3 m (73') of fluvial sand and gravel. The well head was located at an elevation of 1502 m, which indicated that the underlying bedrock strath is 1462 m above sea level (Fig. DR-4). Using this elevation, our new $^{40}Ar/^{39}Ar$ age of 890 ± 20 ka, and a modern river elevation of 1290 m, gives an incision rate of 193 m/Ma. Similarly, using the $^{40}Ar/^{39}Ar$ age from Hanson (2010) of 873 ± 8 ka gives a rate of 197 m/Ma. We consider this a preferred incision point because no intervening material was noted between the flow and the basalt and because the height of the bedrock strath is well known. It is possible that the 1462 m strath (172 m above the modern river) could have been an older terrace preserved above the thalwag at 0.89 Ma. For example, if the 1374 m strath was the thalwag at 890 ka, this would give an incision rate of 94 m/Ma. However, Rice (1980) reported LCR gravels atop the flow indicating that the river was at this level after 890 ka and our preferred interpretation is that the thick alluvium at 1462 m under the Black Point flow reflects the LCR thalwag at 0.89 Ma and that the 1374 strath is a younger terrace that correlates with Cooley's early Wupatki terrace of 61-91 m (estimated to be 450 ka in Table 1) that is inset against Black Point flow and its underlying alluvium. Older studies considered the Black Point flow to be 2.43 Ma (Damon et al., 1974; Rice, 1980; Holm, 2001; Billingsley, 2001), so the new date substantially changes incision rates and confirms rapid rates well above Cameron (C in Fig. DR-3) and above the modern LCR knickpoint (KP in Figure DR-3).

6A. Wukoki flow was reported by Rice (1980) as covering a smooth pediment carved on Triassic strata that sloped down to the LCR. The flow terminates 2.5 km from the LCR but would project to about 85 m above the present channel. The base of the flow on Google Earth is at an elevation of 1405 m and the nearest LCR channel is at 1316 m, so Table 1 shows its height as 89 m. Damon et al. (1974) reported a K-Ar age of 0.87 ± 14 Ma giving an incision rate of 102 m/Ma (Rice reported 97.7 m/Ma). This rate is a maximum rate in the sense that no gravels are known to underlie the flow, but it could be a minimum rate if the K-Ar date is significantly older than the flow age, which was true for the Black Point and Shadow Mountain flows where older K-Ar dates were >twice the later ^{40}Ar-^{39}Ar dates.

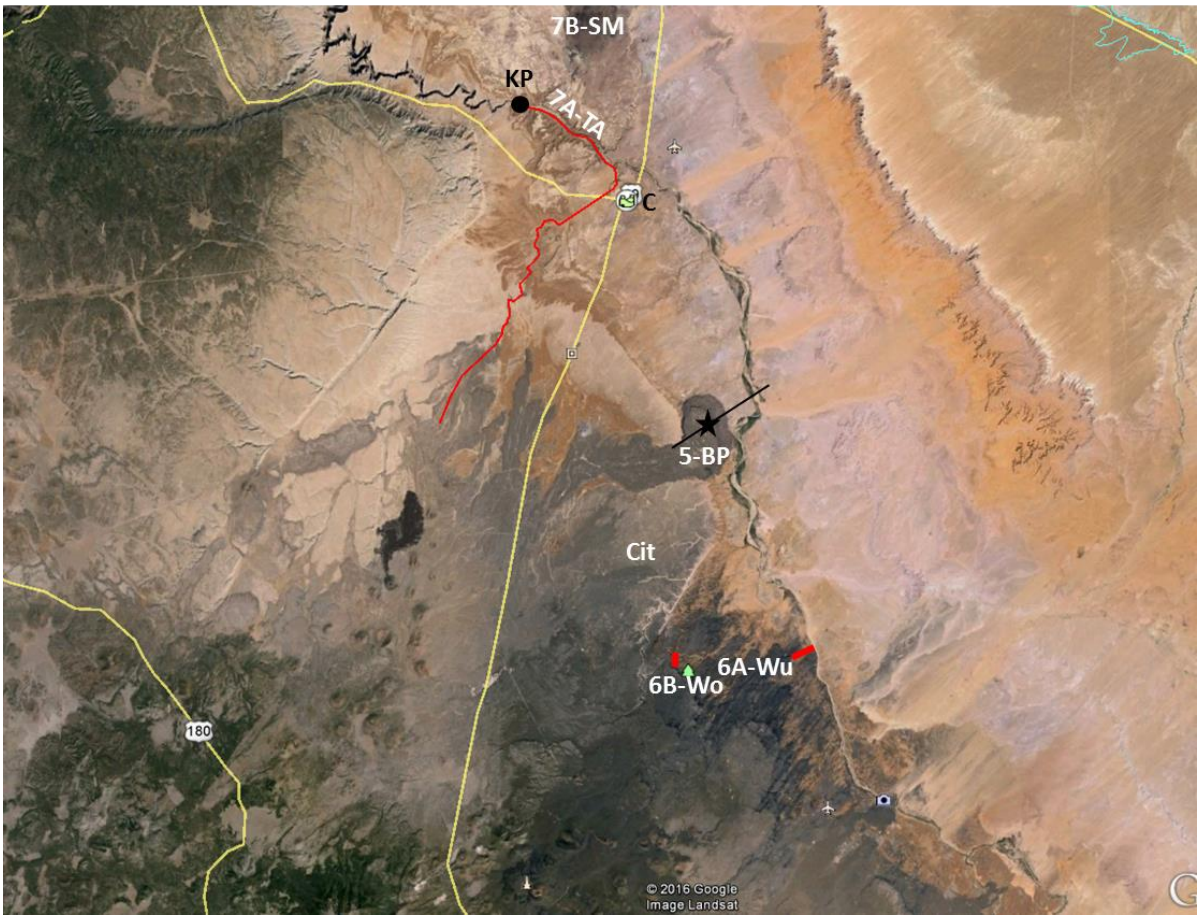

Figure DR-1.3 Image of northern San Francisco volcanic field showing 0.89 Ma Black Point flow from Google Earth; 5-BP; black star is location of drill hole RB No. 5 and the cross section in Fig. DR-4). 6A-Wu is 0.87 Ma Wukoki flow and red line shows ~ 2.5 km distance to nearest LCR channel used for incision estimate. 6B-Wo is 0.81 Ma Woodhouse flow and the red line shows ~ 2 km distance to nearest tributary used for incision estimate. 7A-TA = 0.34 Ma Tappan Spring flow run-out (red line). 7B-SM= eastern edge of the flow is involved in numerous landslide toreva blocks and LCR gravels can be found at
the base of slumped segments. A sample was collected for dating within 1 m of the flow top at an elevation of 1489 m. At the location where the sample was obtained, mass failure at the margins of the Shadow Mountain; C= Cameron; black dot is LCR knickpoint (KP) and start of Paleozoic Gorge of the LCR. Cit= Citadel flow, an undated but potentially useful future incision point.

6B. Woodhouse Mesa flow followed tributary paleovalleys of the LCR. Elston and Young (1981) interpreted the abandoned meanders and gravels in Antelope Creek as Eocene. Holm interpreted the incision to be Quaternary and noted that the complexity of flows and tributary patterns may have been influenced by the Black Point monocline. Holm (2001) showed a map and cross section of Woodhouse Mesa but did not report an incision rate. Table 1 takes the height of the base of the flow (1570 m) relative to ~1450 m elevation of the nearest tributary (Deadman Wash) ~2 km directly north of the dated flow (red line in Fig. DR-3). This incision rate of 148 m/Ma is interpreted to be a maximum tributary incision rate as no gravels are reported beneath this flow. This rate is somewhat lower than the Black Point LCR mainstem rate of 193 m/Ma over about the same 800-900 ka interval.

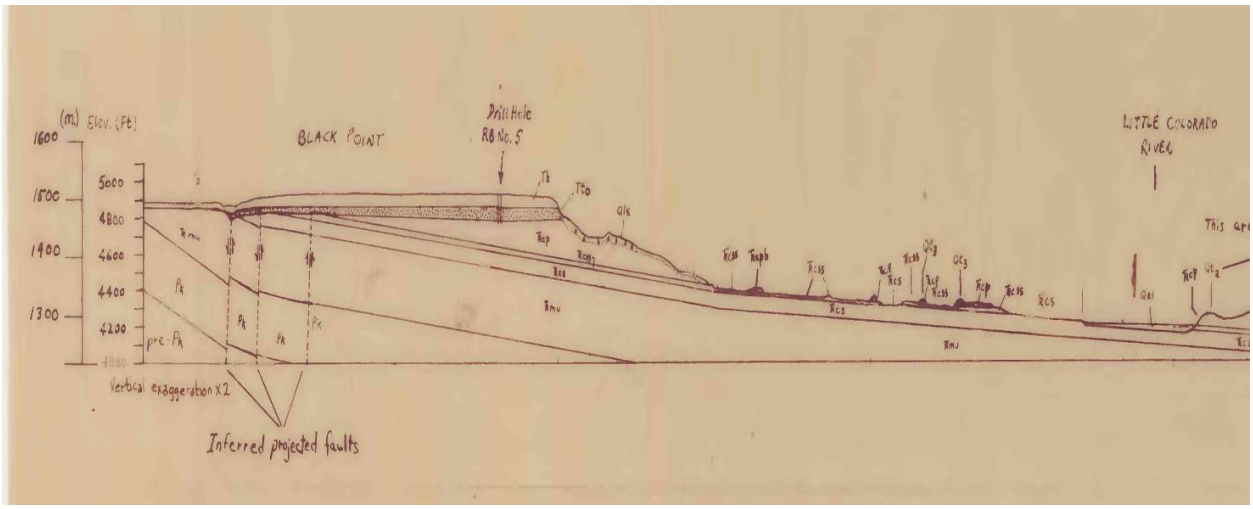

Figure DR-1.4. E-W cross section from Haines and Bowles (1976) showing drill hole RB No. 5 that intersected LCR terrace gravels (unit Tto, stippled) beneath Black Point basalt flow with a bedrock strath cut onto the Petrified Forest Member of the Chinle Formation (Trcp) at an elevation of 1462 m giving an incision rate of 197 m/Ma. Cross section and drill hole locations, are shown in Figure DR-3.

<u>7A. Tappan Spring basalt flow:</u> Basalt samples for $^{40}Ar/^{39}Ar$ dating were collected from the Tappan Spring Flow in the Lower Colorado River Gorge. As noted by Colton (1937) and Rice (1977; 1980) this flow traveled a total of 53-64 km from its source vent in the San francisco volcanic field. It flowed first down Tappen Wash, then spread out to flow both down (~ 11 km) and up (1.6 km) the steep-walled gorge of the paleo LCR. The dated sample was collected about 3 meters above the base of the flow in the lower colonnade portion of the flow (UTM zone 12 460081 3970879, NAD27). The basalt rests on river sand and gravel that is up to about 30 cm thick. Locally the flow has pillow-like structures at its base indicating that the flow filled the river channel when the now-ephemeral river was flowing or the bed was wet. The sand and gravel rests on a bedrock strath of Moenkopi Formation. The height of the bedrock strath was measured with a laser range finder to be 57.2 m above the present river bed of the Lower Colorado River. The thickness of the flow was measured to be 32.25 m. $^{40}Ar/^{39}Ar$ dating of the basalt yields an age of 342 +/- 6 ka which results in a bedrock incision rate of 167 m/Ma. Because the bedrock strath below the gravel is preserved and because the flow rests directly on river gravel, this incision point is considered to be among the most reliable and is considered a "preferred" LCR incision rate in Table 1. Rice (1980) reported the floor of the LCR paleocanyon that was filled with Tappan basalt to have been 48 m above the modern LCR and he used an older K-Ar age of 0.51 Ma from Damon et al. (1974) to calculate a rate of 94 m/Ma. Rice (1977) also reported numerous complexities of aggradation, overtopping of the flow, and migration of the LCR channel in the vicinity of the confluence of Tappan wash and the LCR that post-dated flow emplacement. Also, Rice (1977) reported that the LCR channel near the tip of the basalt outflow has > 30 m of gravel between the present river bed and underlying bedrock as shown by drilling at the "Coconino Damsite". If this depth to underlying bedrock is also present in the sample locality, this would give a bedrock incision amount of > 87 m and a higher incision rate of >270 m/Ma.

<u>7B. Shadow Mountain</u> is a small basaltic volcanic field north of the main San Francisco volcanic field that was built along the Mesa Butte fault. No gravels under basalts were mapped or noted by Conway (et al., 1997) or Condit (1974). The basalt flows are incised by drainages that flow into nearby Moenkopi Wash and the height of base of basalts that are closest to Moenkopi Wash range in height from 50 to 120 m above the level of the wash (Figure DR-4). The lowest elevation (1345 m) flow has a height 50 m

above Moenkopi Wash (at 1295 m). Conway et al. (1997) reported $^{40}Ar/^{39}Ar$ dates of 280 ± 50 and 300 ± 110 ka for two different samples. These ages yield incision rates of 179 and 167 m/Ma respectively which, given the large errors in the ages, agree well with the Tappan flow rate of 167 m/Ma. This suggests that the tributary incision rate for Moenkopi Wash is similar to the mainstem LCR over this time frame. Rice (1980) mapped rounded basalt in gravels and tephra that were derived from Shadow Mountain within terraces about 65-70 m above the modern Hopi Trail Canyon Wash which flows into the LCR at the LCR knickpoint (KP of DR- 1.3) about 2 km downstream of the terraces. Rice concluded the LCR has incised about 70 m since the Shadow Mountain eruptions. He used an older K-Ar age (Damon et al., 1974) of 0.62 Ma and derived an incision rate of 112.9 m/Ma whereas we would get an incision rate of 250 m/Ma for this locality using the newer 0.28 Ma $^{40}Ar/^{39}Ar$ date of Conway et al. (1997). This higher rate would agree reasonably well with the rate calculated assuming 30 m of gravel may fill the LCR at the tip of the Tappan flow. New ages on specific Shadow Mountain flows and on basalt boulders in the terrace gravels are needed to refine these estimates.

MIDDLE REACH- CAMERON TO ST JOHNS

8A, 8B, 8C, 9A, 9B: The base of the lacustrine Lower Bidahochi Formation is contoured based on both outcrop (Dickinson et al., 2013) and drill data (Cooley and Akers, 1962) as shown in Figure 1. The age of the unit is bracketed between the 15.84 Ma Echo Spring Mountain ash (based on a tephrochronology correlation to Buffalo Canyon Ash) that is located ~ 14 m above the base of the section and a 13.71 Ma ash that is about 30 m from the top of the 106-m-thick section (Dallegge et al., 2001). The contours suggest a lake basin depocenter that coincides with the present base of the LCR valley near Saint Johns but deviates ~ 60 km to the NE of the LCR course near Winslow. The highest elevation lacustrine sediment outcrops are about 1950 m elevation compatible with the 200 m measured thickness of the Lower Bidahochi Formation. Long term average incision rates of the LCR valley relative to the 15.8 Ma base of the unit as datum is 4- 20 m/Ma and includes several hundred meters of 11-6 Ma aggradation of the Bidahochi Formation and other sediments as depicted in Figure 6. Long term incision rates based on elevations of the outcrops of 15.19 Wood Chop and 13.7 Ma ash, relative to the modern LCR, are 17 and 31 m/Ma respectively. The combined range of incision rates of 4-31 m/Ma is interpreted to be a preferred long term incision rates for the LCR valley since 13 Ma that reflects slightly greater post-6 Ma erosion than 16-6 Ma aggradation.

#10. Hopi Buttes diatremes and eruptive basalts formed 8.2 to 6.5 Ma and intruded but also interfingered with the upper (fluvial) Bidahochi Formation. Basalt flows overlie and preserve a widespread eruptive surface that is relatively uneroded in the northeastern part of the volcanic field. For these flows, Table 1 reports the approximate elevation of the dated units (most were estimated from Google Earth) and ages are K-Ar ages from Damon and Spencer (2001). Calculated incision rates relative to the LCR are considered maximum denudation rates because no gravels are reported beneath basalts. Dates from diatreme intrusions were also reported as incision rates based on estimated depth below the eruptive surface reported by White (1991). The maar character of the eruptive centers suggests interaction with the groundwater table and the co-location of the Hopi Buttes maar diatremes with the lacustrine Lower Bidahochi Formation depocenter is permissive of the interpretation that the LCR valley bottom remained in approximately the same location as the lacustrine depocenter with a base level of about 1900 from 13.7 to 6.5 Ma. The elevation of the groundwater table likely was close to the elevation of any lake or marsh in the LCR paleovally bottom 6-8 Ma although some relief on the water table is possible. Our preferred long-term average incision rate from the Hopi Buttes volcanic field is the Tuff in Coliseum Marr, which is the closet location to the modern LCR; it gives a maximum incision rate of 50 m/Ma over the last 8.2 Ma. If the age and height of all the volcanic points are averaged, the Hopi Buttes eruptive surface gives an average long term incision rate of 63 m/Ma over the last 7.2 Ma which is also considered a maximum rate.

11. The upper fluvial Bidahochi Formation outcrops (orange in Fig. 1) in a map pattern suggestive of small washes that flowed into the 16-6 Ma valley depocenter located near but NE of the modern course of the LCR. Outcrops reach highest elevations of 2195 to 2255 m northeast of Winslow and St Johns, but these washes likely sloped toward the paleovalley depocenter as tributary drainages. Heights of ~ 700 m above the modern river are shown in Figure 1 as the highest upper Bidahochi outcrop elevations but these are not used as incision points because of projection issues. Highest Bidahochi units are shown in Figure 14A as part of a maximum inferred 6 Ma aggradation paleoprofile that was graded from the ~ 2300 m elevation of Flat Top basalt flow near Springerville (point #16 below) to 1900 m elevations of the Hopi Buttes volcanic field eruptive surface northeast of Winslow. This inferred 6 Ma maximum aggradational surface/ profile for the LCR valley is linked to the speculative 1600 m elevation of the 5 Ma CR-LCR confluences in Figure 14A. No Bidahochi Formation is preserved SW of the LCR, but the inverted topography of Chevelon Butte (incision point # 14) shows a similar landscape elevation at ~6 Ma southwest of the LCR as the lowest Hopi Buttes basalts northeast of the LCR. This, plus the relatively weak Moenkopi bedrock suggests a low-relief 6 Ma paleovalley much like today's but 300-400 m higher.

12A, 12B, 12C. Anderson Mesa- Walnut Creek basalts. As reported by Holm (2001), these basalts are about 50 km SW of the LCR along the Walnut Creek tributary to Diablo Creek that has its confluence with the LCR between Cameron and Winslow. Denudation estimates from these flows are complicated by several normal faults. #12A is the 6.39 Ma Anderson Mesa flow whose base is reported to be at 2180 m relative to nearby Walnut Creek that has incised to 1970 m resulting in an incision rate of 33 m/Ma which we interpret to be a maximum denudation rate. In his estimate, Holm included incision through the flow itself rather than using the base of the flow (rather than bedrock incision as reported in Table 1) and he reported an incision rate of 49 m/Ma since 6 Ma, with "vigorous erosion" starting well after 6 Ma. #12B. The McMillan Mesa flow yields similar results (Table 1). #12C. This basalt is a 859 ka inner canyon flow in Walnut Creek with a base at 2040 m elevation relative to a present creek elevation of about 2022 m yielding an incision rate of 21 m/Ma. Holm reported a rate of 64 m/Ma but also included 37 m of incision through the flow itself for a total of 55 m of incision since 0.859 Ma (rather than bedrock incision, as reported in Table 1). All of these rates are very low and hence are similar to rates seen in the headwaters of the LCR (Fig. 14B). Our interpretation of these low rates is that the post-2 Ma incision acceleration and lower base level of Grand Canyon and the lower LCR have not propagated to these reaches of the upstream tributaries.

13A, 13B—East Sunset Mountain basalt flows form elevated basalt plateaus just north of East Clear Creek, a major tributary canyon that has its confluence with the LCR near Winslow. Holm (2001, p. 62) reported 1.92 Ma and 2.90 Ma ages for the higher flow and concluded that one was likely incorrect. He also reported a younger 1.63 Ma age on a lower inset basalt plateau. **13A.** The 1.92 (or 2.9 Ma) basalt eminates from a cinder cone and flowed south toward East Clear Creek. Its base is at 1945 m elevation where it flowed to within 2 km of modern East Clear Creek tributary in a place where the East Clear Creek Canyon floor is at an elevation of about 1725 (from Google Earth) yielding a tributary incision rate of 115 m/Ma which is considered a maximum rate in Table 1. If the older 2.9 Ma age is correct, this flow would yield a rate of 76 m/Ma. **13B.** The 1865 m elevation of the base of the lower inset flow relative to the 1690 m elevation of the floor of East Clear Creek (from Google Earth) gives an incision rate of 107 m/Ma since 1.63 Ma. Holm reported an average incision rate of 86 m/Ma, but it is not clear how this value was calculated. This is an important incision site that needs additional study as it may help constrain the 2-3 Ma change in incision rates shown in Figure 14B. From existing data we infer a maximum tributary incision rate of 80-120 m over the last ~2 Ma for this location.

14. Chevelon Butte basalt forms an isolated basalt-capped plateau located between East Clear Creek and Chevelon Creek tributaries to the LCR. This point was used by Cather et al. (2008) to define a 6 Ma paleosurface (flat in his Fig. 14) and post-6 Ma incision/ denudation of ~ 520 m or 87m/Ma (in his Fig. 15). Table 1 shows the base of the flow at 2075 m relative to the East Clear Creek tributary at 1750 m

elevation (from Google Earth) yielding a 51 m/Ma tributary incision rate which could be considered we interpret to be a maximum denudation rate or a maximum tributary incision rate for East Clear Creek over the last 6 Ma.

15. The Cooley et al. (1969) surfaces and terraces were interpreted (in their Plate 3) to be erosional surfaces that record progressive incision of the LCR valley. Many of the higher surfaces are likely surfaces of diachronous age and variable incision significance such that additional correlation and dating is needed to test Cooley's mapping and correlations. Nevertheless, we have now directly dated several of the surfaces and terraces and present the dates, interpretations, and hypothetical correlation of surfaces in Table 1. Figure 13 is an attempt to digitize and georeference the mapping of Cooley et al., 1969, Plate 3 and is reasonably accurate at the scale presented. From oldest, our interpretations of the Cooley et al. (1969) surfaces and terraces are as follows. **The Valencia surface** (L-1 of Cooley et al., 1969, Plate 3) is likely of composite age, but we interpret it in Figure 13 to largely post-date the Chuska Sandstone and pre-date the Lower Bidahochi Formation and hence to be fragments of the landscape that developed during the post-Chuska erosion event described by Cather et al. (2008) during 25-15 Ma incision of the LCR paleovalley and carving of the East Kaibab paleocanyon. Cooley et al. (1969) correlated it with the Zuni surface of Gregory (1947) but we interpret the latter to be more closely related to the 6-8 Ma fluvial upper Bidahochi drainage system. **Hopi Buttes eruptive surface** (L1 of Cooley et al., 1969) is a term used in this paper for a diachronous surface in the Hopi Buttes volcanic field onto which basalts were erupted 6-8 Ma. It has been variably dissected by post-6 Ma incision of the modern LCR valley and it elevation is constrained by the base of basalts of this age in the northeastern parts of the volcanic field and by estimates of depth below the eruptive surface that have been made for Maar diatremes of the southwestern volcanic field (White, 1991). As discussed above, the post-basalt erosion estimates for Hopi Buttes basalts suggest 50-65 m/Ma maximum denudation rate of the LCR valley in the past 6 Ma. This elevation may also approximate a local base level for fluvial deposition of the upper Bidahochi Formation and the maximum aggradation level of the LCR paleovalley prior to integration for the Colorado River through Grand Canyon as shown in Figure 14A**.** Crooked Ridge, White Mesa alluvium, and Moenkopi Plateau were all mapped by Cooley et al. (1969) as part of the L2A "early Black Point surface". However, new ^{40}Ar-^{39}Ar sanidine dating confirms that these are all about 2 Ma and distinctly older than the Black Point basalt flow hence we assign a ~ 2 Ma age to the mapped L2A surfaces in the Black Mesa area. The correlation of these surfaces to areas to the southeast and northwest (Cooley et al., C-1 surfaces) needs additional testing. The "late Black Point surface" of Cooley et al. (1969, L-2, L-2B, L-2C) included the Blue Canyon plateau (#4 of Table 1) which contains an ash that correlates with the ~ 1 Ma Bishop- Glass Mountain Tuff (Hereford et al., 2016). Other surfaces mapped as L-2B by Cooley et al. (1969) may also be approximately 1 Ma. The Black Point terrace is here defined as the strath beneath the gravels that underlie the 890 ka Black Point basalt (# 5 in Table 1). This seems to be close to the same age and landscape position to Cooley et al.'s late Black Point surface such that the surfaces may be pediments graded to the Black Point river terrace which is now the highest recognized LCR river terrace at 172 m above the LCR. The "Wupatki terraces" of Cooley et al. (1969) are river terraces in the Cameron-Winslow area that record glacial-interglacial aggradation- incision fluctuations during overall progressive bedrock incision of the LCR. Five identified terrace treads in this area (mapped as L-3, L-3A, and L-3B) are at heights of 61-91 m, 46-61 m, 23-30m, 15, and 9 m above the modern LCR (Cooley et al., 1969). The 340 ka Tappan flow (#7A of Table 1) now dates the 57 m strath terrace near Cameron as 340 ka. Cooley et al. (1969) correlated these LCR terraces with higher terraces along the Colorado and San Juan rivers (C-5, C-5A, C-5B) at heights of 122-152m, 61-91 m, 30-60m, 15-30m, and 9-15m.

UPPER REACH- ST JOHNS TO MOUNT BALDY

Basalts of the Springerville volcanic field range in age from 8.9 Ma to about 0.5 Ma (Condit et al., 1999) and provide a record of interaction of the LCR with the developing volcanic field in the headwaters of the LCR. The caveats about our interpretation for the basalt-contrained incision points are that: 1) K-Ar

ages are of variable reliability and ^{40}Ar-^{39}Ar ages are only available for some of the basalts. 2) The places the basalts were dated (stars in Figs. 15 and 16) are generally not the optimum locations for incision estimates such that our incision estimates (lines below the stars in Fig. 16) reflect assumed correlations of flows based on mapping by Condit et al. (1999). 3) Knickpoints in the modern profile and inferred paleoprofiles reflect the low erodibility of basalts that filled paleochannels. 4) Sirrine (1958) mapped and studied the gravels but additional systematic work is needed on age relations between gravels and basalts (Figs. 16 and 17). 5) Embid (2008) projected heights of basalt bases and tops, and of mapped gravel terraces, but these are subject to the usual projection and correlation ambiguities. 6) The geologic complexity of estimating incision rates in a developing volcanic complex transected by a regional river system are substantial because the slopes of the constructional volcanic surfaces, the run-out basalt flow geometries, and the inferred incision rates reflect a combination of changes in far-field river gradient (downstream baselevel fall/ headwater uplift) AND elevation increases associated with local lava flow emplacement. For example, post-3 Ma flows show aggradation (younger flows atop older ones) upstream of the main LCR upper knickpoint, but incision (younger flows inset into older flows) below it. In spite of the various limitations and the need for further work, our analysis suggests two main observations. 1) Many flows have "run-out" geometries (thin flows with long longitudinal extent relative to their width) suggestive that basalts flowed down and preserved paleochannels. 2) Once solidified, the basalt surfaces were hard to erode and now form elevated plateaus (inverted topography) with older flows preserved higher in the landscape than younger ones. These conclusions indicate that the basalts, and especially the basalt run-outs and distal areas below the major knickpoint, record progressive semi-steady incision of this part of the LCR (Fig. 16).

16. Flat Top basalt (sample SM-5 of McIntosh and Cather, 1994) yielded an ^{40}Ar-^{39}Ar isochron of 6.8 ± 0.02 Ma. It overlies gravels of the Fence Lake Formation that have been correlated with the fluvial Bidahochi Formation. The base of the basalt is 299 m above the LCR ~ 4 km east of Springerville yielding a maximum incision rate of 44 m/Ma.

17. Fissure Vent basalt samples 771 and 801C from Cooper et al. (1990) yielded K-Ar ages of 5.31 ± 0.11 and 6.52 ± 0.12/6.66 ± 0.12 (two aliquots) respectively. This flow overlies Triassic Moenkopi Formation and appears to be a run-out along a tributary channel to the LCR similar to the modern wash on its west side that parallels the modern LCR. Figure 16 shows that its base projects about 120-155 m above the LCR over a distance of about 20 km yielding a tributary incision rate of 18-24 m/Ma using the 6.52 age, and 23-29 using the 5.31 age. At the tip of the flow, its base is about 200 m above the LCR yielding an LCR incision rate of 31-38 m/Ma. These are interpreted to be maximum rates as gravels are not known below the flow. Examination of all the ~ 6 Ma flows in Figure 16 suggests that early Springville flows may preserve a convex reach and/or knickpoint in the upper LCR drainage system that was present before 6 Ma perhaps due to 9 to 6 Ma building of the early Springerville volcanic field. This flow should be re-dated near its tip where it crosses highway 180 and where its base is about 200 m above the modern LCR (estimated from non-landslid outcrops in Google Earth).

18. South Fork Campground flow (sample AWL-7-77 of Laughlin et al., 1980) yielded a K-Ar age of 6.03 ± 0.43 ka. It is from the mesa just south of South Fork Campground and is reported to overlie gravels. Its flow base is about 274 m above the modern LCR (estimated from Google Earth) yielding an incision rate of 45 m/Ma which is in good agreement with the rate calculated from Flat Top basalt and is interpreted as a preferred incision rate for the upper LCR over this timeframe. However, samples 21A (3.06 Ma) and 21B (2.94 Ma) are in the same reach of the river and are directly adjacent to the modern floodplain suggesting low post-3 Ma incision rates such that 6 to 3 Ma incision rates may have been ~ 80 m/Ma in this area.

19. Black Mesa flow forms an inverted basalt mesa with a channel-like map geometry east of the LCR but the age of the flow at its farthest runout is uncertain, where it sits on (or is adjacent to) Tg1 gravels of

Sirrine (1958). We tentatively use the ^{40}Ar-^{39}Ar age of 6.03 ± 0.02 Ma from SMC-1 (McIntosh and Cather, 1996) which is from a basalt just east of the NM-AZ stateline overlying Fence Lake Formation (Bidahochi equivalent) east of Cow Springs draw, paired with a height of 245 m measured above the LCR at the tip of the outflow, to derive an incision rate of 41 m/Ma which is interpreted as a maximum rate. Other dated basalts that might correlate with this flow are 2.46-2.37 Ma but these are likely younger flows inset into or overlying the older flow (see # 22 below). This flow needs to be re-dated near its northern tip.

20. Coyote Wash flow forms a run-out basalt platform just east of the LCR near Lyman Lake. At the farthest tip of the run-out its base is 135 m above the LCR (estimated from Google Earth). Sample AWL-3-77 from Laughlin et al. (1980) yielded a K-Ar date of 3.67 ± 0.12 Ma on a flow that may be correlative with Coyote Wash flow. The dated sample is from a roadcut along Highway 60 about 6 km east of Springerville. The base of this flow is about 120 m above Coyote Creek yielding a tributary incision rate of 33 m/Ma relative to Coyote Creek and, if this age correlates with the flow at the tip of the run-out, an LCR incision rate of 37 m/Ma. A new date from the tip of the Coyote Wash run-out is needed to confirm this assumption.

21A. Springerville flow; AWL-42-74 (Laughlin et al., 1979) is from a sample that yielded a K-Ar age of 3.06 ± 0.08 from a flow that borders the flood plain of the upper LCR south of Springerville. The base of the flow (~ 2150 m) is about the same elevation as the LCR floodplain (2145 m) which gives a near-zero (2 m/Ma) incision rate at this location.

21B. Springerville flow AWL-40-74 (Laughlin et al. 1979) is probably the same flow as AWL-42-74 and gave a K-Ar age of 2.94 ± 0.14 Ma that is within error the same age. Laughlin et al (1979) described the sample as in a roadcut along Highway 60, 6.8 km east of Springerville. Its flow base is about 25 m above the LCR yielding an LCR rate of 9 m/Ma.

22. Mesa Parada flow: M1160 of McIntosh and Cather (1994) is inset into the Black Mesa and yielded an ^{40}Ar-^{39}Ar isochron age of 2.37 ± 0.04 Ma. If this date were used for the tip of Black Mesa, it would yield an incision rate of 105 m/Ma but because it is inset, we prefer the 6.03 Ma age from #19. A new date near the tip of the run-out and additional mapping is needed before the correct age for this incision point can be verified.

23. Escudilla Mountain flow UAKA82-194 is from an inverted basalt mesa about 1.5 km west of and directly above the LCR near Lyman Lake. It yielded a K-Ar date of 1.98 ± 0.06 (Aubele et al., 1986). The base of the flow is at an elevation of 1930 m relative to the LCR at the outflow of Lyman Lake Dam at 1810 m (from Google Earth) yielding an incision rate of 60 m/Ma. Qg2 gravels of Sirrine are mapped beneath this flow such that this flow provides an estimate for the age of that terrace. Because gravels are present, this incision rate is interpreted as a preferred LCR incision rate.

24. AWL-5-77 yielded a K-Ar date of 1.67 ± 0.09 (Laughlin et al., 1980) from the flow that forms the lip of the basalt gorge at the major knickpoint just upstream of Lyman Lake. Below the knickpoint, the base of the basalt is 1940 m elevation relative to the LCR at 1880 m yielding an incision rate of 36 m/Ma. Upstream of the knickpoint, the LCR flows within this flow indicating no net bedrock incision above the knickpoint.

25. 717MR: Cooper et al. (1990) reported a K-Ar date of 1.56 ± 0.03 on a basalt run-out (now an inverted basalt mesa) about 25 km west from sample 17 and west of Figure 15. The base of this basalt is at an elevation of about 1835 m at the tip of the mesa (from Google Earth) and the adjacent dry tributary to the LCR (500 m west, just upstream of where it crosses Concho Rd) is 1715 m, yielding a tributary incision rate of 77 m/Ma over the last 1.56 Ma. The date is about 17 km SSE of the tip of the mesa but the run-out geometry of this thin flow makes this a preferred tributary incision rate.

26. AWL 6-77 is from a flow that overlies #24 (1.67 ka) and is one of the younger flows in the Springerville volcanic field (youngest = 0.5 Ma; Condit et al., 1999). It yielded a K-Ar date of 75 ± 0.03 but it has a normal magnetic polarity suggesting its age may be closer to 620 ka (Condit et al., 1999). This flow is mapped from the dated locality north into the LCR valley (Condit et al., 1999). At its closest point to the LCR (within 100m of the flood plain), the base of the flow is at an elevation of about 1870 m relative to the LCR at 1845 m giving an incision rate of 33 m/Ma using the 0.75 age and 40 m/Ma using the 0.62 age.

27. T21- EE07-81A is the oldest dated travertine sample that also directly overlies a strath; it is 304 ± 86 ka and is from the southern end of the Salado platform. The base of the travertine is at an elevation of 1827 m, overlying 1 m of gravels that in turn rest on a strath 26 m above the LCR. This yields an incision rate of 86 m/Ma.

28. T23: EE-09-7 is from a mound next to Lyman Lake dam and is dated at 281 ka. It gives an age of 281 ± 15 ka. The strath is 43 m above the LCR giving an incision rate of 153 m/Ma.

29. T28: K04-SPV-2 is from the northern end of Lyman Lake along the paved road; it gave a U-series age of 255 ± 6 ka and an incision rate of 94 m/Ma (Fig. DR-5).

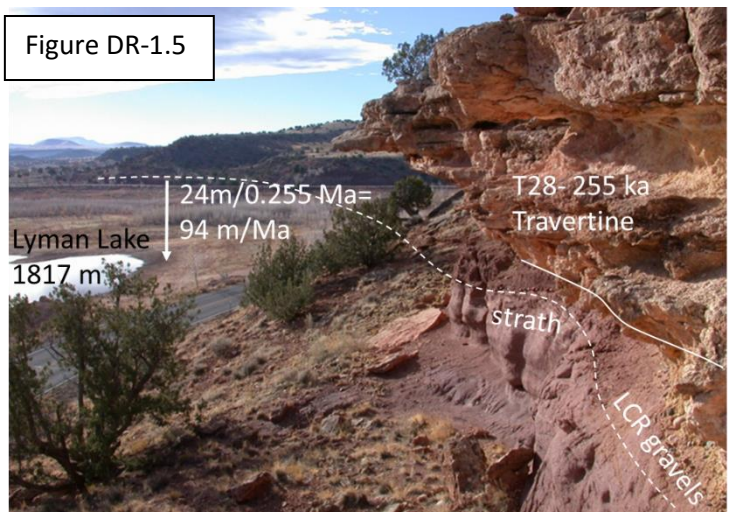

30. EE07-84A was sampled several m above a strath that underlies the Salado travertine platform just north of Lyman Lake. It gives an age of 239 ± 3 ka. The strath is 26 m above the floodplain yielding an incision rate of 109 m/Ma (Fig. DR-6).

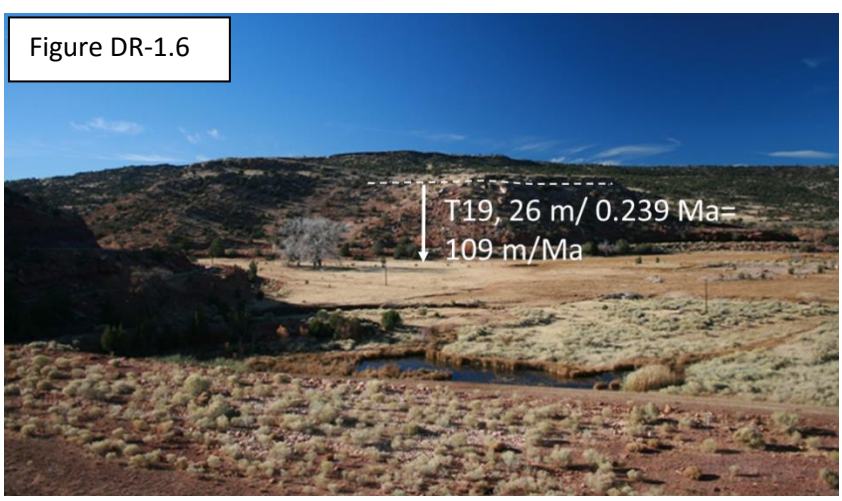

31. T26: K04-SPV-5C is from a mound deposit near the Lyman Lake dam. It overlies LCR river gravels that in turn overlie a strath that is 30 m above the LCR floodplain; this gives an incision rate of 134 m/Ma (Fig. DR-7).

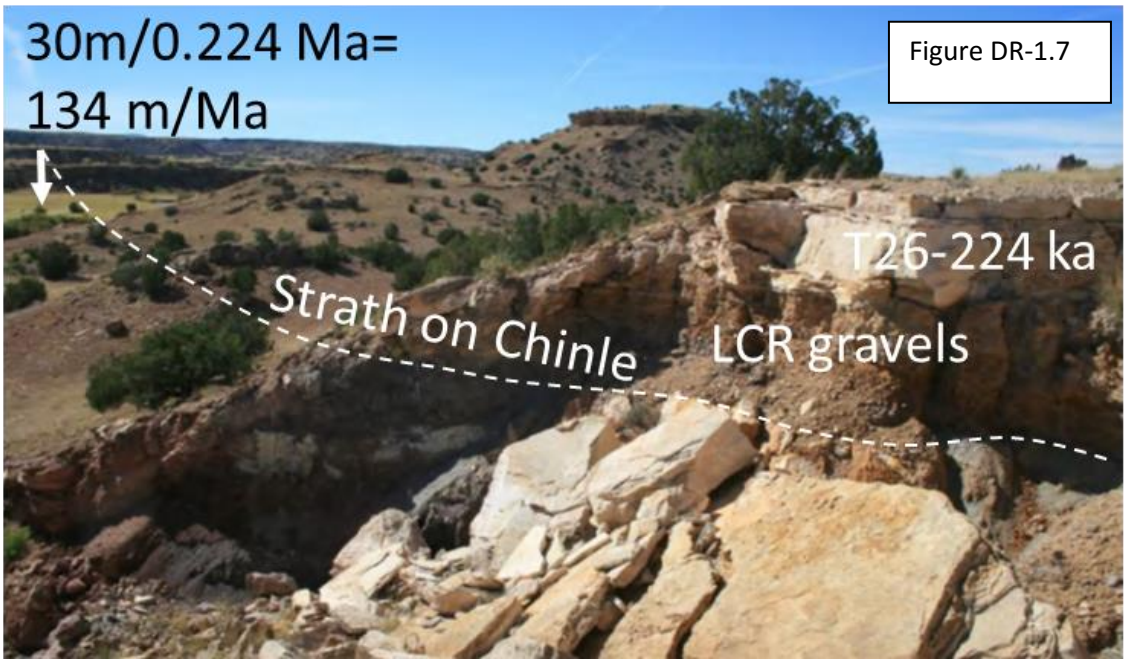

32- 34. T40: EE06-LL, EE07-75-AR and EE06-LL are all from the bases of individual mounds between Lyman Lake and Salado Springs and all overly river gravel/strath contacts. They are dated at 97, 78, and 101 ka respectively and show an average river incision rate in the last 100 ka of 257, 309, and 269 m/Ma.

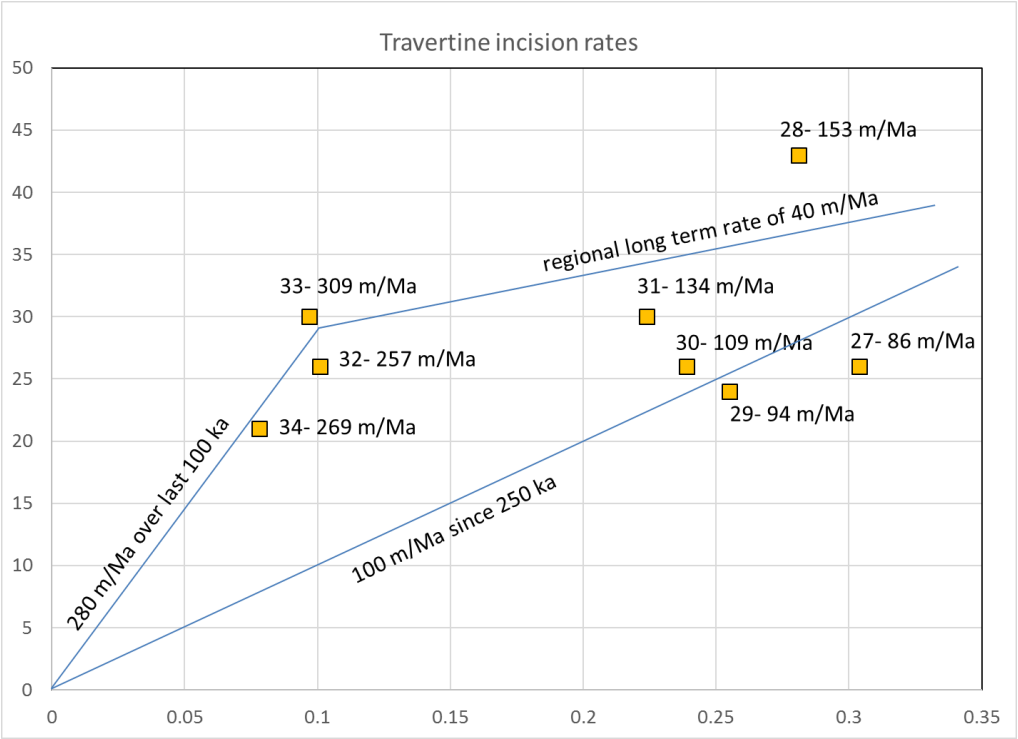

Figure DR-1.8. Incision rates calculated from U-series ages of travertines that overlie bedrock straths near Lyman Lake. Rapid incision over the last 100 ka is suggested by strath heights of 20-30 m for these travertines. 200-300 ka travertines overlie variable strath heights and could be interpreted in terms of ~100 m/Ma rates over this time period, or as compatible with the ~40 m/Ma rates seen for the previous 6 Ma as depicted in Fig. 14.

EASTERN LCR HEADWATER TRIBUTARIES

Eastern tributaries to the LCR (with confluences above Holbrook Arizona) are shown in profile in Figure DR-5; these include the Rio Peurco of the West, Zuni River, Carrizo Wash/ Largo Creek, and their upper tributaries. Rio Peurco of the West and Largo Creek have lower gradient smooth concave-up profiles that differ markedly from the modern LCR headwaters. Zuni river is also lower gradient but has knickpoints that reflect basalt flows in the channel. These lower gradient profiles may have been earlier headwaters and/or reflect the softer bedrock in areas away from the young basaltic volcanism at Springerville. $^{40}Ar/^{39}Ar$ dates from basalts in the region of these eastern tributaries were published in McIntosh and Cather (1994) and are summarized in Figure 14. Table 1 lists these ages as well as heights above the modern channels taken from cross sections drawn by McIntosh and Cather (1994) and also estimated from Google Earth. Love and Connell (2005) also discuss some of these basalts in terms of drainage evolution although they do not focus on long term bedrock incision rates and they come to somewhat different results involving aggradation/incision histories (mentioned in Table 1). Our conclusion based on plotting age versus heights for all the basalts is that they record low but semi-steady progressive bedrock incision over the last 6 Ma (Fig. 14).

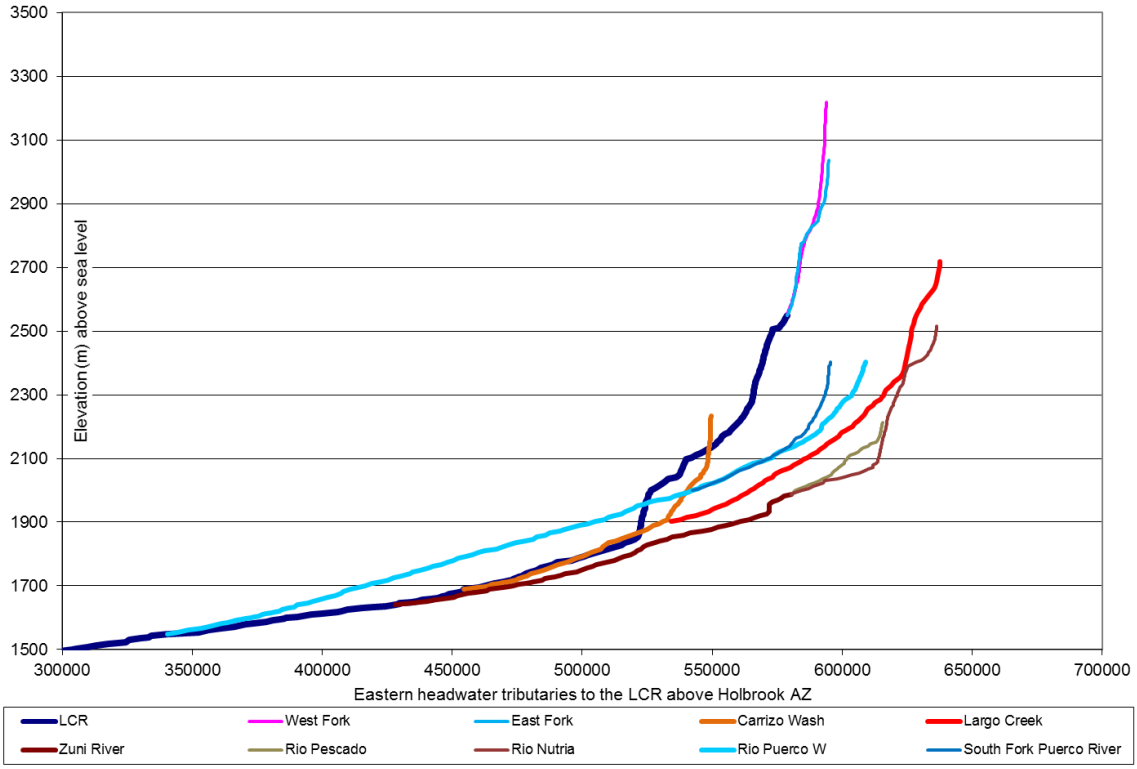

Figure DR-1.9. Profiles of eastern tributaries to the LCR (above Holbrook Arizona) include the Rio Peurco of the West, Zuni River, Carrizo Wash/ Largo Creek, and their upper tributaries. Rio Peurco of the West and Largo Creek have lower gradient smooth concave-up profiles that differ markedly from the modern LCR headwaters.

35. TM-11-13-1 Tejana Mesa basalt forms a mesa adjacent to Largo Creek; it was dated by the K-Ar method by Dethier et al (1986) to be 6.73 ± 0.18 Ma. The flow overlies Fence Lake Formation gravels (correlated with fluvial upper Bidahochi) and underlies Quemado Formation gravels. The cross section from McIntosh and Cather (1994) shows this flow to cascade off the top of Tejana Mesa toward Largo Creek and get as low as 2140m. The height of the base of the flow on mesas on both sides of Largo Creek are 2230 m relative to elevation of the Largo Creek bed at 2060 m giving a maximum incision rate of 25 m/Ma. Incision rate is 12 m/Ma using the base of the cascading flow and assuming it is the same age as the mesa top flows.

36. NM-1159 Mesa N of Blaines Lake gave an Ar-Ar date of 6.08 ± 0.04 Ma (McIntosh and cather, 1994) and is at an elevation of 2190 m relative to the closest point along Aqua Fria Creek of 2100 m, giving a tributary incision rate of 15 m/Ma.

37. SMC-4 Cimarron Mesa basalt was dated by McIntosh and Cather (1994) and gave an ^{40}Ar-^{39}Ar plateau age of 6.05 ± 0.02. Their cross section shows the base of the flow at elevation of 2241 m relative to Blaines Lake along the Aqua Fria Creek at 2115 m and Largo Creek at 2060 m. This gives a tributary incision rate of 21 m/Ma relative to Aqua Fria Creek and 30 m/Ma relative to Largo Creek.

38. SMC-1 Cow Springs (Black Mesa vent area?) basalt gave an ^{40}Ar-^{39}Ar isochron age of 6.03 ± 0.02 Ma. This area may be the vent area or upflow continuation of the Black Mesa flow (# 19 of Table 1). The flow overlies gravels of the Fence Lake Formation and the elevation of the sample is 2378 m and base of the flow is about 2360 relative to the 2170 m elevation of Cow Springs draw giving a tributary incision rate of 32 m/Ma relative to Cow Springs Draw and an LCR incision rate (from the tip of Black Mesa) of 41 m/Ma.

39. Basalt of Red Hill Draw sample SM-2 gave an ^{40}Ar-^{39}Ar plateau age of 5.20 ± 0.03 Ma. It overlies the Fence Lake Formation. Based on the cross section of McIntosh and Cather (1994) the base of the flow is at an elevation of 2270 m relative to Cow Springs draw at an elevation of 2060 m giving a tributary incision rate of 40 m/Ma. Their cross section shows this flow either interbedded with or possibly inset into Fence Lake Formation.

40. Basalt of Nutrioso Basin AWL-8-77 gave a K-Ar age of 3.87 ± 0.03 Ma (Laughlin et al., 1980). It overlies the Quemado Formation (?). The elevation of the base of the flow at 2251 m relative to Nutrioso Creek at 2110 m yields a tributary incision rate of 26 m/Ma.

41. Basalt of Nutrioso Basin AWL-3-77 gave a K-Ar age of 3.67 ± 0.12 Ma (Laughlin et al., 1980). It overlies the Quemado Formation (?). Its elevation of 2225 m relative to Nutrioso Creek at 2110 m yields a tributary incision rate of 31 m/Ma.

42. SMC-3 basalt of Cow Springs basin gave an ^{40}Ar-^{39}Ar plateau age of 2.46 ± 0.04 Ma (McIntosh and Cather, 1994). It overlies the Quemado Formation. Its elevation of 2276 m relative to Coyote Creek at 2170 m yielding a tributary incision rate of 43 m/Ma.

43. NM-1156 is a basalt from the Red Hill basin that gave an ^{40}Ar-^{39}Ar plateau age of 1.51 ± 0.01 Ma (McIntosh and Cather, 1994). Its base is at an elevation of 2166 m relative to Agua Fria Creek (Blaines Lake) at 2117 m giving a maximum incision rate of 32 m/Ma.

44. NM-1157 basalt Red Hill basin gave an ^{40}Ar-^{39}Ar plateau age of 0.97 ± 0.14 Ma (McIntosh and Cather, 1994). It is interbedded with the Quemado Formation east of Blaines Lake. Its elevation is 2149, with the base of the flow at about 2145 m, relative to Aqua Fria Creek at 2112 m yields a tributary incision rate of 34 m/Ma.

Section DR-2 Thermochronology

Contents:

Section DR-2 Thermochronology modeling
Table DR-2.1 Table of key thermochronology samples
Figure DR-2.2 Age-elevation and eU-age data from LCR-region
Figure DR-2.3 Youngest age –elevation plot for LCR samples
Section DR-2.4 Geologic constraint boxes imposed on HeFTy models
Section DR-2.5 Sample by sample modeling details for samples A through N
Figure DR-2.6 Comparison of models with and without the Rim Gravel constraint box
Figure DR-2.7 Comparison of models with and without the Bidahochi constraint box

Thermochronologic modeling. This paper presents thermal history models of available apatite (U-Th)/He (AHe) thermochronological data from Flowers et al. (2008) and Lee et al. (2013) using the program HeFTy 1.7.4 (Ketcham et al., 2005). Constrained time-temperature (t-T) paths are generated by inverse modeling using the RDAAM (Radiation Damage Accumulation and Annealing Model) diffusion model (Shuster et al., 2006; Flowers et al., 2009). Input parameters for the apatite AHe models include: the equivalent spherical radius of the grains; an alpha stopping distance of 35 μm; and alpha calculation set to `ejection only', so no implantation; an rmr0 value of 0.83 typical for apatite-CaF; the corrected age with an assigned 20% uncertainty; and concentrations of uranium, thorium, and samarium. Table DR-2.1 shows sample locations and information. HeFTy takes predicted results from t-T paths and compares them to observed data and a goodness of fit (GOF) is calculated. GOF indicates the probability of failing the null hypothesis which states that the modelled data and the observed data are statistically different. High values of GOF indicate a high probability that the null hypothesis can be rejected and there is hence a good match to the measured data. GOF values >0.05 are defined as acceptable agreement between modelled and observed data; values >0.5 are regarded as good fits (Ketchum et al., 2005). All thermal models trace the detrital grains from their Precambrian crystallization age through exhumation, deposition, reburial by Mesozoic strata, and post-Laramide cooling (Section DR-2.4). The pre-Laramide portion of the path allows for buildup of radiation damage in crystals that reside above or within the AHe partial retention zone for extended time periods (Fox and Shuster, 2014). A temperature of 15 ± 10ºC is used to represent near-surface conditions, which encompasses the 25ºC maximum surface temperature used for conversions of temperature to depth in this paper and also includes a more realistic 10ºC surface temperature.

In some samples, HeFTy inverse modeling was not able to produce any good or acceptable time-temperature paths using all analyzed grains from a given sample. For example, there were zero acceptable paths generated after ~1 million random path attempts for the 8 grains in sample E (CP05-7), and this was true with and without the earliest (pre-deposition, Precambrian) constraint box. This suggests that complicating factors such as inclusions or zoning in grains, variable early lattice damage among detrital grains of different crystallization age and burial history, variable He retentiveness (Fox and Shuster, 2014), grain boundary phases, helium implantation, and other complexities of helium diffusion are not completely described by the RDAAM model. For these samples, subsets of 5 to 7 grains were modeled as guided by positive-slope eU-age correlations among a subset of grains and through trial and error to maximize the

number of grain constraints that would produce time-temperature paths in HeFTy. The resulting multigrain time-temperature paths generated for each sample show the number of grains used, and excluded in the models (Table DR-2.1). In each case, HeFTy was run until 100 good paths (GOF= 0.5) were generated.

TABLE OF KEY THERMOCHRONOLOGY SAMPLES DISCUSSED IN TEXT

Sample #	Latitude	Longitude	Elevation (m)	Rock type	AHe age range (Ma)	eU range (ppm)	Apatite grains modeled	Ave. (range) of GOF for modeled grains	Grains not modeled
A. CP06-3B	35.53166	-111.3457	1417	Moenkopi	18-64	21-84	1, 3, 6, 7	0.72 (0.49-0.98)	2, 5
B. CP06-5	34.97482	-110.5206	1519	Moenkopi	18-42	6-152	1, 2, 3, 4, 5, 6, 8	0.58 (0.18-1.0)	7
C. CP06-6	34.83569	-110.1447	1628	Moenkopi	20-25	16-42	1, 2, 3, 4, 5	0.69 (0.40-0.92)	-
D. CP06-7	34.60621	-110.0888	1704	Moenkopi	21-33	9-36	1, 2, 3, 6	0.55 (0.20-0.96)	-
E. CP05-7	35.92422	-111.7297	1910	Moenkopi	21-49	17-36	3, 4, 5, 6, 8	0.65 (0.24-0.98)	1, 2, 7
F. CP05-3A	35.70257	-112.1317	1816	Moenkopi	22-74	18-72	1, 3, 5, 8, 10	0.58 (0.33-0.96)	2, 7, 9
G. CP05-2	35.64722	-112.124	1833	Moenkopi	28-83	24-38	1, 3, 4, 5, 7, 9	0.72 (0.17-0.99)	2, 6, 8
H. CP06-10	34.26573	-110.0916	1916	Moenkopi	30-46	20-97	1, 2, 4, 5, 6, 7	0.72 (0.26-0.98)	8
I. CP06-20	34.78654	-111.1358	1957	Moenkopi	41-58	23-115	1, 2, 3, 5, 10, 11, 12	0.74 (0.27-0.97)	-
J. CP05-1	35.46021	-112.3126	1870	Moenkopi	43-66	28-138	4,6,7,8,11,12,13	0.64 (0.28-1.0)	2,5,10
K. CP06-12	34.36629	-110.445	2025	Moenkopi	47-57	25-171	1, 2, 3, 4, 5	0.82 (0.37-1.0)	-
L. CP06-19	34.5991	-111.24	2122	Moenkopi	48-61	9-75	1, 2, 5, 6	0.83 (0.67-0.98)	-
M. CP06-17	34.30494	-110.9428	2062	Esplanade	53-63	5-33	1, 3, 4, 5	0.76 (0.41-0.97)	-
N. CP06-29F	35.68541	-112.6067	1802	Moenkopi	59-75	9-89	2, 3, 4, 5, 6	0.69 (0.48-0.84)	-

Table DR-2.1 Thermochronology samples modeled in this study (analytical data are in Flowers et al., 2008); sample locations shown in Fig. 1, HeFTy thermal models are shown in figures 6-8 of the paper and modeling details, by sample, are in Section DR-2.5 (see below).

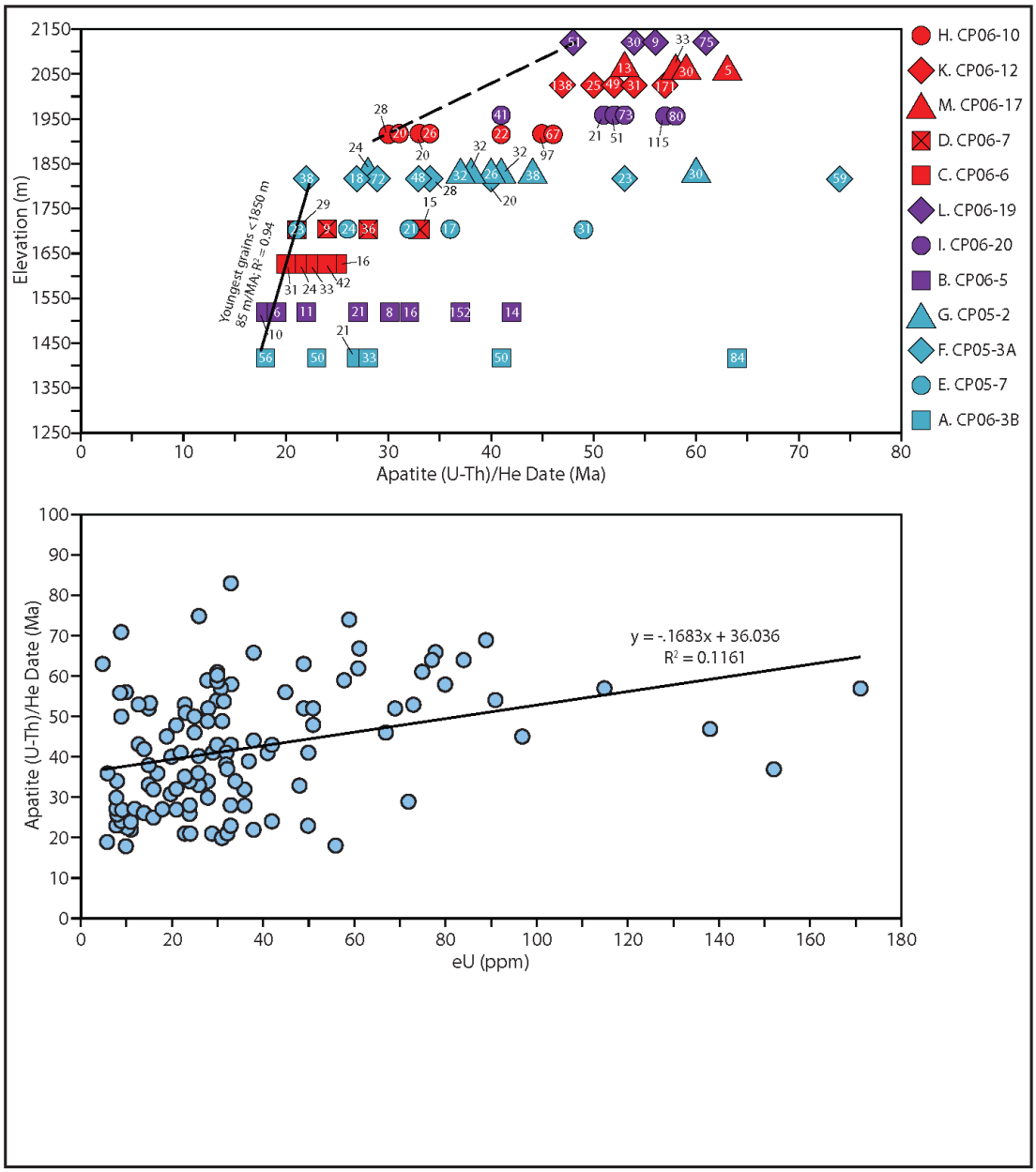

Figure DR-2.2 Age-elevation and eU-age data from LCR-region apatite thermochronology. A) Age- elevation plot for Little Colorado River thermochronology samples. Blue is Cameron transect; Purple is Winslow transect, Red is Holbrook transect. All samples show a wide range of detrital apatite ages; white numbers inside the symbols are eU values for each apatite grain. B) Age- eU plot for all LCR thermochronology samples. Details of age-eU relationships for each sample are shown below.

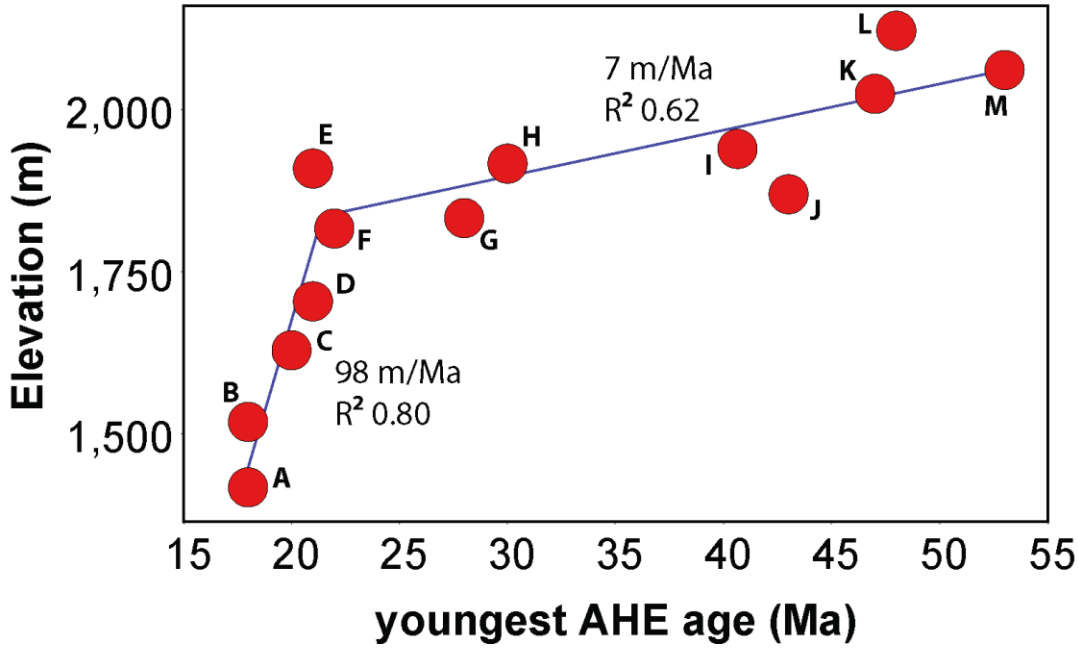

Figure DR-2.3. Youngest age- elevation plot of the LCR samples using the youngest AHe age shows a kink in the age-elevation diagram at ~ 20 Ma that is compatible with HeFTy models that show an onset of rapid cooling ~ 20 Ma. However, the ~700 m difference in elevation of the samples would correspond to only ~17 ºC for geothermal gradients of ~ 25 ºC/km. The samples have a wide horizontal spacing such that cooling is interpreted to reflect a combination of vertical denudation and NE-directed horizontal cliff retreat

SECTION DR-2.4 Geologic constraint boxes imposed on the HeFty models

1) Grains are assumed to have been 100-300 ºC from 1.4 to 1.0 Ga. This is supported by detrital zircon studies of the Moenkopi Formation that show that >50% of zircons (by inference apatite) crystallization ages are Precambrian (Anderson, 2006). ^{40}Ar-^{39}Ar studies indicate that Precambrian basement rocks in the region cooled through K-spar closure temperatures of ~ 150 ºC by 1.25- 1.0 Ga (Timmons et al., 2005). The effect of this constraint box is minimal but it may realistically simulate the accumulation of radiation damage in a majority of the detrital apatite grains prior to their deposition in the Triassic (Fox and Shuster, 2014). Models in figures of the paper are clipped to only show the last 100 Ma, but examples of the full paths are in DR-2.

2) All grains were in the surface environment during lower Triassic fluvial deposition, so all paths were forced through a depositional constraint box of 10-25 ºC from 230-250 Ma.

3) A pre-Laramide constraint box was used with a very broad temperature range: 40-140 ºC from 80-90 Ma. The wide temperature range permits uncertainty of the original thickness of upper Triassic, Jurassic, and Cretaceous strata in this area as well as uncertainties in the evolution of geothermal gradients, thermal conductivities, the role of groundwater, and surface temperatures. This constrain box allows the AHe data themselves to constrain modeled maximum Laramide temperature as well as cooling paths during and following the Laramide orogeny.

4) A “Rim Gravel” constraint was applied to samples high on the Mogollon slope where mid-Tertiary gravels overlie Triassic and Permian rocks in close proximity to thermochronology samples. Samples J and N are close to the Music Mountain Formation and hence must have cooled to near-surface conditions of 10-30 ˚C by 65-55 Ma. Samples I, J, K, L, and M are near to outcrops of Rim Gravels and hence must have cooled to temperatures of 10-30 ˚C by 50-30 Ma. Comparison of models run with and without this constraint box are shown in DR-2.7. Model runs with the constraint box for samples H and I produced more realistic t-T paths relative to models run without this constraint box and hence these models were used in Figures 7 and 8 of the main text. For all the other samples, the models run with and without the constraint box are essentially the same so we preferred to us the models without the constraint box in the main text in order for the thermochronology data to independently predict t-T paths.

5) A Bidahochi constraint box was applied to samples near the modern LCR (samples A, B, C, and D) that are within 10-100 km laterally of the exposed lower Bidahochi Formation lacustrine beds. For these samples (and possibly for the others such as H and I), the ~ 16 Ma paleosurface is geologically constrained to be at ~1770-1900 m modern elevation (Fig. 1; Cooley and Akers, 1961; Dickinson, 2013). Note that all of the samples were likely within ~ 300 m vertically (~7.5 ºC) of the 16 Ma paleosurface and hence were probably near surface temperatures by 16 Ma. Nevertheless, this constraint box was not used for the higher elevation samples on the Kaibab uplift as the monoclinal topography likely introduced variation in the thickness of overlying strata and the original western extent of the Bidahochi Formation is unknown (Dickinson, 2013). However, a sensitivity test in DR 2.7 shows that models developed with and without this constraint box are very similar for all the LCR samples.

(5) The final constraint was to force samples to cool to modern surface temperatures of 10-25 ºC (Karlstrom et al., 2014). In the following discussion, where we convert temperature to depth, we use a surface temperature of 25 ºC and geothermal gradient of 25 ºC/km which may provide a realistic (Wernicke, 2011; Flowers et al. 2008), and/or minimum (Karlstrom et al., 2014) depth estimate for reconstructed paleosurfaces.

SECTION DR-2.5 Sample by sample modeling details for samples A through N

Section DR-2.5 Sample by sample modeling details for samples A through N

Figure DR-2.5A Cameron Transect – Sample A (CP06-3B)

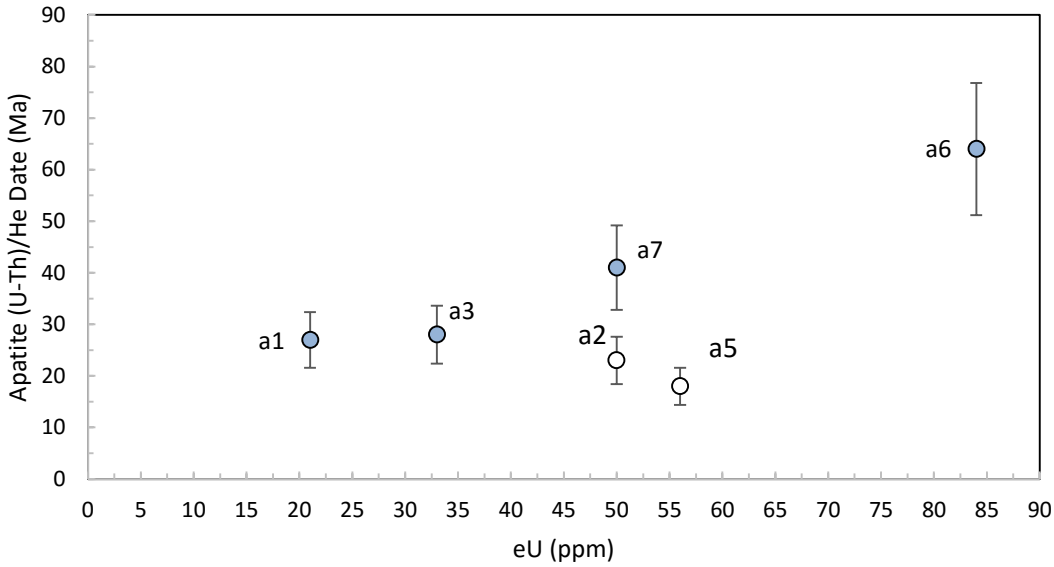

The thermal history model for sample CP05-7 includes 5 individual AHe dates, shown in blue. Grains not used in modeling are in white. a2 and a5 were excluded because their age doesn't increase with increasing eU, which would be expected. Uncertainties for each grain are set at 20% of the corrected grain age.

Thermal History Models

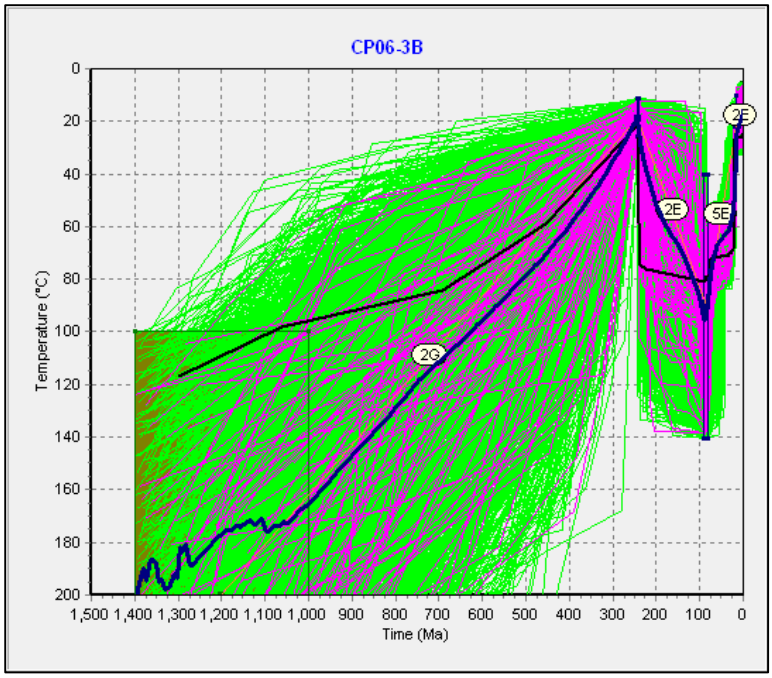

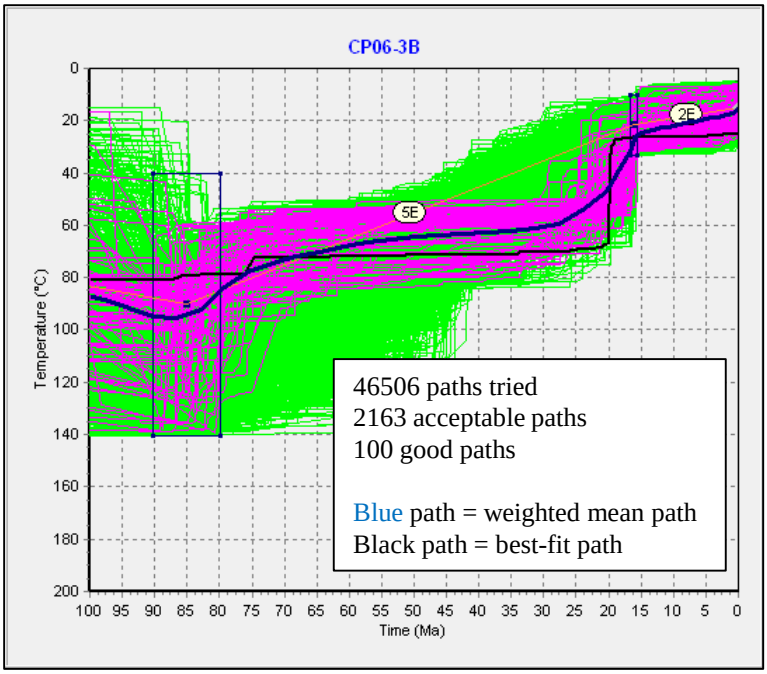

AHe Modeling Results

a1 corrected age: 27.0 ± 5.4 Ma
model age: 23.3 Ma
GOF: 0.49

a3 corrected age: 28.0 ± 5.6 Ma
model age: 28.2 Ma
GOF: 0.98

a6 corrected age: 64.0 ± 12.8 Ma
model age: 67.3 Ma
GOF: 0.86

a7 corrected age: 41.0 ± 8.2 Ma
model age: 35.9 Ma
GOF: 0.53

Comparison of Corrected Ages to Model Ages

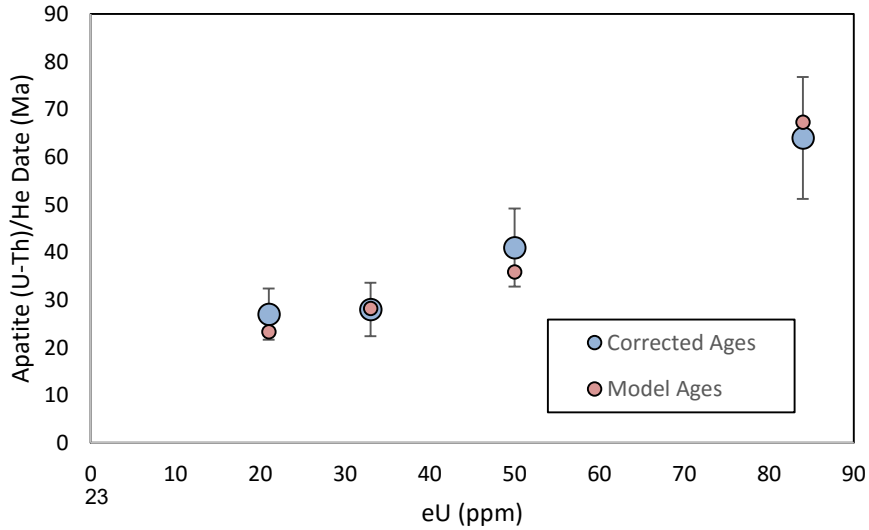

Figure DR-2.5B Winslow Transect – Sample B (CP06-5)

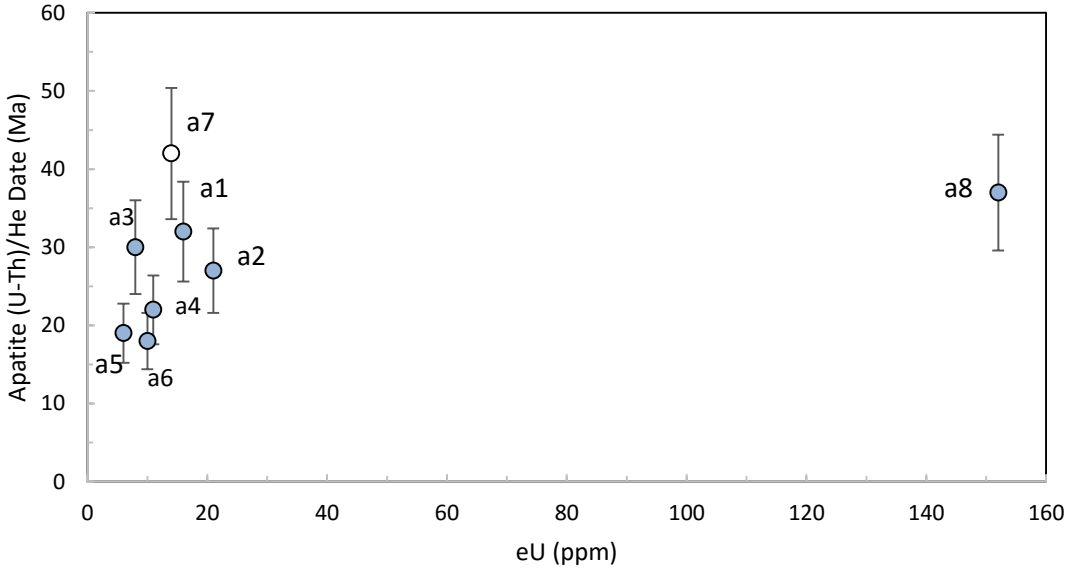

The thermal history model for sample CP06-5 includes 7 available AHe dates, shown in blue. A single grain, a7, was not used in modeling because HeFTy only accepts 7 AHe dates, and a7 is anomalously old compared with the rest. Uncertainties for each grain are set at 20% of the corrected grain age.

Thermal History Models

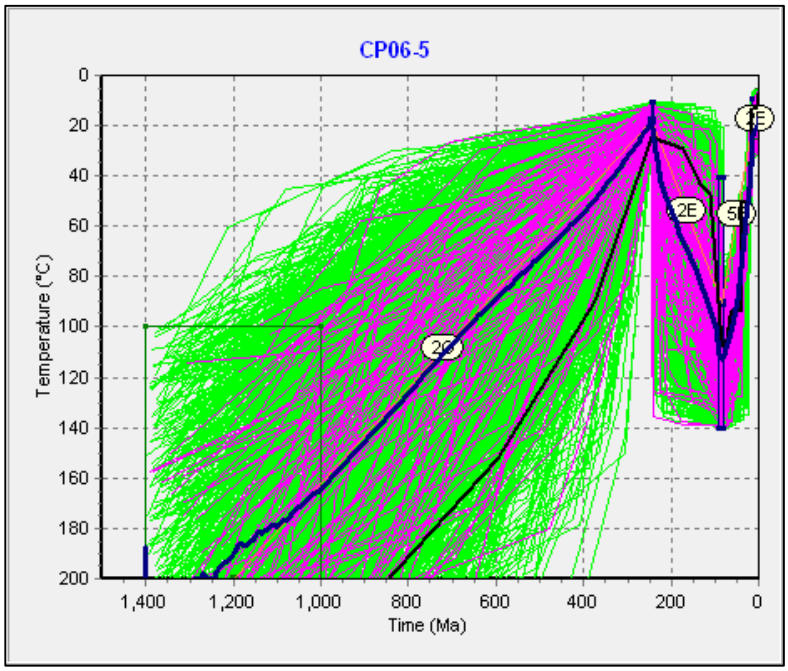

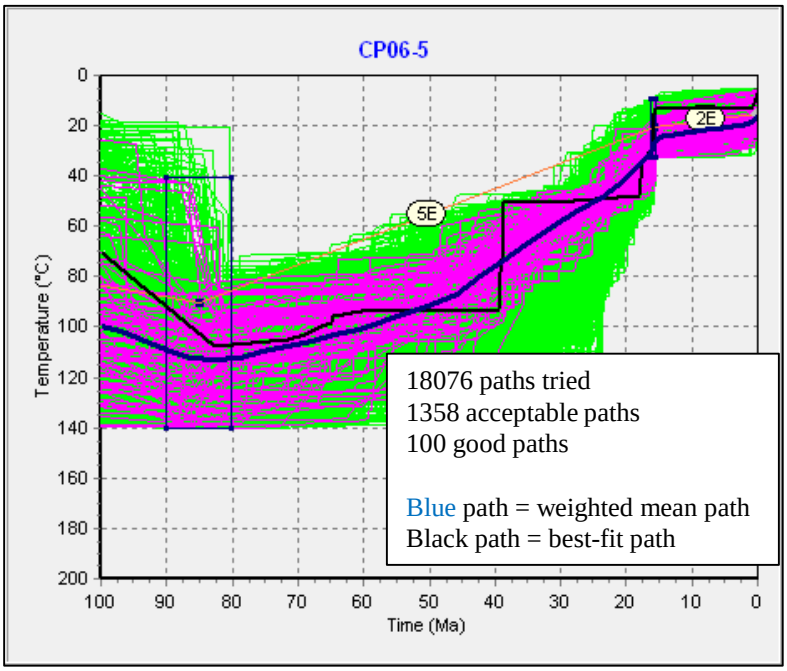

AHe Modeling Results

a1 corrected age: 32.0 ± 6.4 Ma
model age: 25.2 Ma
GOF: 0.28

a2 corrected age: 27.0 ± 5.4 Ma
model age: 27.0 Ma
GOF: 1.00

a3 corrected age: 30.0 ± 6.0 Ma
model age: 23.2 Ma
GOF: 0.26

a4 corrected age: 22.0 ± 4.4 Ma
model age: 20.6 Ma
GOF: 0.76

a5 corrected age: 19.0 ± 3.8 Ma
model age: 21.2 Ma
GOF: 0.58

a6 corrected age: 18.0 ± 3.6 Ma
model age: 22.6 Ma
GOF: 0.18

a8 corrected age: 37.0 ± 7.4 Ma
model age: 37.2
GOF: 0.98

Comparison of Corrected Ages to Model Ages

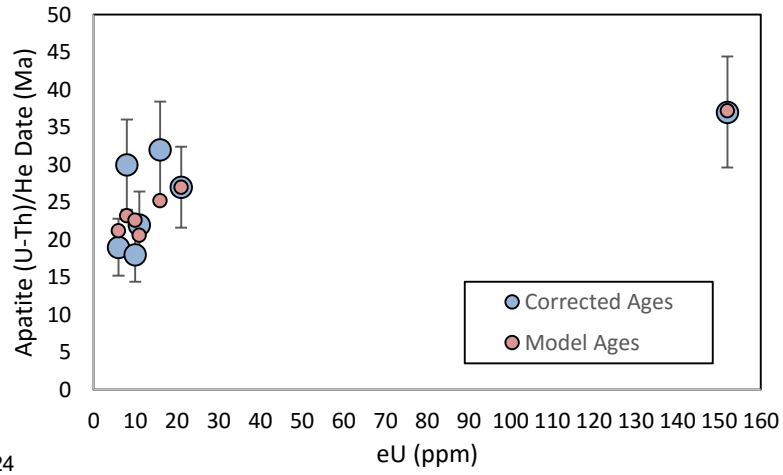

Figure DR-2.5C Holbrook Transect – Sample C (CP06-6)

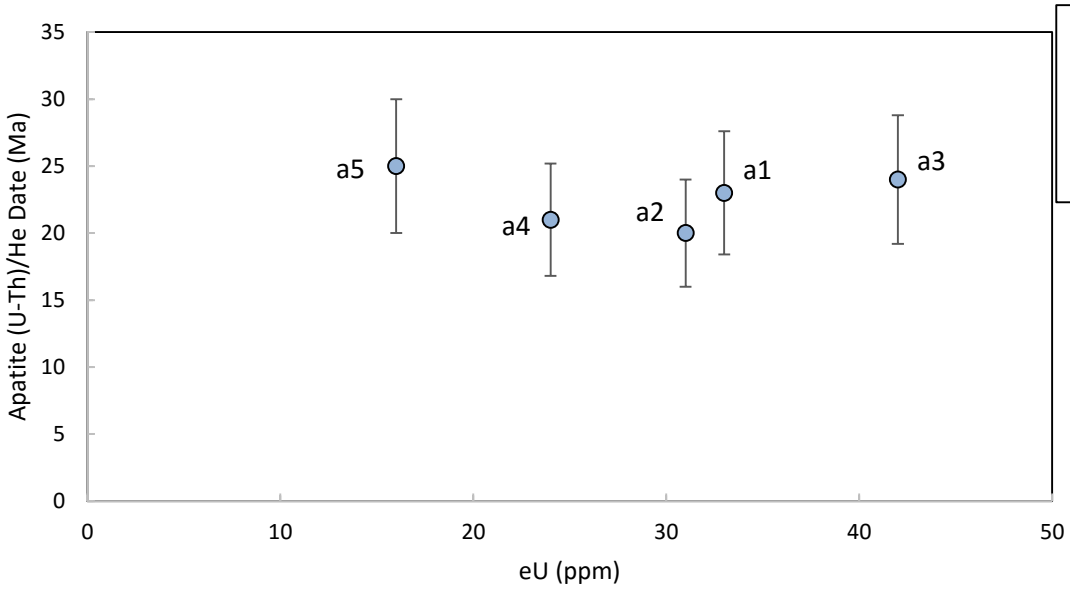

The thermal history model for sample CP06-6 includes all 5 available AHe dates. Uncertainties for each grain are set at 20% of the corrected grain age.

Thermal History Models

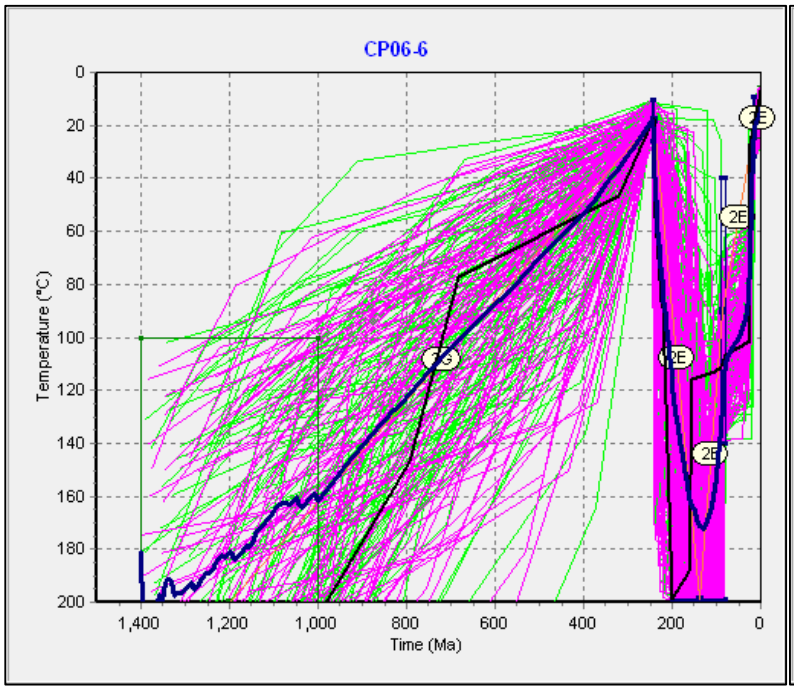

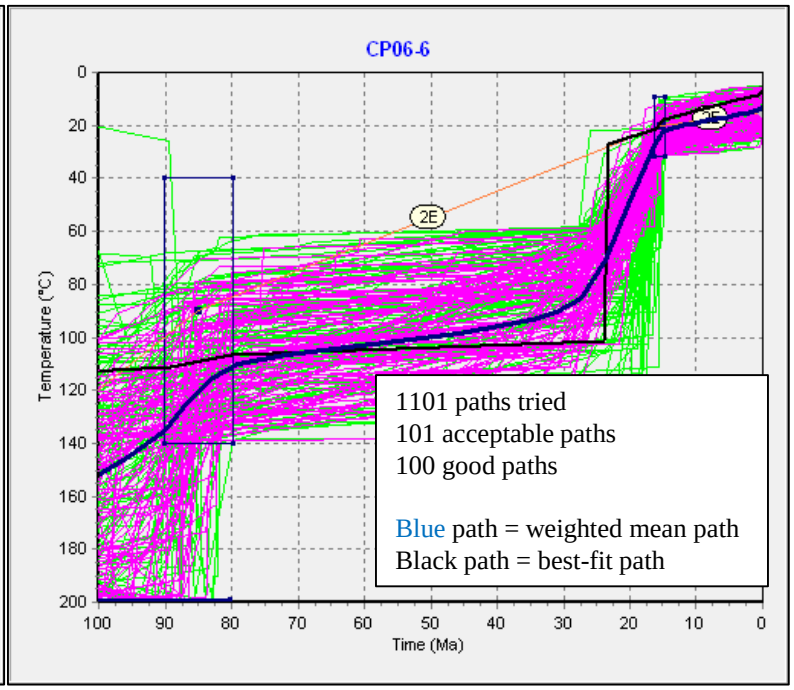

AHe Modeling Results

a1 corrected age: 23.0 ± 4.6 Ma
model age: 23.5 Ma
GOF: 0.92

a4 corrected age: 21.0 ± 4.2 Ma
model age: 23.3 Ma
GOF: 0.57

a2 corrected age: 20.0 ± 4.0 Ma
model age: 23.4 Ma
GOF: 0.40

a5 corrected age: 55.0 ± 5.0 Ma
model age: 23.0 Ma
GOF: 0.69

a3 corrected age: 24.0 ± 4.8 Ma
model age: 23.3 Ma
GOF: 0.88

Comparison of Corrected Ages to Model Ages

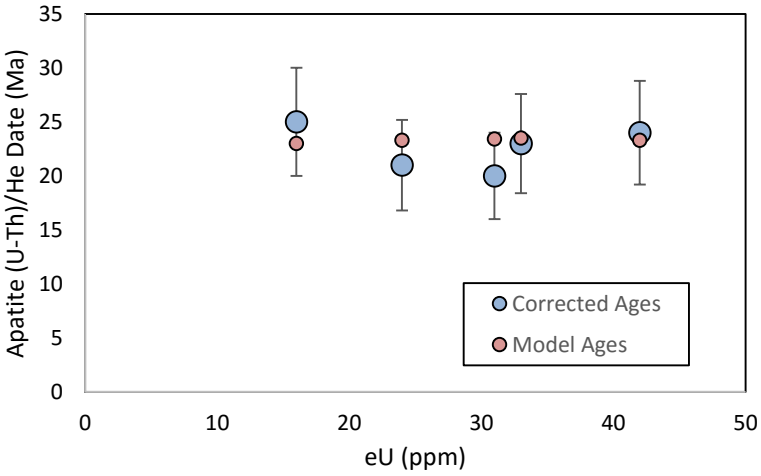

Figure DR-2.5D Holbrook Transect – Sample D (CP06-7)

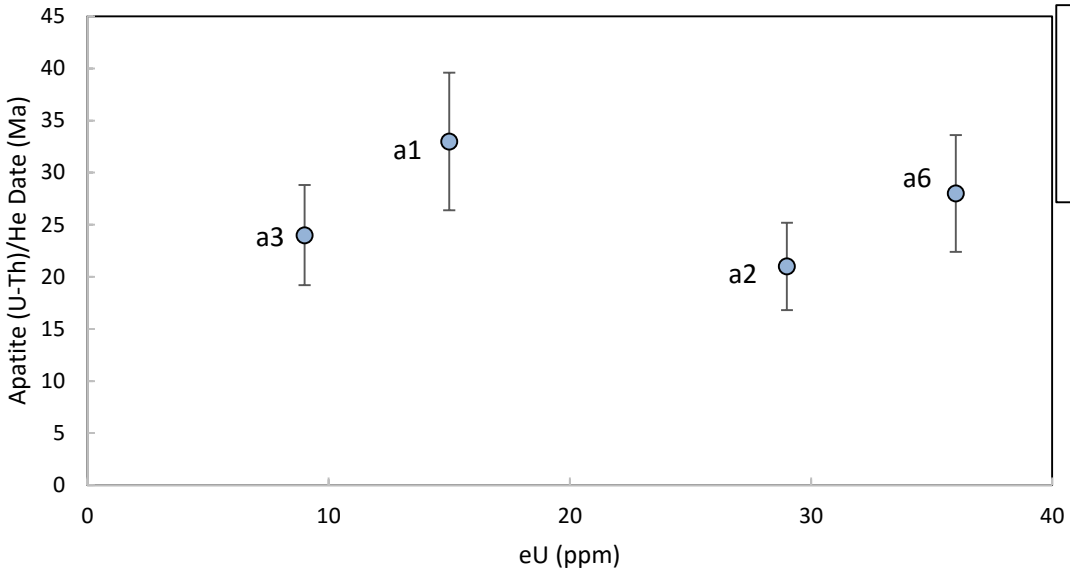

The thermal history model for sample CP06-7 includes all 4 available AHe dates. Uncertainties for each grain are set at 20% of the corrected grain age.

Thermal History Models

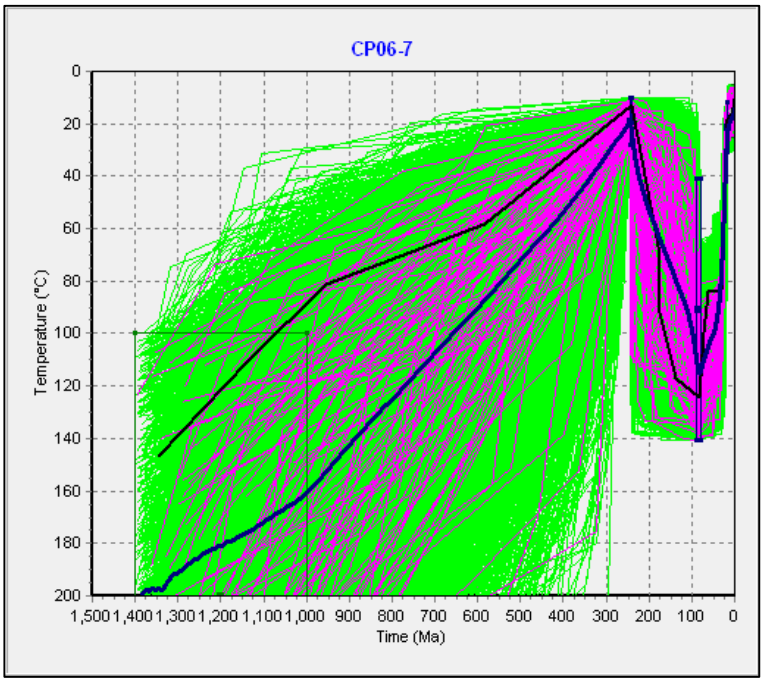

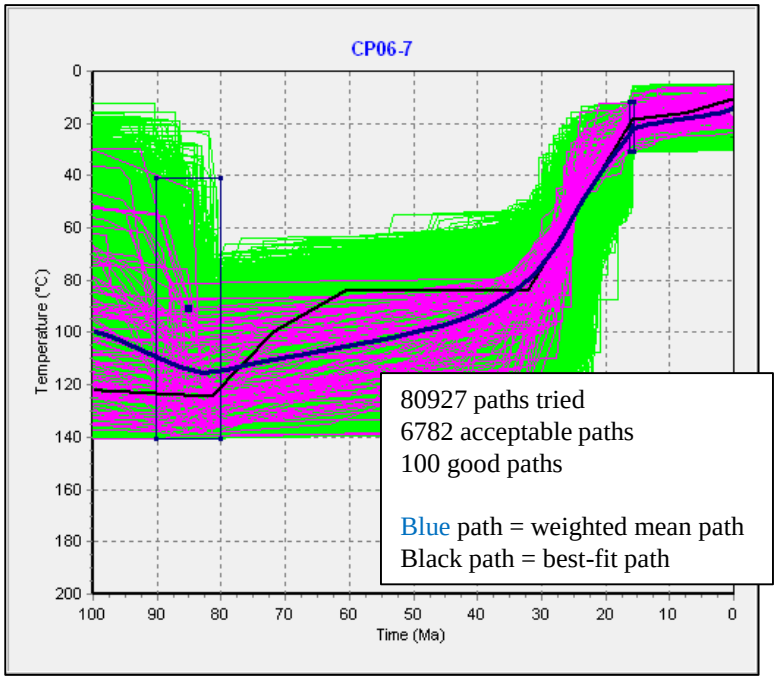

AHe Modeling Results

a1 corrected age: 33.0 ± 6.6 Ma
model age: 24.4 Ma
GOF: 0.20

a2 corrected age: 21.0 ± 4.2 Ma
model age: 25.9 Ma
GOF: 0.21

a3 corrected age: 24.0 ± 4.8 Ma
model age: 24.2 Ma
GOF: 0.96

a6 corrected age: 28.0 ± 5.6 Ma
model age: 26.1 Ma
GOF: 0.83

Comparison of Corrected Ages to Model Ages

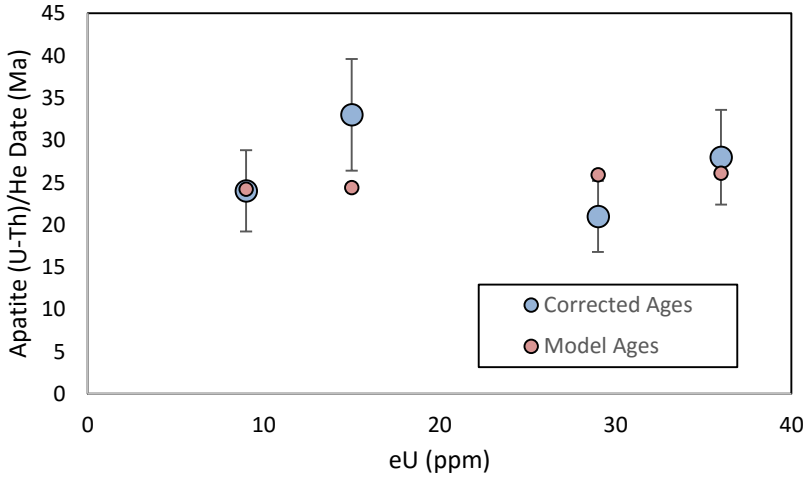

Figure DR-2.5E Cameron Transect – Sample E (CP05-7)

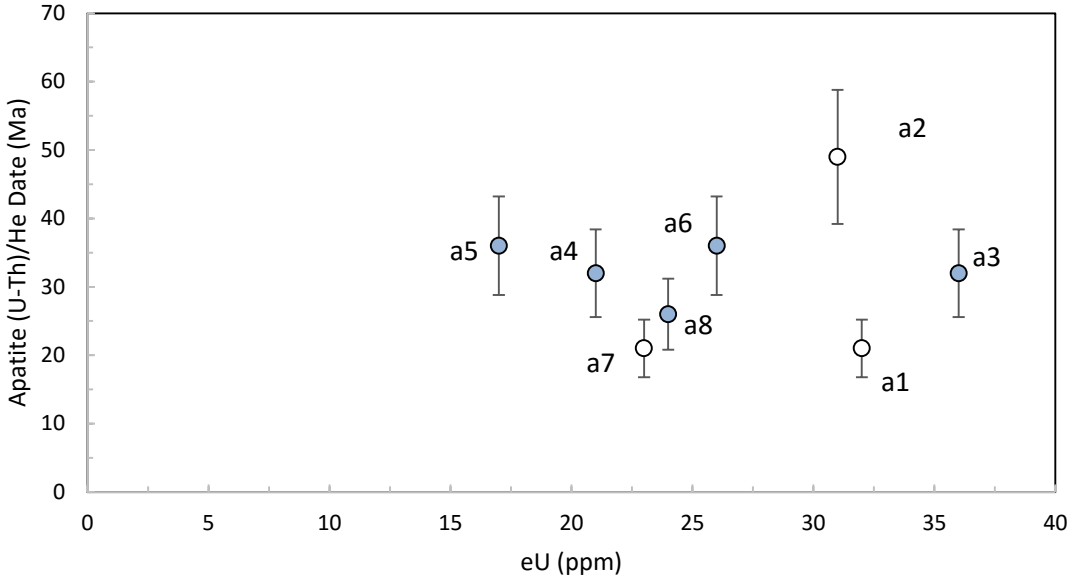

The thermal history model for sample CP05-7 includes 5 individual AHe dates, shown in blue. Grains not used in modeling are in white. a1, a2 and a7 were excluded because of difficulties in modeling these grains along with the rest. Uncertainties for each grain are set at 20% of the corrected grain age.

Thermal History Models

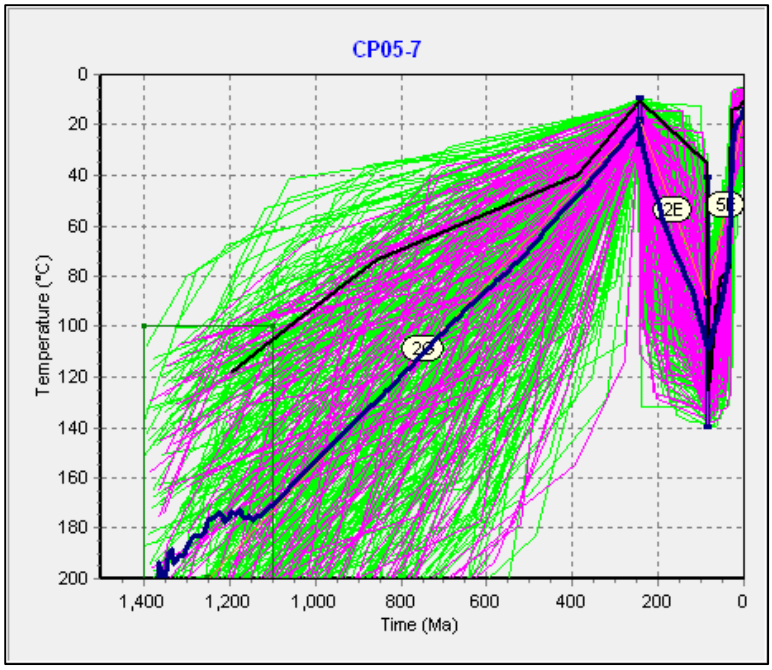

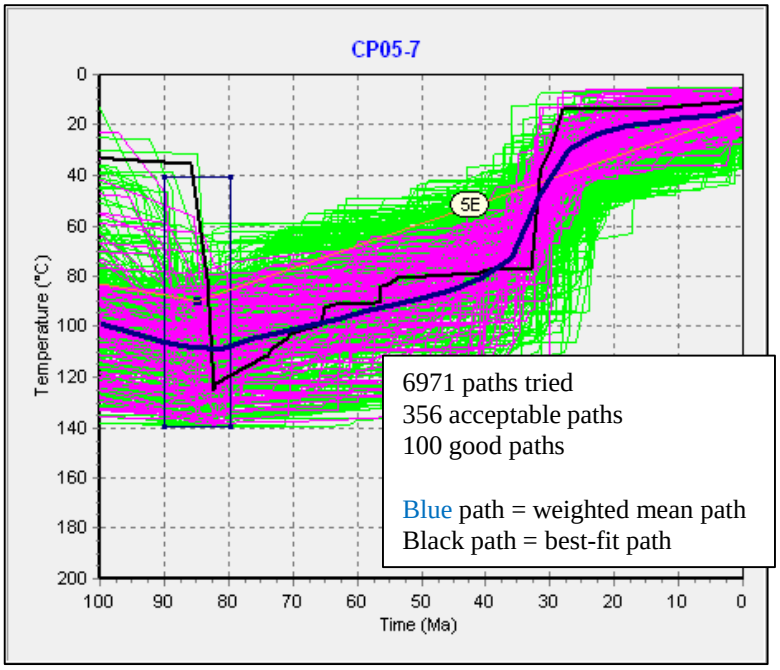

AHe Modeling Results

a3 corrected age: 32.0 ± 6.4 Ma
model age: 32.4 Ma
GOF: 0.94

a4 corrected age: 32.0 ± 6.4 Ma
model age: 32.2 Ma
GOF: 0.98

a5 corrected age: 36.0 ± 7.2 Ma
model age: 31.5 Ma
GOF: 0.53

a6 corrected age: 36.0 ± 7.2 Ma
model age: 31.9 Ma
GOF: 0.57

a8 corrected age: 26.0 ± 5.2 Ma
model age: 32.0 Ma
GOF: 0.24

Comparison of Corrected Ages to Model Ages

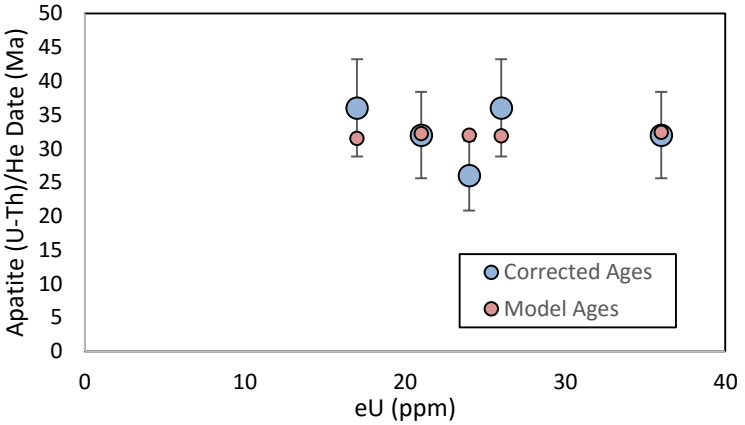

Figure DR-2.5F Cameron Transect – Sample F (CP05-3A)

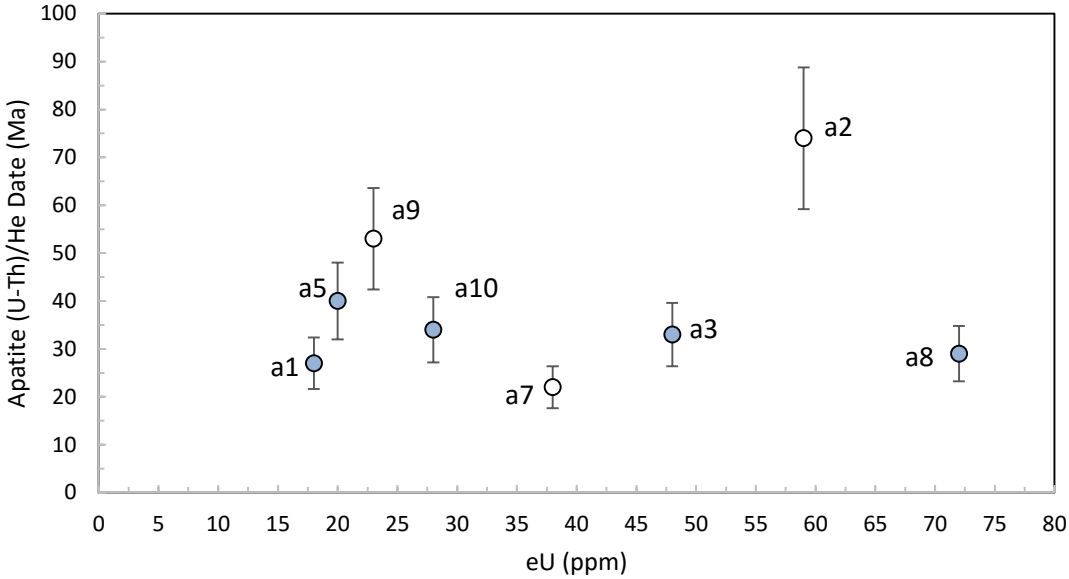

The thermal history model for sample CP05-3A includes 5 individual AHe dates, shown in blue. Grains not used in modeling are in white. a2, a7 and a9 were excluded because of difficulties in modeling these grains along with the rest. Uncertainties for each grain are set at 20% of the corrected grain age.

Thermal History Models

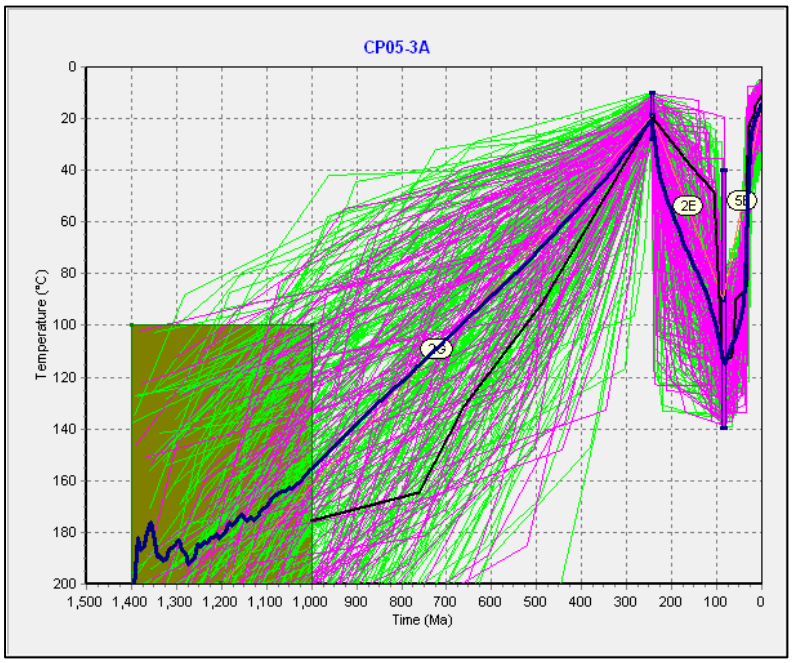

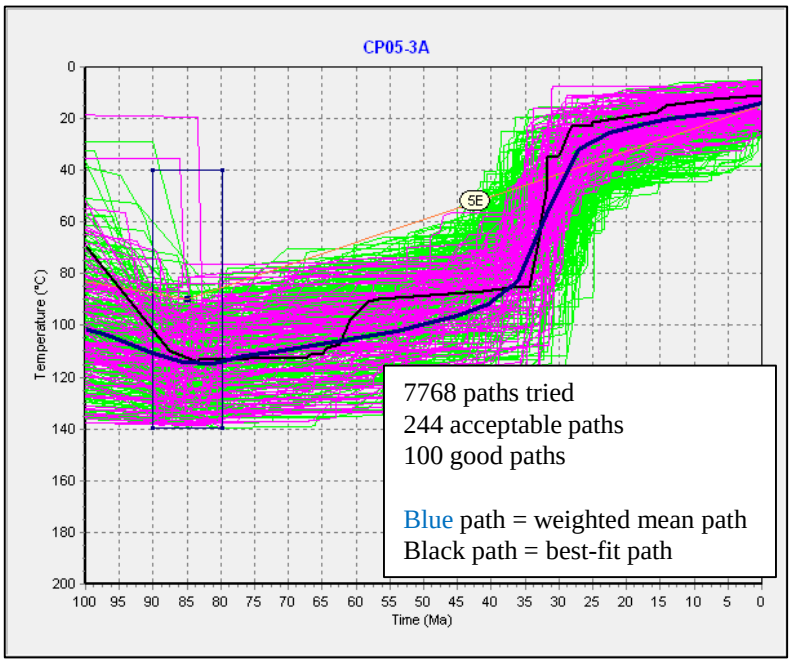

AHe Modeling Results

a1 corrected age: 27.0 ± 5.4 Ma
model age: 32.0 Ma
GOF: 0.35

a8 corrected age: 29.0 ± 5.8 Ma
model age: 33.1 Ma
GOF: 0.48

a3 corrected age: 33.0 ± 6.6 Ma
model age: 32.6 Ma
GOF: 0.96

a10 corrected age: 34.0 ± 6.8 Ma
model age: 32.2 Ma
GOF: 0.79

a5 corrected age: 40.0 ± 8.0 Ma
model age: 32.1 Ma
GOF: 0.33

Comparison of Corrected Ages to Model Ages

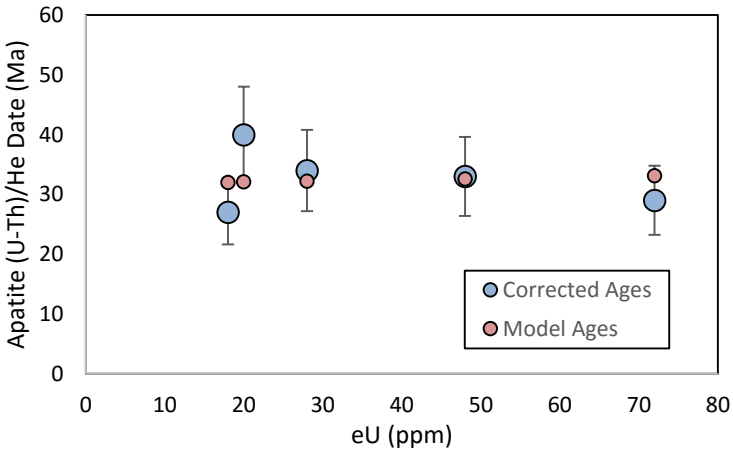

Figure DR-2.5G Cameron Transect – Sample G (CP05-2)

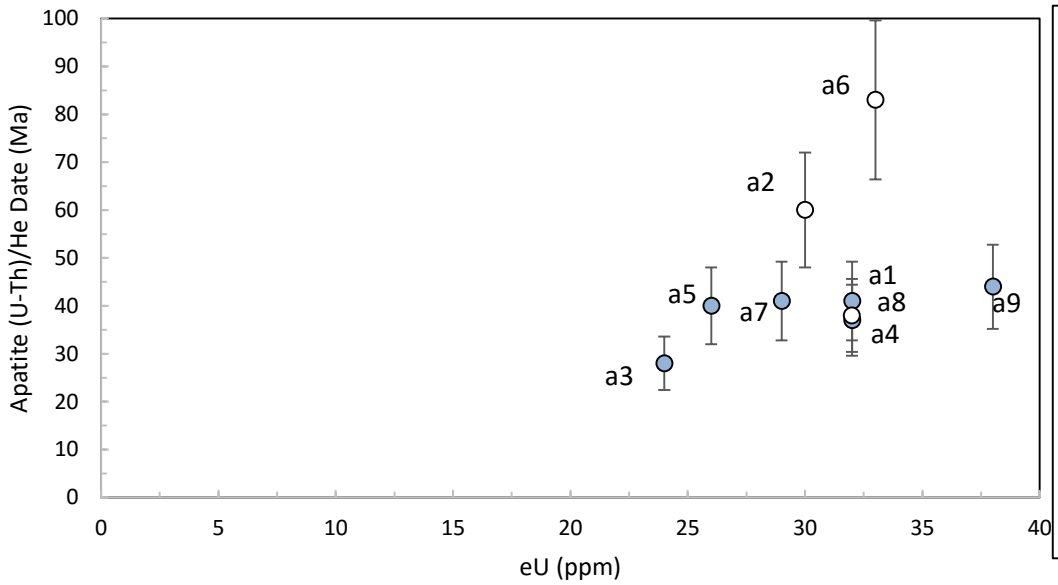

The thermal history model for sample CP05-2 includes 6 individual AHe dates, shown in blue. Grains not used in modeling are in white. Excluding a4 makes very little difference because it is nearly identical to a1 and a8, which were included. a2 and a6 were excluded because their apparently old age cannot be justified by higher eU, and they would not model with the rest of the grains. Uncertainties for each grain are set at 20% of the corrected grain age.

Thermal History Models

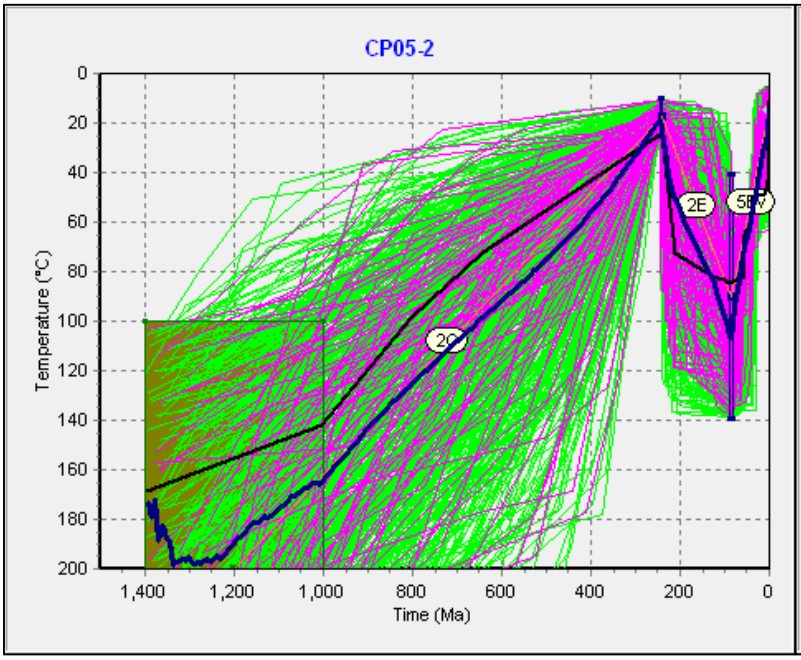

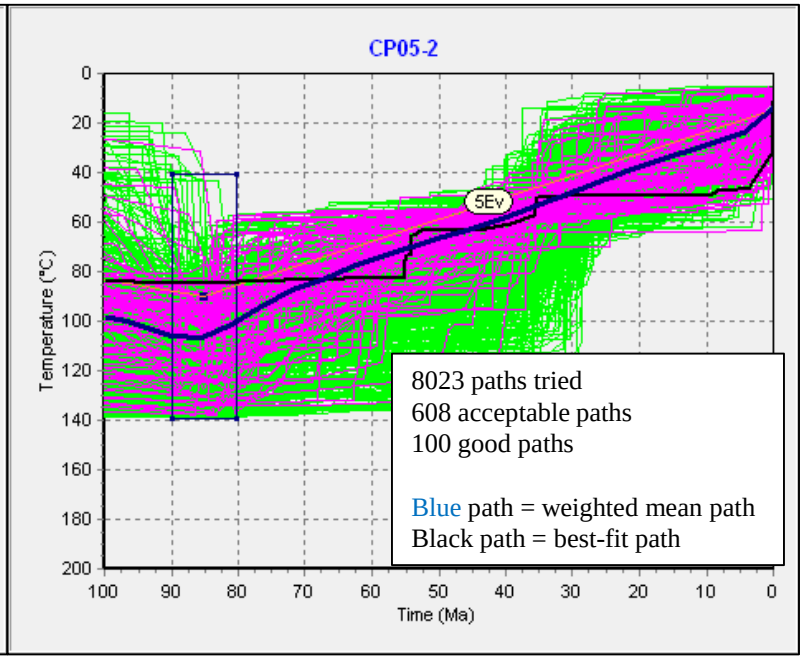

AHe Modeling Results

a1 corrected age: 41.0 ± 8.2 Ma
model age: 38.8 Ma
GOF: 0.79

a5 corrected age: 40.0 ± 8.0 Ma
model age: 35.3 Ma
GOF: 0.56

a3 corrected age: 28.0 ± 5.6 Ma
model age: 35.8 Ma
GOF: 0.17

a7 corrected age: 41.0 ± 8.2 Ma
model age: 40.7 Ma
GOF: 0.96

a4 corrected age: 37.0 ± 7.4 Ma
model age: 35.3 Ma
GOF: 0.82

a9 corrected age: 44.0 ± 8.8 Ma
model age: 44.2
GOF: 0.99

Comparison of Corrected Ages to Model Ages

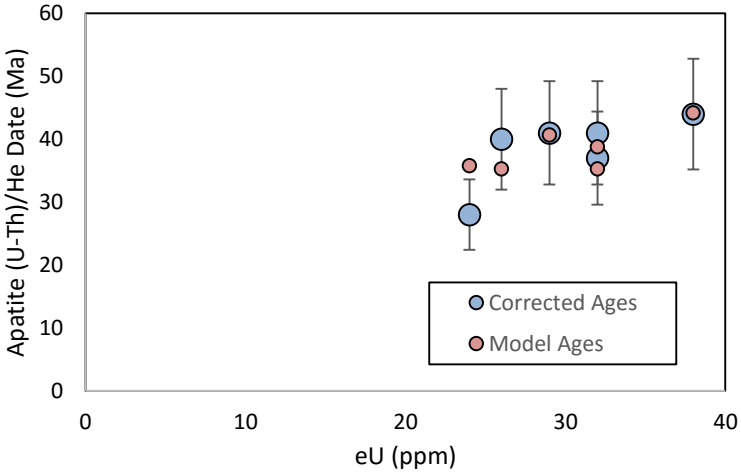

Figure DR-2.5H Holbrook Transect – Sample H (CP06-10)

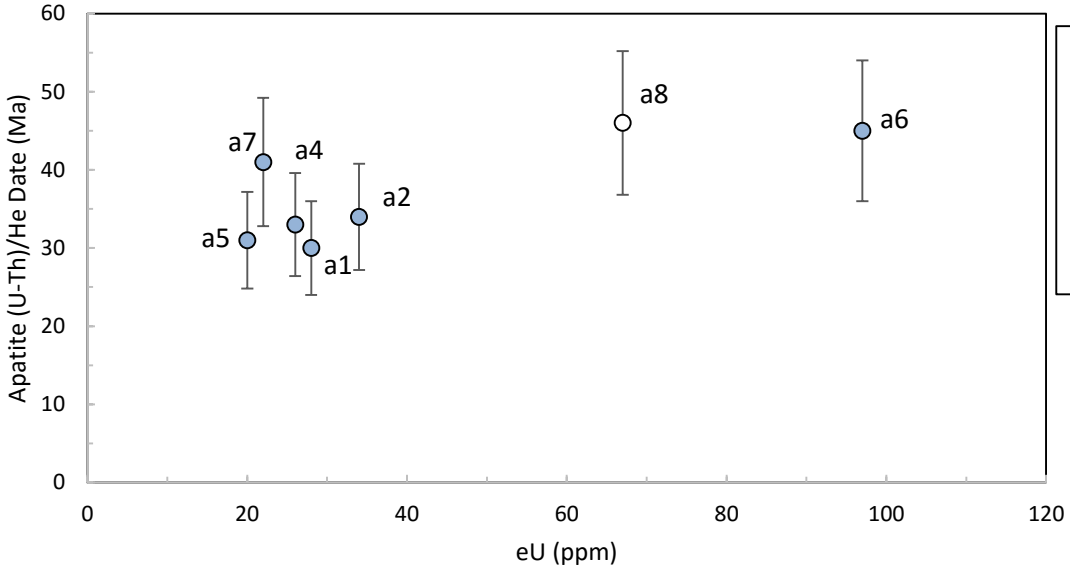

The thermal history model for sample CP06-10 includes 6 out of the 7 available AHe dates, shown in blue. The single date not used in modeling is in white. Uncertainties for each grain are set at 20% of the corrected grain age.

Thermal History Models

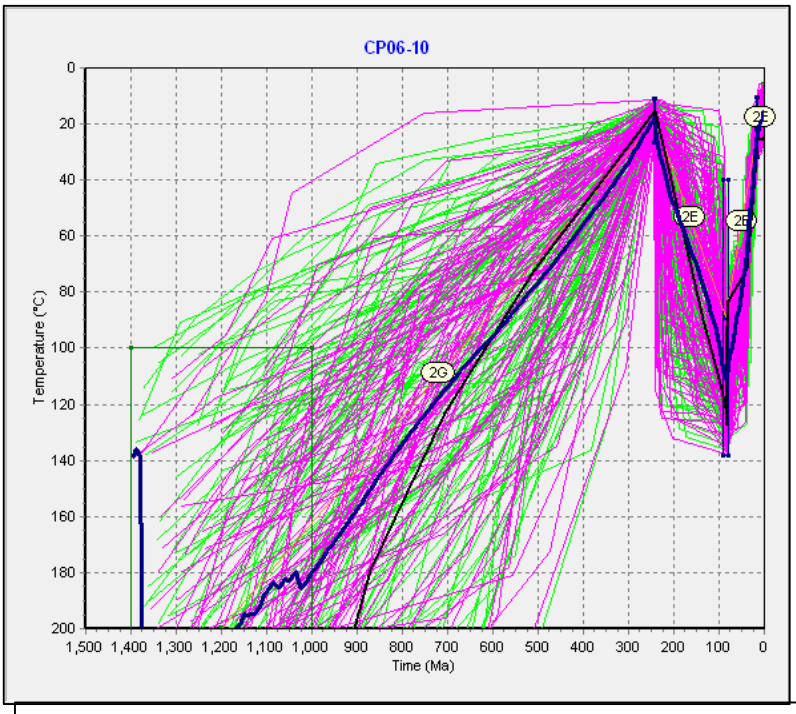

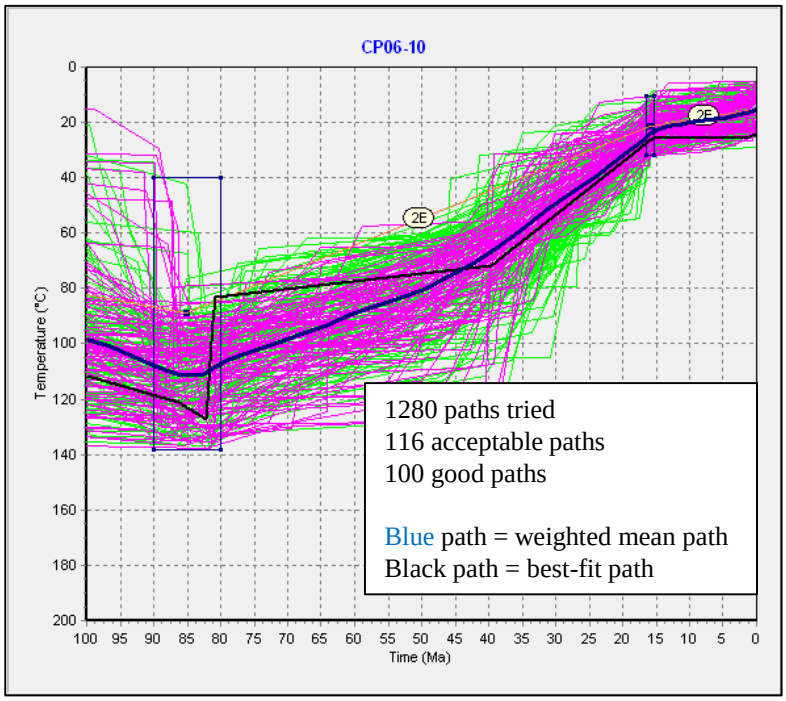

AHe Modeling Results

a1 corrected age: 30.0 ± 6.0 Ma
model age: 32.2 Ma
GOF: 0.92

a2 corrected age: 34.0 ± 6.8 Ma
model age: 33.7 Ma
GOF: 0.88

a4 corrected age: 33.0 ± 6.5 Ma
model age: 33.2 Ma
GOF: 0.98

a5 corrected age: 31.0 ± 6.2 Ma
model age: 30.6 Ma
GOF: 0.97

a6 corrected age: 45.0 ± 9.0 Ma
model age: 34.8 Ma
GOF: 0.26

a7 corrected age: 41.0 ± 8.2 Ma
model age: 31.1
GOF: 0.28

Comparison of Corrected Ages to Model Ages

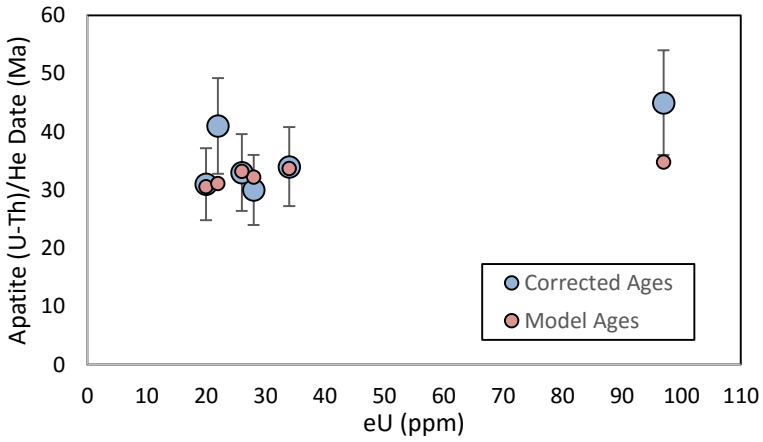

Figure DR-2.5I Winslow Transect – Sample I (CP06-20)

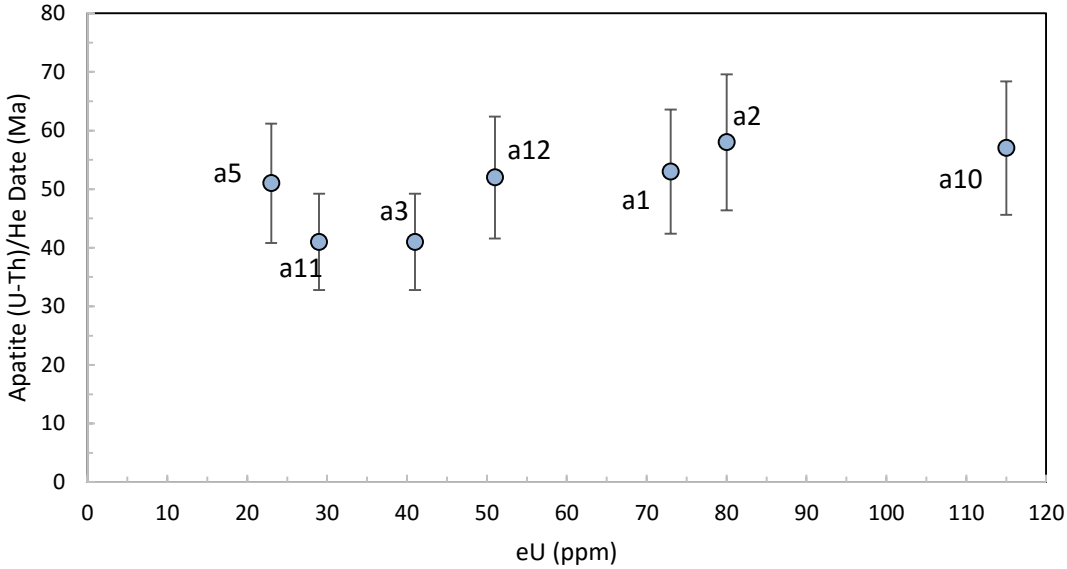

The thermal history model for sample CP06-20 includes all 7 available AHe dates, shown in blue. Uncertainties for each grain are set at 20% of the corrected grain age.

Thermal History Models

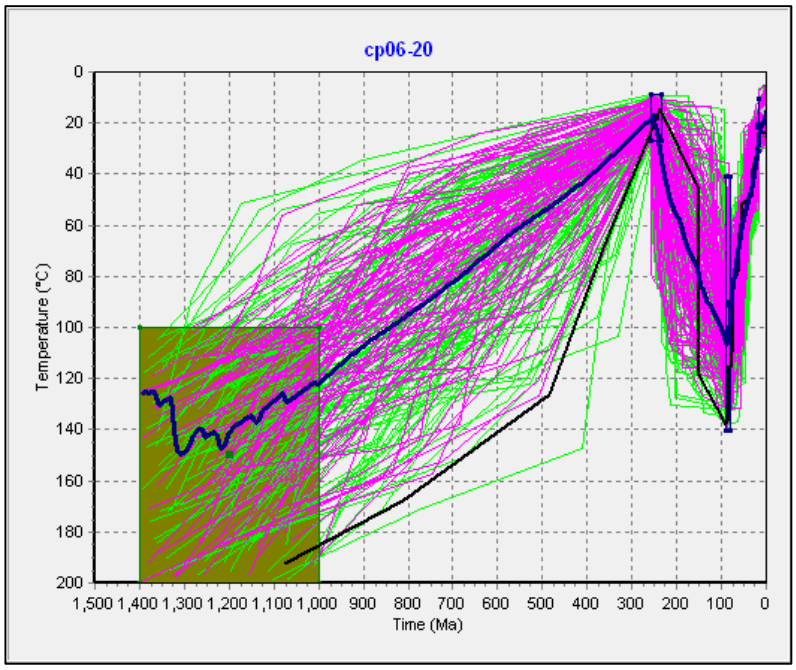

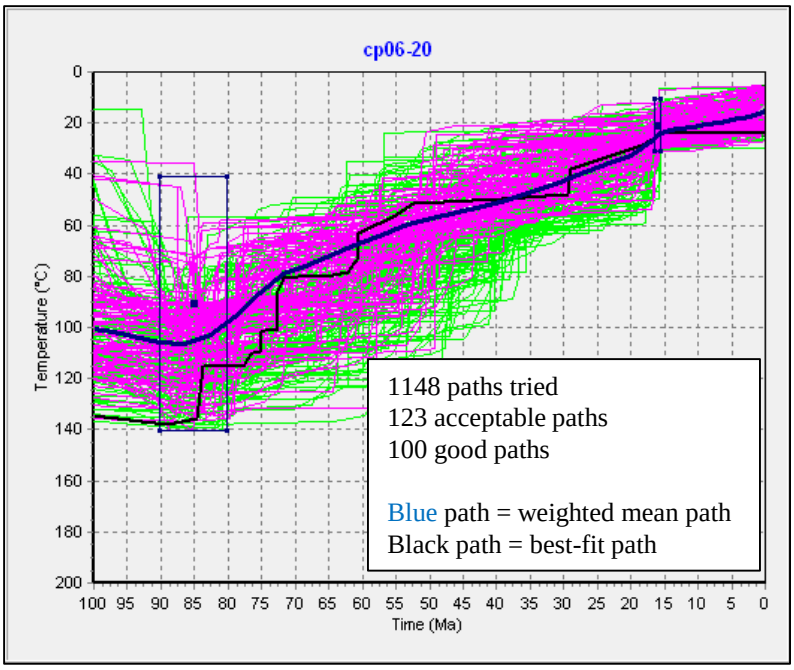

AHe Modeling Results

a1 corrected age: 53.0 ± 10.6 Ma
model age: 53.0 Ma
GOF: 0.96

a2 corrected age: 58.0 ± 11.6 Ma
model age: 53.7 Ma
GOF: 0.71

a3 corrected age: 41.0 ± 8.2 Ma
model age: 46.3 Ma
GOF: 0.52

a5 corrected age: 41.0 ± 10.2 Ma
model age: 48.6 Ma
GOF: 0.81

a10 corrected age: 57.0 ± 11.4 Ma
model age: 57.6 Ma
GOF: 0.97

a11 corrected age: 41.0 ± 8.2 Ma
model age: 50.0 Ma
GOF: 0.27

a12 corrected age: 52.0 ± 10.4 Ma
model age: 51.2 Ma
GOF: 0.94

Comparison of Corrected Ages to Model Ages

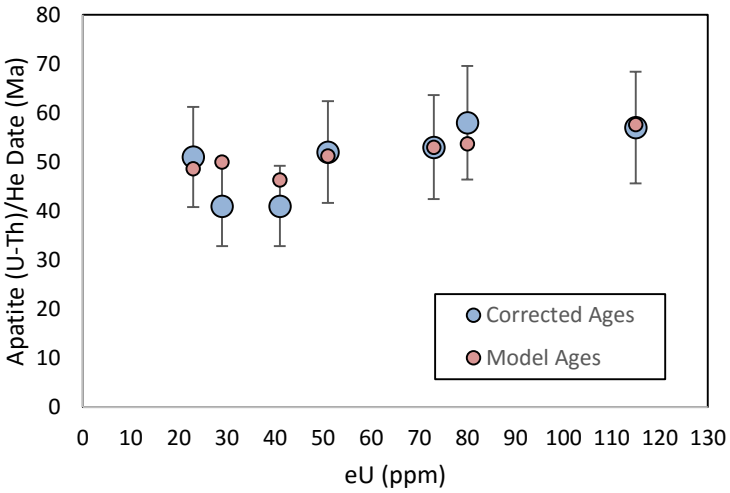

Figure DR-2.5J Cameron Transect – Sample J (CP05-1)

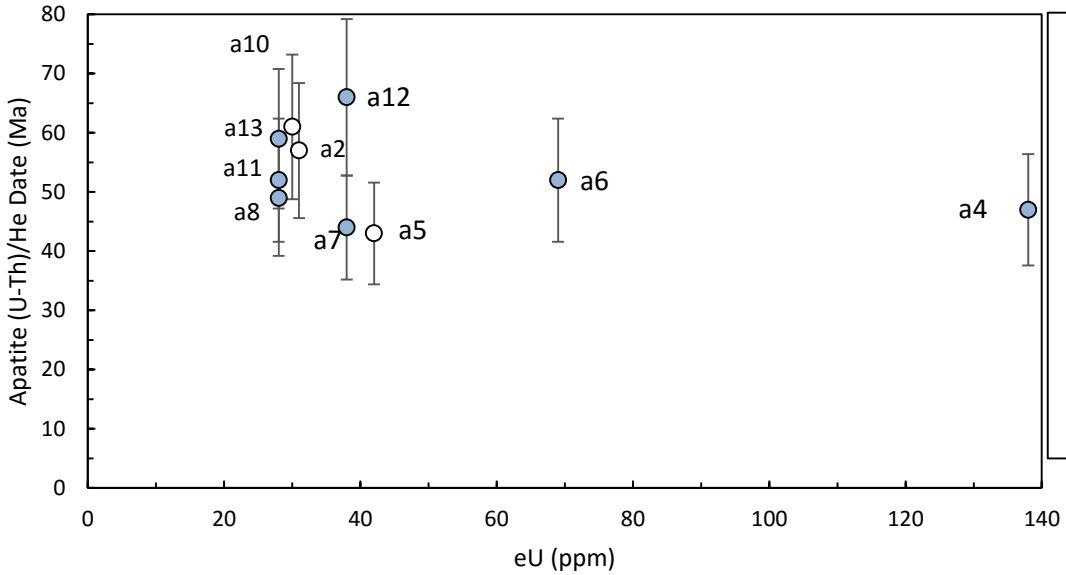

The thermal history model for sample CP05-1 includes 7 individual AHe dates, shown in blue. Grains not used in modeling are in white. Excluding these three grains makes very little difference in the resulting thermal history model because they are very similar in age and eU to nearby grains. Uncertainties for each grain are set at 20% of the corrected grain age.

Thermal History Models

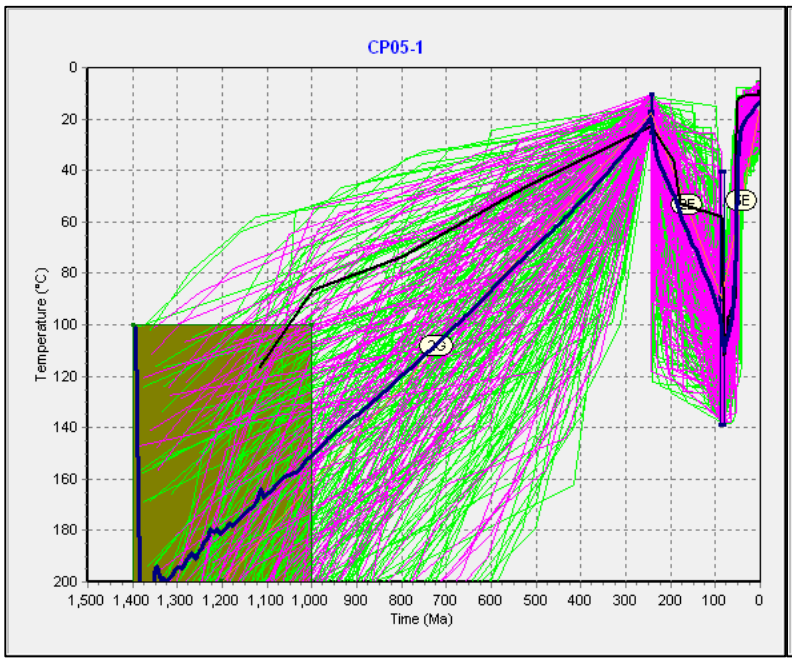

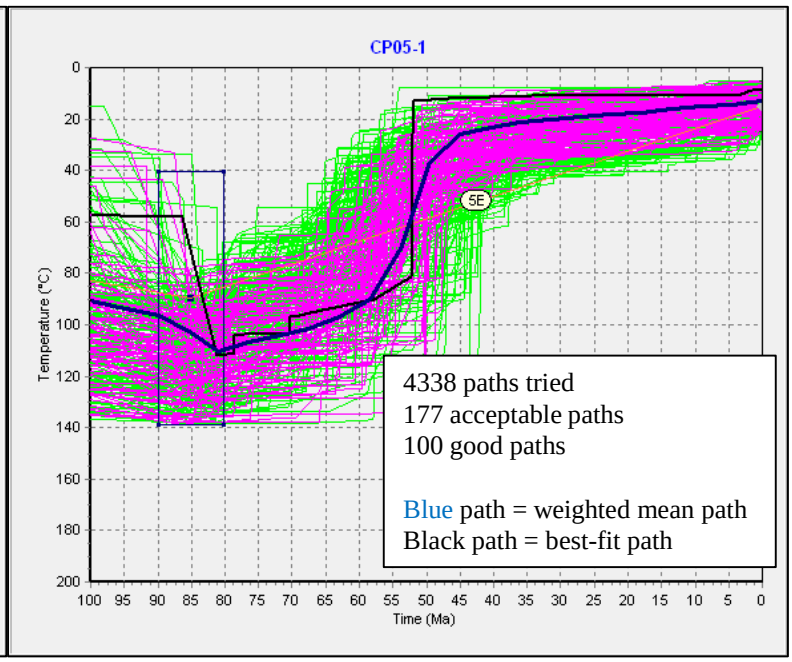

AHe Modeling Results

a4 corrected age: 47.0 ± 9.4 Ma
model age: 52.3 Ma
GOF: 0.58

a11 corrected age: 52.0 ± 10.4 Ma
model age: 51.6 Ma
GOF: 0.97

a6 corrected age: 52.0 ± 10.4 Ma
model age: 52.0 Ma
GOF: 1.00

a12 corrected age: 66.0 ± 13.2 Ma
model age: 51.8 Ma
GOF: 0.28

a7 corrected age: 44.0 ± 8.8 Ma
model age: 51.7 Ma
GOF: 0.38

a13 corrected age: 59.0 ± 11.8 Ma
model age: 50.8
GOF: 0.48

a8 corrected age: 49.0 ± 9.8 Ma
model age: 51.4 Ma
GOF: 0.81

Comparison of Corrected Ages to Model Ages

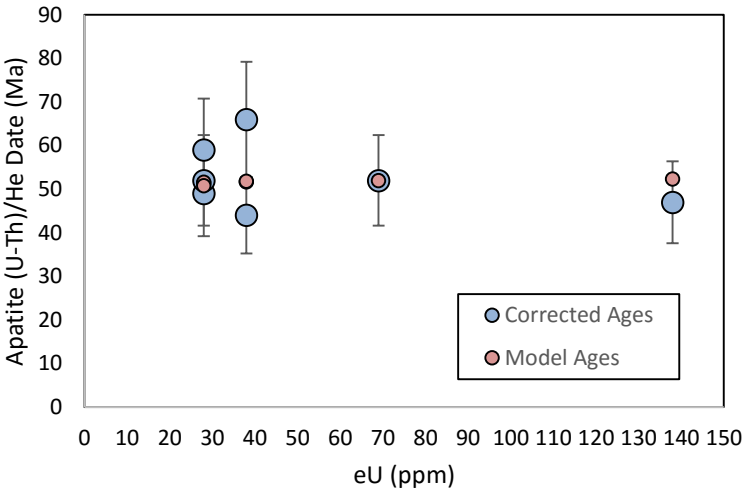

Figure DR-2.5K Holbrook Transect – Sample K (CP06-12)

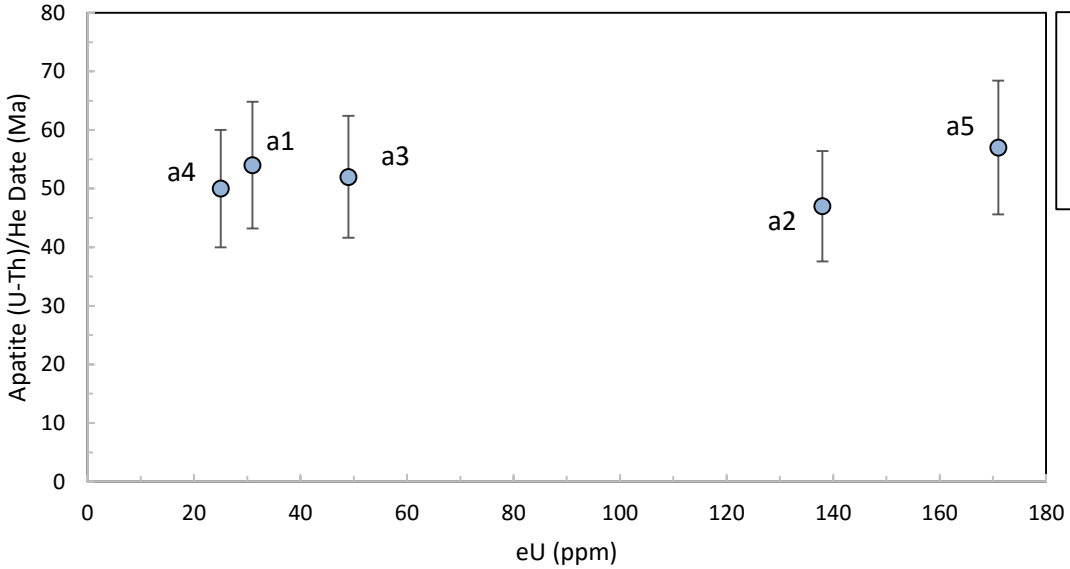

The thermal history model for sample CP06-12 includes all 5 available AHe dates, shown in blue. Uncertainties for each grain are set at 20% of the corrected grain age.

Thermal History Models

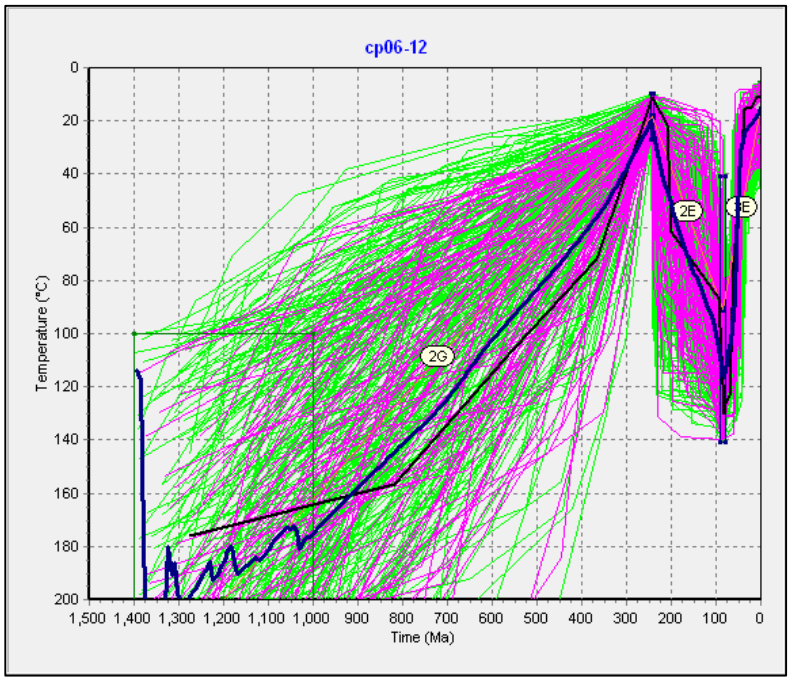

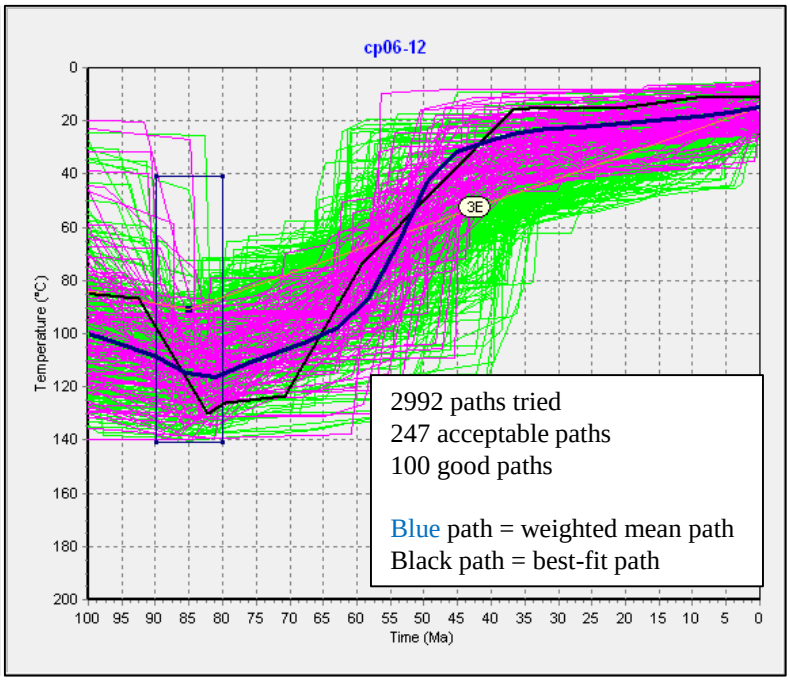

AHe Modeling Results

a1 corrected age: 54.0 ± 10.8 Ma
model age: 50.9 Ma
GOF: 0.78

a2 corrected age: 47.0 ± 9.4 Ma
model age: 55.4 Ma
GOF: 0.37

a3 corrected age: 52.0 ± 10.4 Ma
model age: 52.0 Ma
GOF: 1.00

a4 corrected age: 50.0 ± 10.0 Ma
model age: 50.2 Ma
GOF: 0.99

a5 corrected age: 57.0 ± 11.4 Ma
model age: 56.8 Ma
GOF: 0.98

Comparison of Corrected Ages to Model Ages

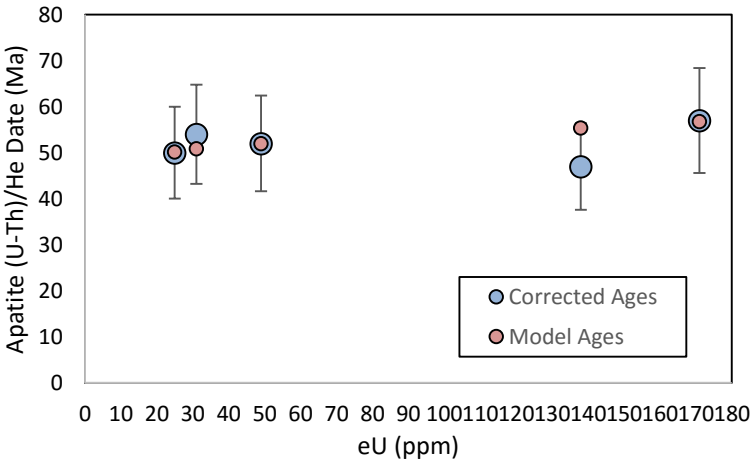

Figure DR-2.5L Winslow Transect – Sample L (CP06-19)

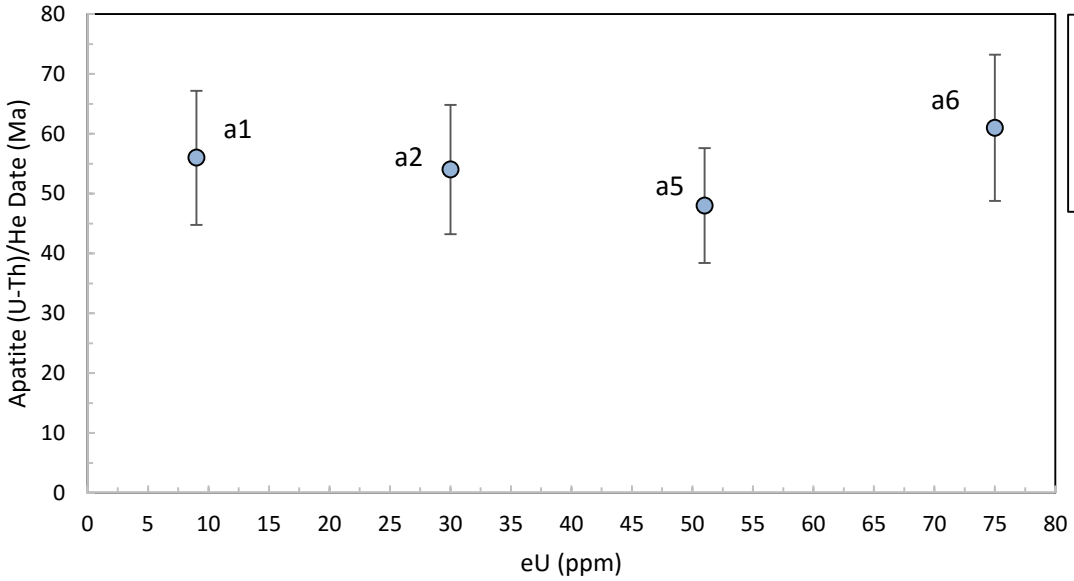

The thermal history model for sample CP06-19 includes all 4 available AHe dates, shown in blue. Uncertainties for each grain are set at 20% of the corrected grain age.

Thermal History Models

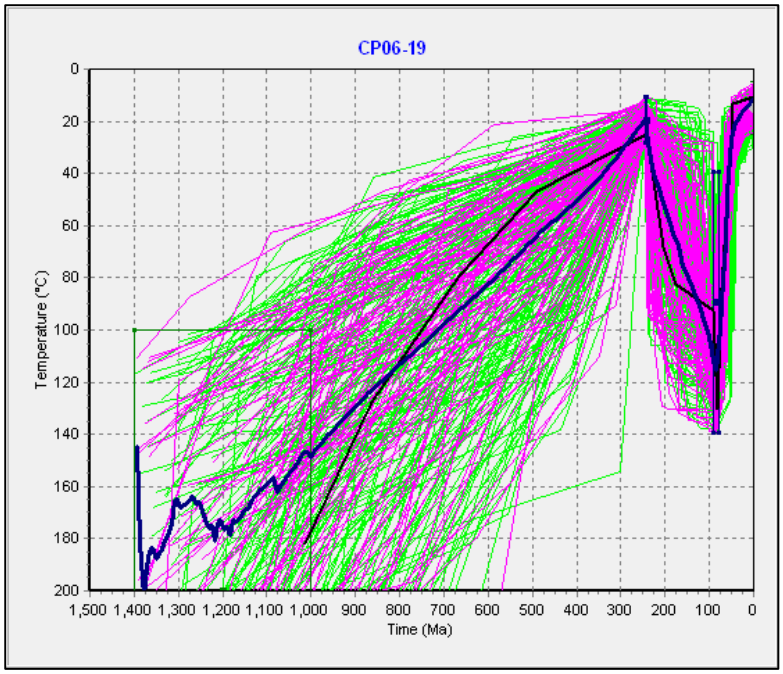

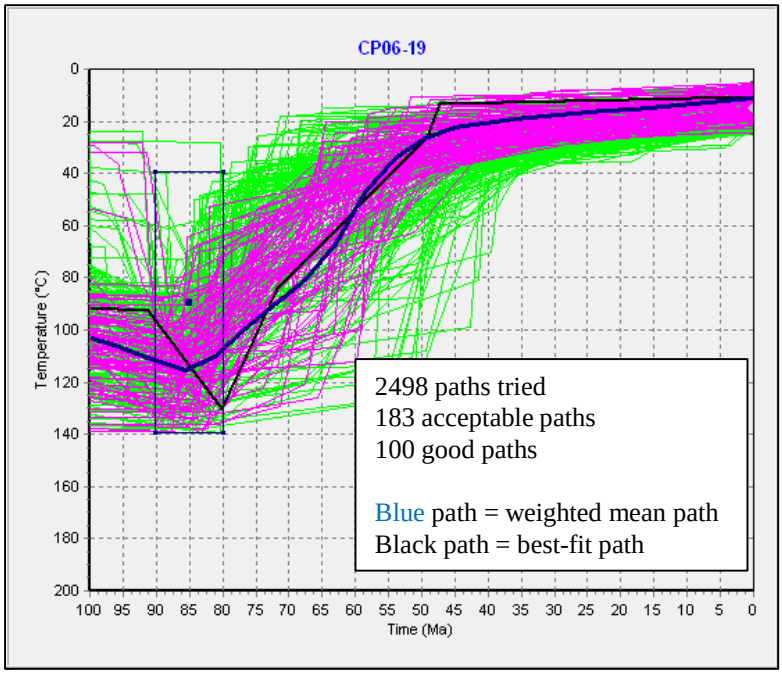

AHe Modeling Results

a1 corrected age: 56.0 ± 11.1 Ma
model age: 53.0Ma
GOF: 0.77

a2 corrected age: 54.0 ± 10.8 Ma
model age: 56.3 Ma
GOF: 0.98

a5 corrected age: 48.0 ± 9.6 Ma
model age: 57.8 Ma
GOF: 0.67

a6 corrected age: 61.0 ± 12.2
model age: 59.6 Ma
GOF: 0.88

Comparison of Corrected Ages to Model Ages

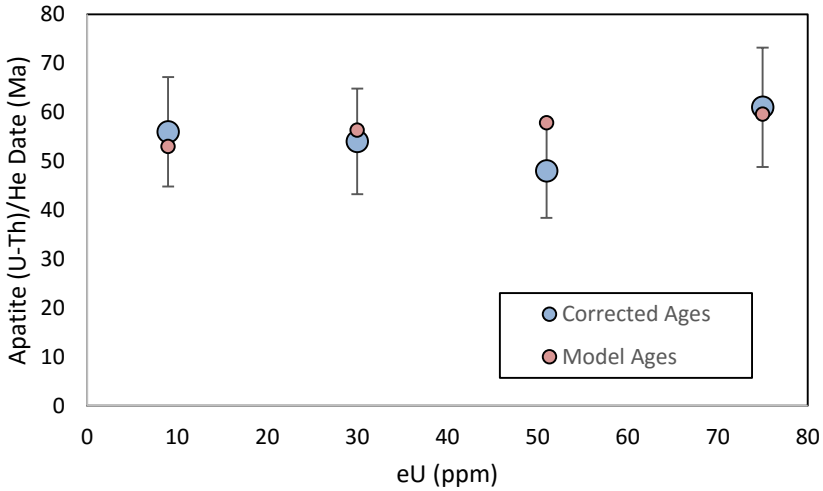

Figure DR-2.5M Holbrook Transect – Sample M (CP06-17)

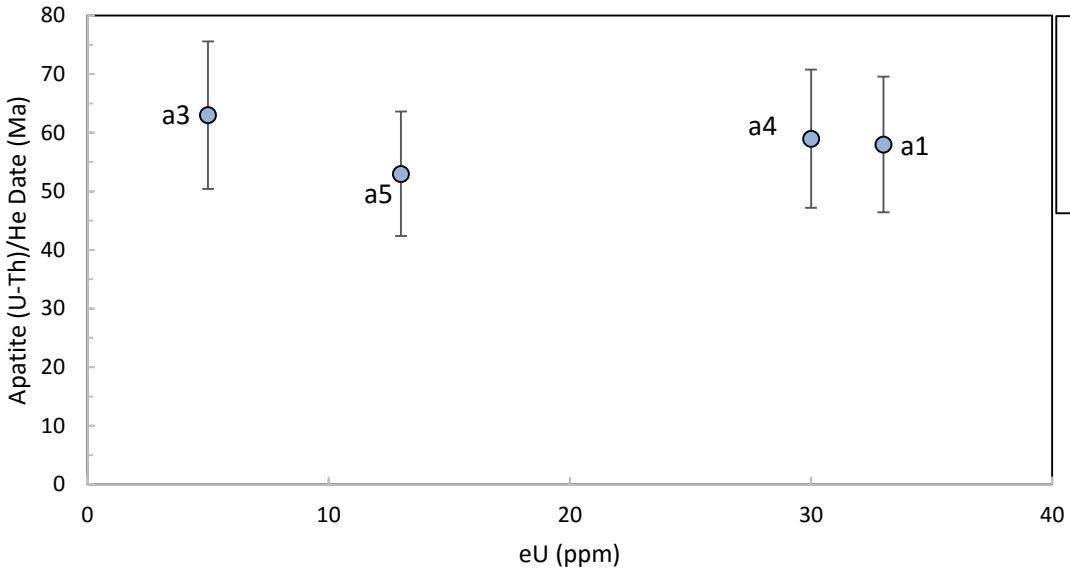

The thermal history model for sample CP06-17 includes all 4 available AHe dates, shown in blue. Uncertainties for each grain are set at 20% of the corrected grain age.

Thermal History Models

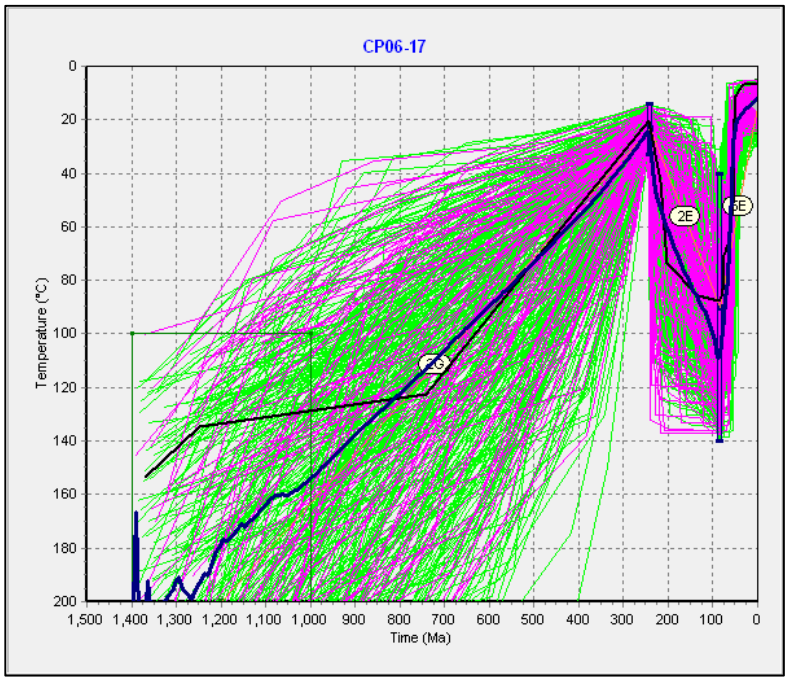

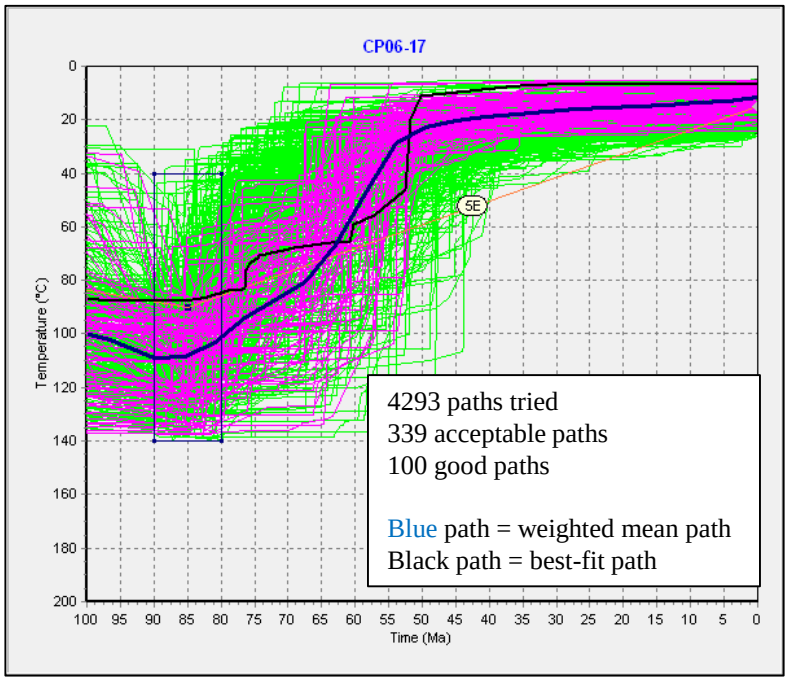

AHe Modeling Results

a1 corrected age: 58.0 ± 11.6 Ma
model age: 58.5 Ma
GOF: 0.97

a3 corrected age: 63.0 ± 12.6 Ma
model age: 52.5 Ma
GOF: 0.41

a4 corrected age: 59.0 ± 11.8 Ma
model age: 56.7 Ma
GOF: 0.85

a5 corrected age: 53.0 ± 10.6 Ma
model age: 55.3 Ma
GOF: 0.82

Comparison of Corrected Ages to Model Ages

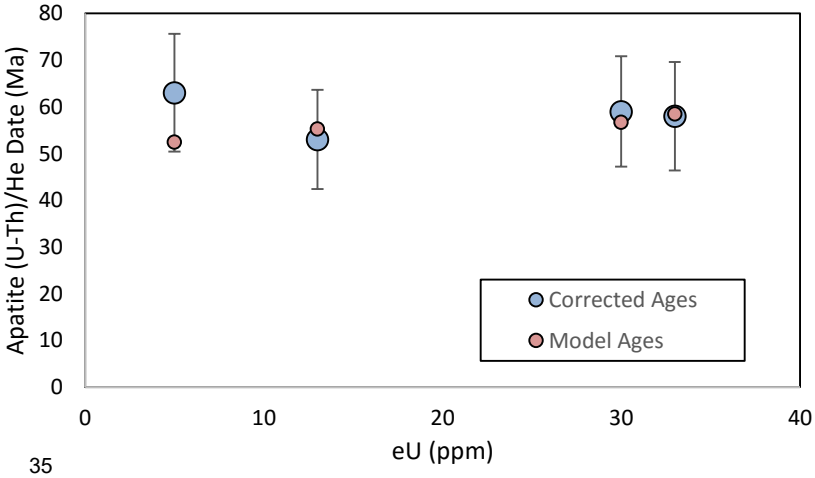

Figure DR-2.5N Cameron Transect – Sample N (CP06-29F)

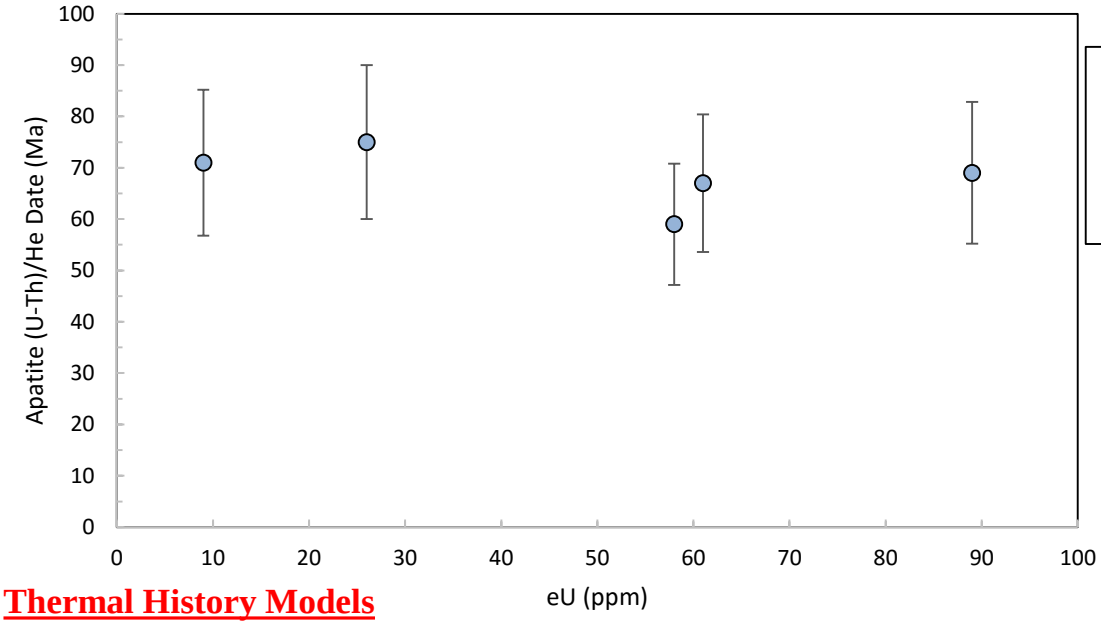

The thermal history model for sample CP06-29F includes all 5 individual AHe dates, shown in blue. Uncertainties for each grain are set at 20% of the corrected grain age.

Thermal History Models

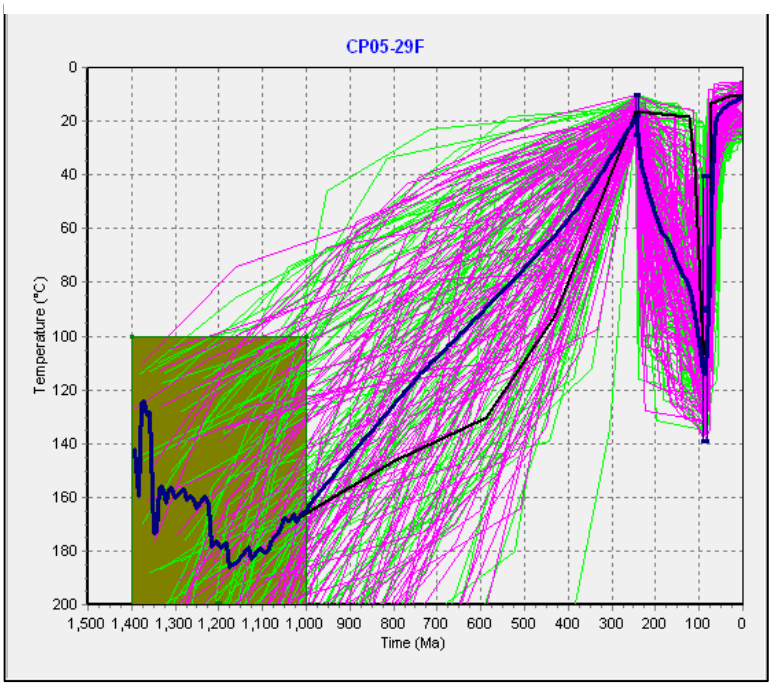

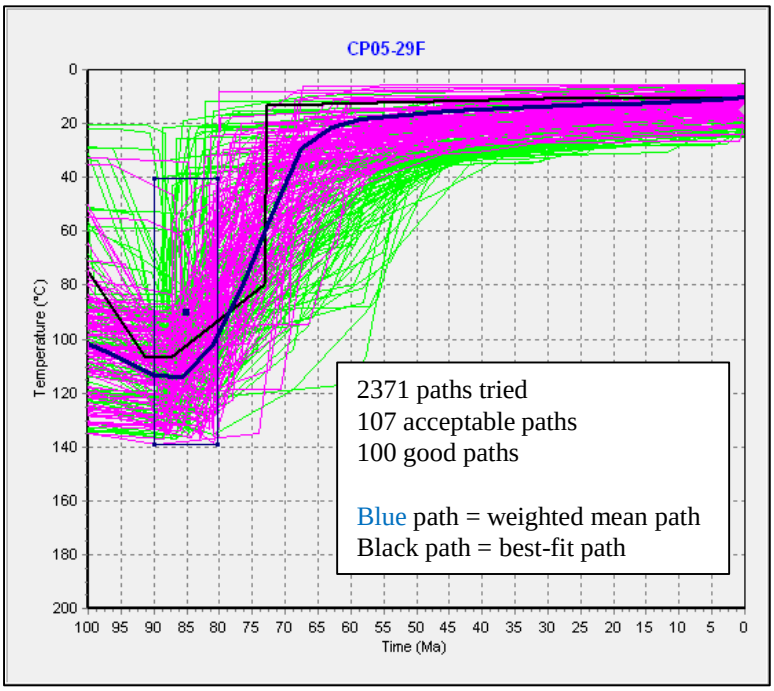

AHe Modeling Results

a2 corrected age: 73.0 ± 14.6 Ma
model age: 70.4 Ma
GOF: 0.84

a5 corrected age: 64.0 ± 12.8 Ma
model age: 72.7 Ma
GOF: 0.48

a3 corrected age: 74.0 ± 14.8 Ma
model age: 69.1 Ma
GOF: 0.72

a6 corrected age: 78.0 ± 15.6 Ma
model age: 72.1 Ma
GOF: 0.73

a4 corrected age: 67.0 ± 13.4 Ma
model age: 72.7 Ma
GOF: 0.67

Comparison of Corrected Ages to Model Ages

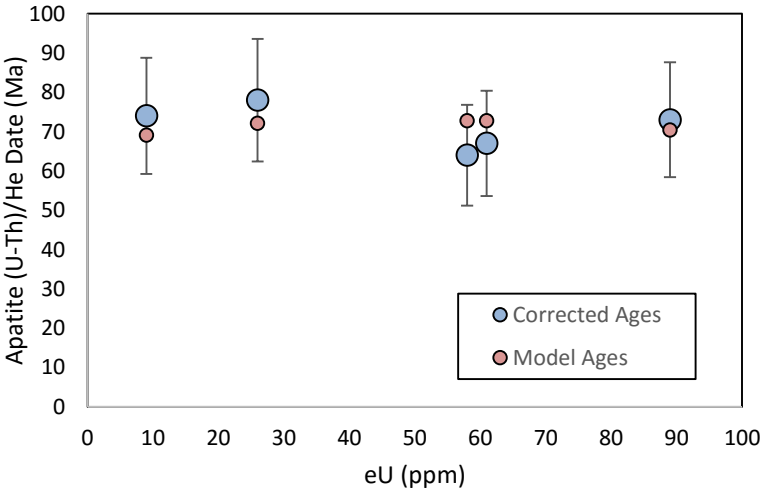

Figure DR-2.6. Comparison of HeFTy models with and without Rim Gravel constraint

With Rim Gravel Constraint

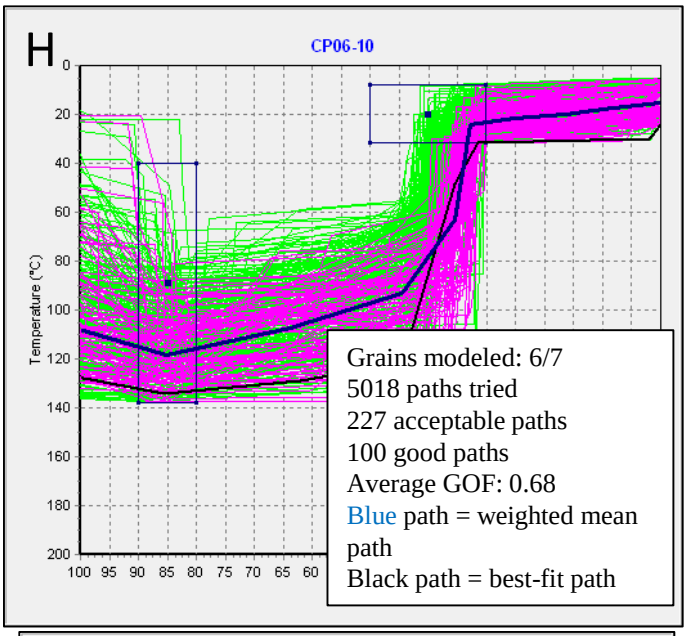

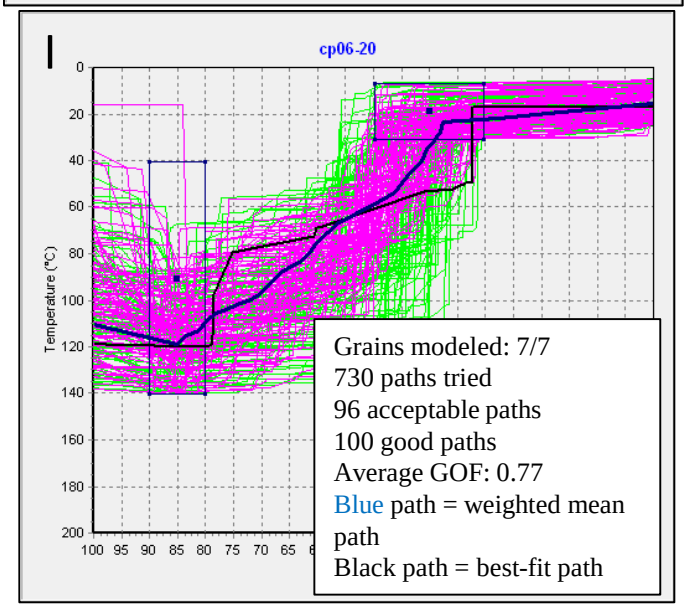

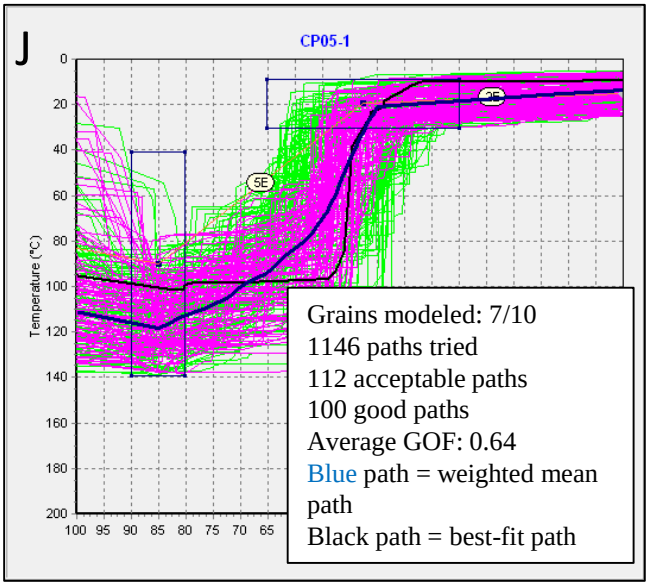

Without Rim Gravel Constraint

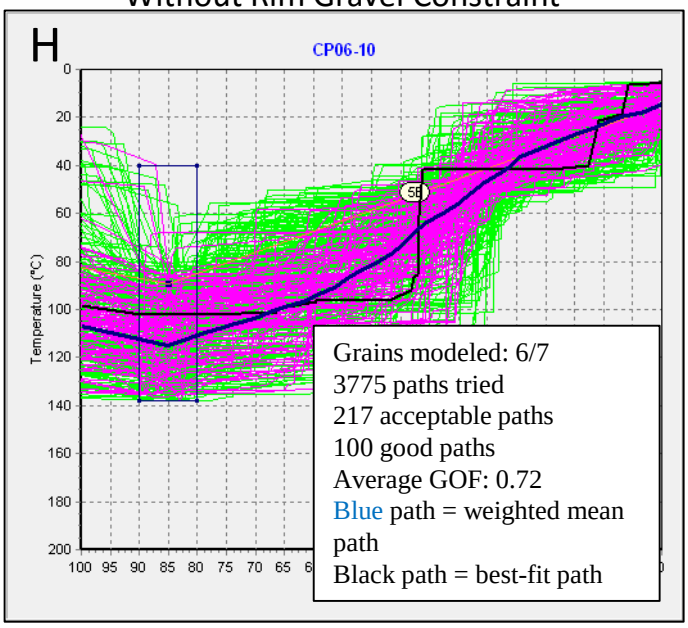

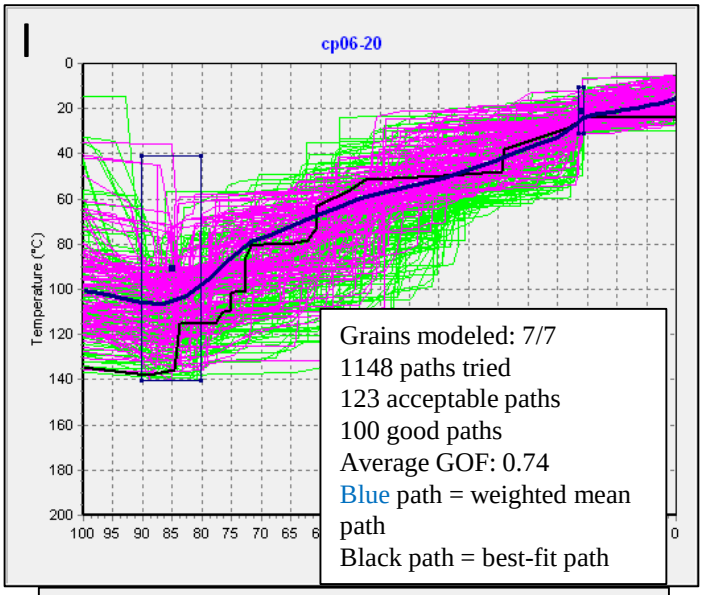

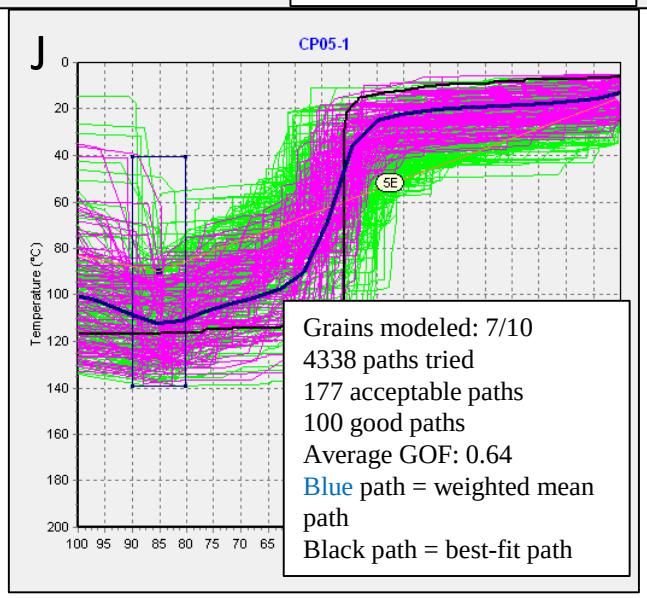

Figure DR-2.6. Comparison of HeFTy models with and without Rim Gravel constraint (continued).

With Rim Gravel Constraint

Without Rim Gravel Constraint

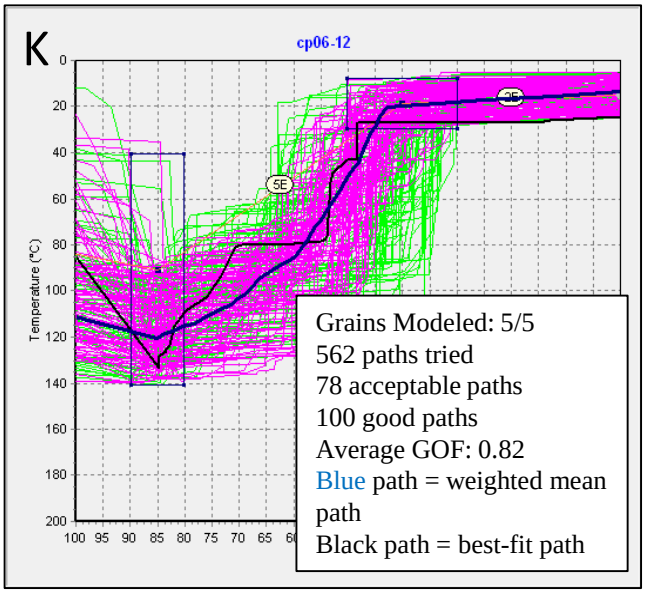

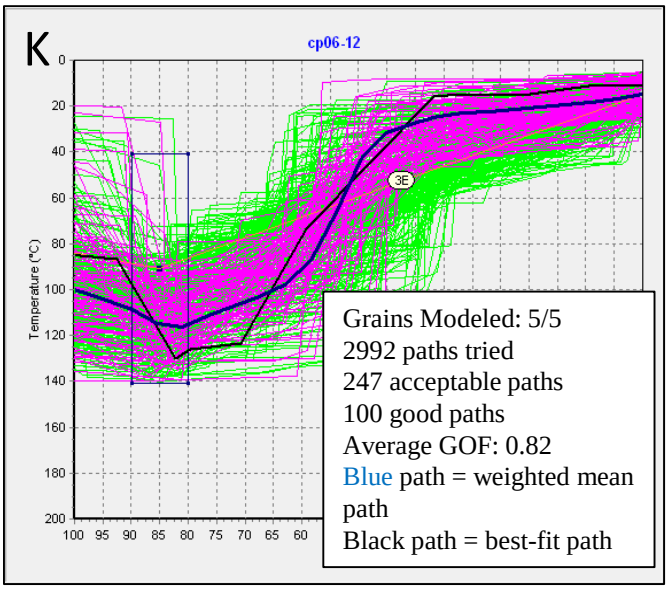

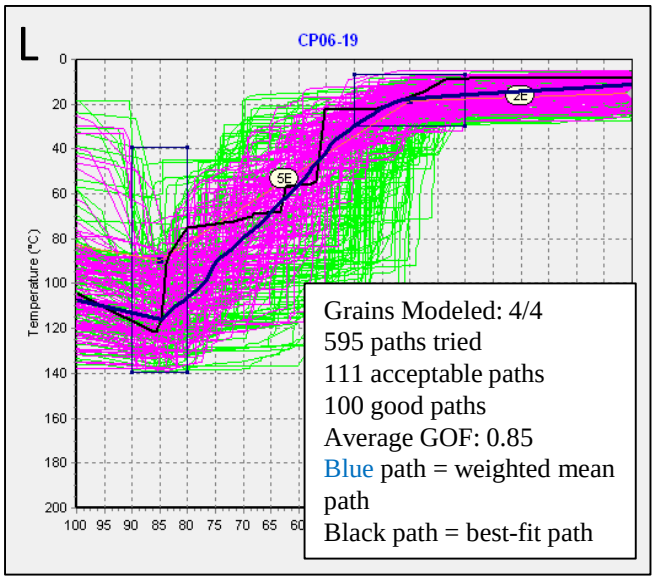

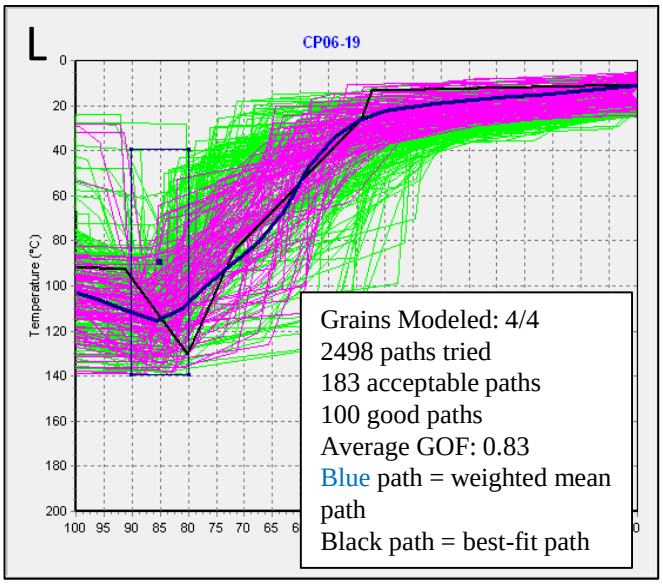

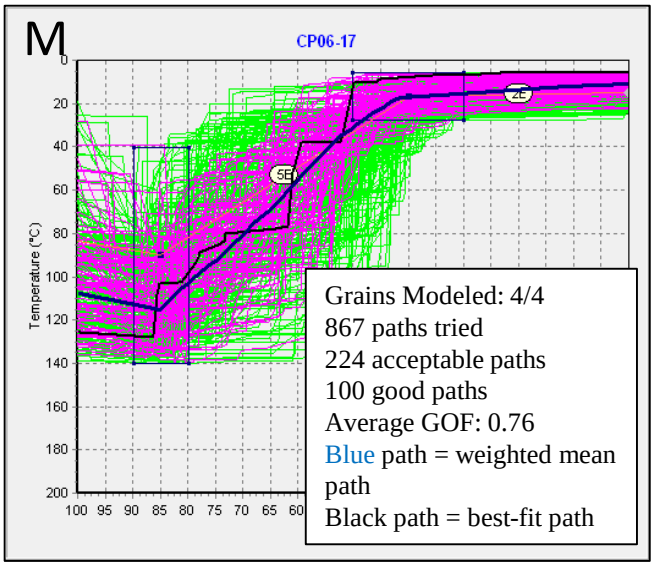

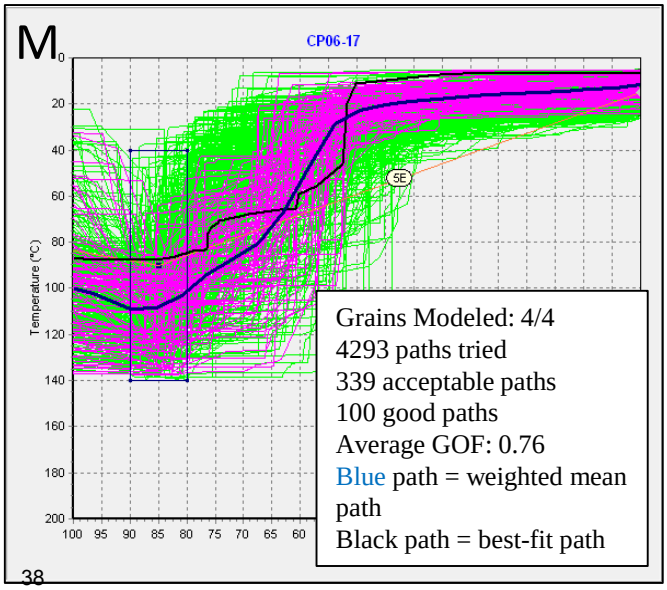

Figure DR-2.7. Comparison of HeFTy models with and without Bidahochi constraint

With Bidahochi Constraint

Without Bidahochi Constraint

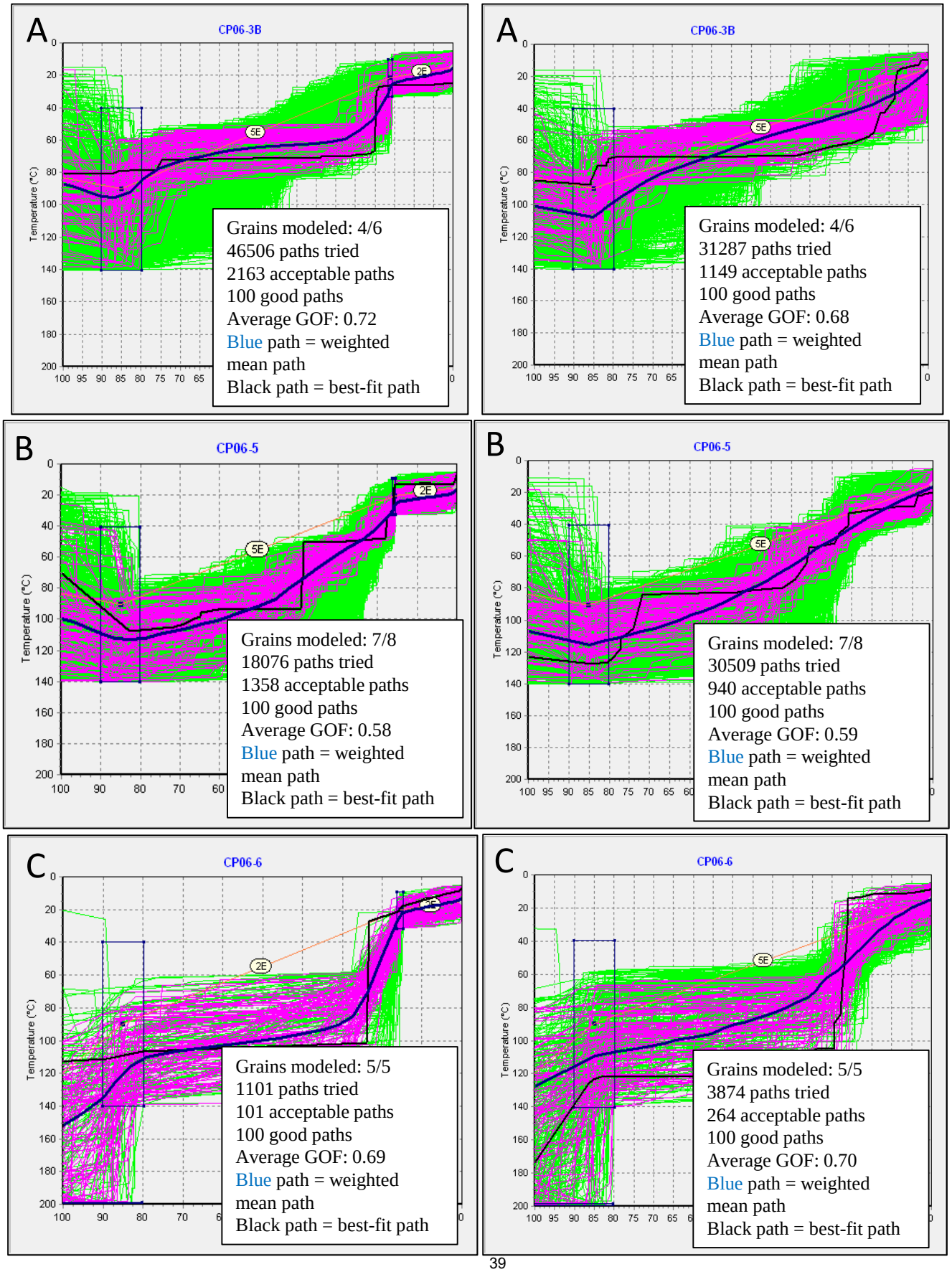

Figure DR-2.7. Comparison of HeFTy models with and without Bidahochi constraint (continued).

With Bidahochi Constraint

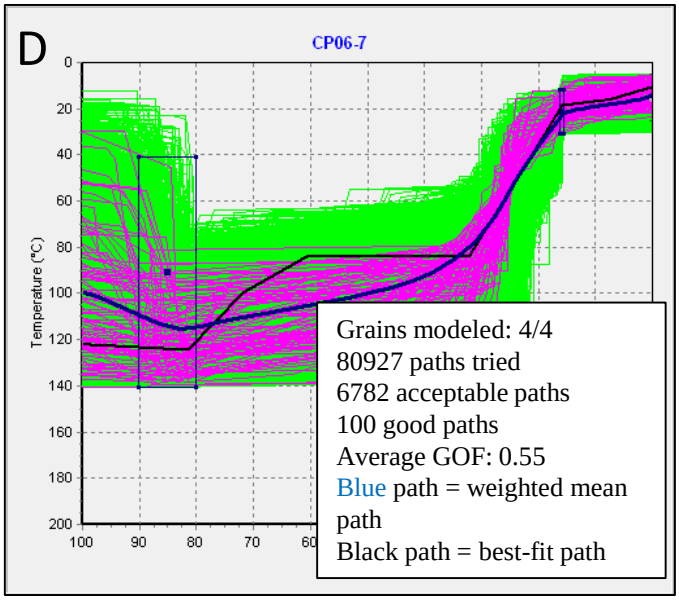

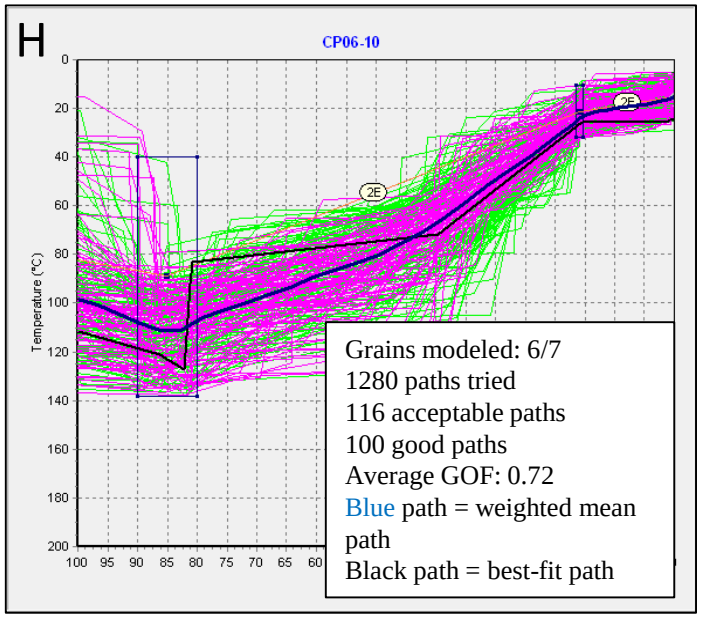

Without Bidahochi Constraint

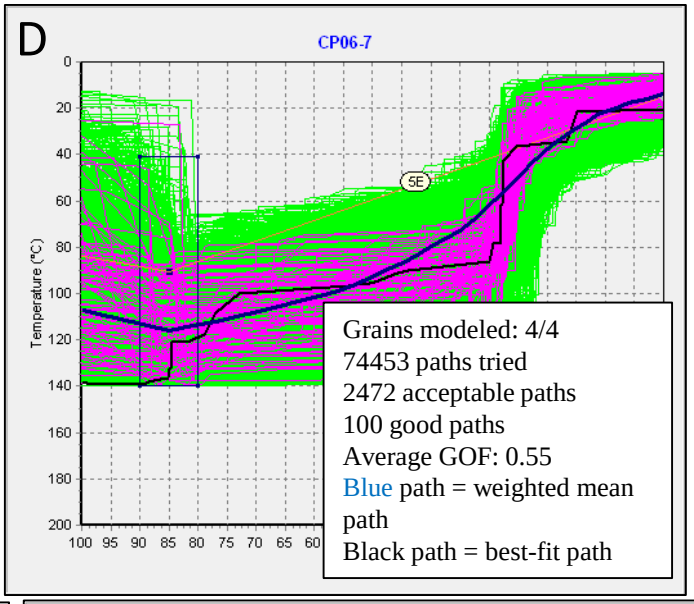

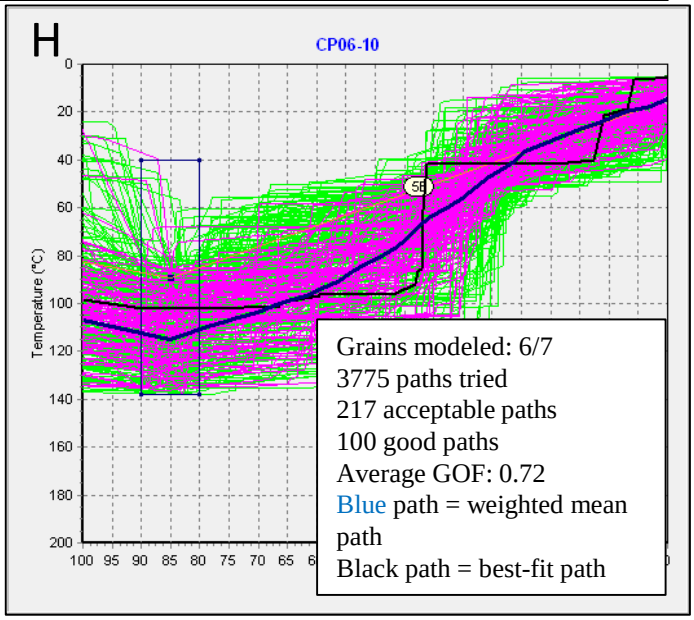

Table DR-3.1. Analytical methods

40Ar/39Ar Methods

Sample preparation and irradiation:

Groundmass concentrated by coarse crushing and picking fragments visibly free of phenocrysts.
Sanidine separated by standard heavy liquid, magnetic and hand-picking techniques.
Basalt or sandine were loaded into machined Al discs and irradiated in 3 separate batches
in central thimble, USGS TRIGA reactor, Denver, CO.
NM-229 & NM-231, 1 hour
NM-238, 10 hours
NM-279, 16 hours
Neutron flux monitor Fish Canyon Tuff sanidine (FC-2). Assigned age = 28.201 Ma Kuiper et al., 2008).

Instrumentation: Basalts

Mass Analyzer Products 215-50 mass spectrometer on line with automated all-metal extraction system.
Basalt samples step-heated using a 50 W CO_2 laser or double vacuum resistance furnace.
CO_2 samples heated for 60 seconds
Reactive gases removed by 5 or minute exposure to two SAES GP-50 getters. One operated at ~450°C and one at 20°C.
Gas also exposed to a W filament operated at ~2000°C and a cold finger operated at -140°C.
Furnace sample heated for 8 minutes
Gas exposed to a GP-50 Getter during heating
Gas cleaned in 2nd stage after heating for 7 minutes with two SAES GP-50 getters. One operated at ~450°C and one at 20°C.
Gas also exposed to a W filament operated at ~2000°C.

Instrumentation: Sanidine

Thermo-Fisher Scientific ARGUS VI mass spectrometer on line with automated all-metal extraction system.
System = Jan
Multi-collector configuration: 40Ar-H1, 39Ar-Ax, 38Ar-L1, 37Ar-L2, 36Ar-L3
Amplification: H1, L1, L2 1E12 Ohm Faraday, AX 1E13 Ohm Faraday, L3 - CDD ion counter, deadtime 14 nS.
Laser single crystal total fusion.
Samples fused for 30 seconds at 3 W using a 75W Photon-Machines CO2 laser.
Reactive gases removed by 30 second reaction with 1 SAES NP-10 getter operated at 1.6 A
and 1 D-50 getter operated at room temperature.

Analytical parameters:

Mass Analyzer Products 215-50 Analyses:
Electron multiplier sensitivity averaged 5 x 10^{-17} and 1 x 10^{-16} moles/pA for laser and furnace systems, respectively.
Total system blank and background:
Furnace = 140 .5, 0.2, 1.7, 0.5 x 10-^{17} moles for masses 40, 39, 38, 37, 36, respectively.
Laser = 225, 6, 1.0, 1.6, 8.5 x 10^{-17} moles for masses 40, 39, 38, 37, 36, respectively.
J-factors determined to a precision of ~± 0.1% by CO_2 laser-fusion of 6 single crystals
from 6 radial positions around the irradiation tray.
ARGUS VI Analyses:
Instrument sensitivity averaged 5 x 10^{-17} moles/fA.
Total system blank and background:
Laser = 3, 0.1, 0.05, 0.01, 0.01 x 10^{-17} moles for masses 40, 39, 38, 37, 36, respectively.
J-factors determined to a precision of ~± 0.02% by CO_2 laser-fusion of 6 single crystals
from 13 radial positions around the irradiation tray.

	ID	Power (Watts/°C)	$^{40}Ar/^{39}Ar$	$^{37}Ar/^{39}Ar$	$^{36}Ar/^{39}Ar$ (x 10^{-3})	$^{39}Ar_K$ (x 10^{-15} mol)	K/Ca	$^{40}Ar^*$ (%)	^{39}Ar (%)	Age (Ma)	±1σ (Ma)	eating At Re	Comment	Irrad.	Ar40_Disc	Ar40_DiscEr
	K05-LCR-TAP2, Groundmass Concentrate, 392.98 mg, J=0.0002277±0.09%, D=1.005±0.001, NM-229C, Lab#=59401-01															
	A	625	33.75	1.691	111.8	2.46	0.30	2.5	0.7	0.35	0.14	685	Groundmas	NM-229C	1.005	0.001
	B	700	3.431	0.8834	9.119	27.6	0.58	23.4	9.0	0.333	0.010	420	Groundmas	NM-229C	1.005	0.001
	C	750	2.052	0.6794	4.347	37.4	0.75	39.9	20.3	0.339	0.006	420	Groundmas	NM-229C	1.005	0.001
	D	800	2.165	0.7235	4.762	45.7	0.71	37.5	34.0	0.337	0.007	420	Groundmas	NM-229C	1.005	0.001
	E	875	2.413	0.7100	5.486	55.4	0.72	35.0	50.6	0.350	0.007	420	Groundmas	NM-229C	1.005	0.001
	F	975	2.954	0.8727	7.434	51.3	0.58	27.8	66.1	0.342	0.008	420	Groundmas	NM-229C	1.005	0.001
	G	1075	3.941	1.214	10.91	35.1	0.42	20.5	76.6	0.337	0.010	420	Groundmas	NM-229C	1.005	0.001
	H	1250	10.10	1.137	32.42	45.7	0.45	6.0	90.3	0.253	0.022	420	Groundmas	NM-229C	1.005	0.001
	I	1700	30.88	6.412	103.9	32.2	0.080	2.3	100.0	0.297	0.062	420	Groundmas	NM-229C	1.005	0.001
	Integrated age ± 1σ			n=9		332.9	0.36	K2O=1.43%		0.325	0.012			NM-229C		
	Plateau ± 1σ	steps A-I		n=9	MSWD=2.37	332.9	0.55 ±0.22		100.0	0.339	0.005			NM-229C		
	K05-LCR-BP, Groundmass Concentrate, 88.38 mg, J=0.0002034±0.26%, D=1.001±0.001, NM-238E, Lab#=59864-01															
X	A	3	193.7	6.768	660.7	0.243	0.075	-0.5	0.6	-0.35	0.52	60	Groundmas	NM-238E	1.001	0.001
	B	4	24.12	2.586	72.56	1.93	0.20	12.0	5.2	1.077	0.065	60	Groundmas	NM-238E	1.001	0.001
	C	6	7.421	1.665	17.67	9.44	0.31	31.4	27.8	0.867	0.016	60	Groundmas	NM-238E	1.001	0.001
	D	8	6.593	1.078	14.48	15.2	0.47	36.4	64.3	0.892	0.012	60	Groundmas	NM-238E	1.001	0.001
	E	9	8.729	1.030	21.46	4.02	0.50	28.2	74.0	0.917	0.027	60	Groundmas	NM-238E	1.001	0.001
	F	12	14.18	1.732	40.19	3.58	0.29	17.2	82.6	0.910	0.039	60	Groundmas	NM-238E	1.001	0.001
	G	15	22.66	3.783	69.57	3.04	0.13	10.6	89.8	0.897	0.056	60	Groundmas	NM-238E	1.001	0.001
X	H	20	32.93	5.787	103.4	1.72	0.088	8.7	94.0	1.068	0.093	60	Groundmas	NM-238E	1.001	0.001
X	I	30	50.54	12.24	162.9	1.37	0.042	6.7	97.3	1.28	0.13	60	Groundmas	NM-238E	1.001	0.001
X	J	50	76.48	18.30	257.6	1.15	0.028	2.5	100.0	0.71	0.19	60	Groundmas	NM-238E	1.001	0.001
	Integrated age ± 1σ			n=10		41.7	0.20	K2O=0.89%		0.907	0.023			NM-238E		
	Plateau ± 1σ	steps B-G		n=6	MSWD=2.31	37.2	0.37 ±0.14		89.3	0.891	0.013			NM-238E		
	K06-REDB-1, groundmass, 22.07 mg, J=0.0022887±0.09%, D=1.005±0.001, NM-231C, Lab#=59491-01															
	A	3	12.22	4.075	34.45	2.12	0.13	19.5	1.5	9.97	0.51	60	Groundmas	NM-231C	1.005	0.001
	B	4	5.678	1.434	12.35	5.61	0.36	37.8	5.3	8.95	0.23	60	Groundmas	NM-231C	1.005	0.001
	C	5	3.598	0.7940	4.822	8.57	0.64	62.2	11.2	9.33	0.11	60	Groundmas	NM-231C	1.005	0.001
	D	6	3.016	0.7334	2.900	16.0	0.70	73.6	22.1	9.245	0.065	60	Groundmas	NM-231C	1.005	0.001
	E	8	2.811	0.7151	2.268	21.4	0.71	78.2	36.8	9.161	0.058	60	Groundmas	NM-231C	1.005	0.001
	F	10	2.773	0.7646	2.155	21.6	0.67	79.3	51.6	9.158	0.053	60	Groundmas	NM-231C	1.005	0.001
	G	13	2.789	1.046	2.352	23.2	0.49	78.1	67.6	9.083	0.054	60	Groundmas	NM-231C	1.005	0.001
X	H	16	2.594	1.805	2.016	17.5	0.28	82.8	79.5	8.949	0.074	60	Groundmas	NM-231C	1.005	0.001
X	I	18	2.692	2.925	2.755	11.0	0.17	78.7	87.1	8.84	0.10	60	Groundmas	NM-231C	1.005	0.001
X	J	30	3.021	0.1188	5.394	18.9	4.3	47.4	100.0	5.97	0.13	60	Groundmas	NM-231C	1.005	0.001
	Integrated age ± 1σ			n=10		145.9	0.47	K2O=1.11%		8.709	0.047			NM-231C		
	Plateau ± 1σ	steps A-G		n=7	MSWD=1.54	98.5	0.61 ±0.22		67.6	9.165	0.035			NM-231C		
	K07-SHIV-1, groundmass, 20.32 mg, J=0.002293±0.09%, D=1.005±0.001, NM-231C, Lab#=59492-01															
	A	3	19.83	3.729	64.84	1.13	0.14	5.0	1.1	4.2	1.0	60	Groundmas	NM-231C	1.005	0.001
	B	4	6.012	2.489	17.11	3.71	0.20	19.3	4.9	4.86	0.26	60	Groundmas	NM-231C	1.005	0.001
	C	5	2.797	1.842	5.467	4.63	0.28	47.6	9.6	5.56	0.17	60	Groundmas	NM-231C	1.005	0.001
	D	6	2.125	1.679	3.138	10.4	0.30	62.8	20.1	5.570	0.097	60	Groundmas	NM-231C	1.005	0.001
	E	8	1.937	1.544	2.535	13.5	0.33	67.8	33.8	5.483	0.072	60	Groundmas	NM-231C	1.005	0.001
	F	10	1.857	1.621	2.263	13.5	0.31	71.1	47.4	5.510	0.073	60	Groundmas	NM-231C	1.005	0.001
	G	13	1.750	1.908	2.081	18.6	0.27	73.7	66.2	5.387	0.072	60	Groundmas	NM-231C	1.005	0.001
X	H	16	1.838	2.000	2.545	14.8	0.26	67.9	81.1	5.210	0.080	60	Groundmas	NM-231C	1.005	0.001
X	I	18	2.128	4.229	3.708	7.38	0.12	64.8	88.6	5.77	0.16	60	Groundmas	NM-231C	1.005	0.001
X	J	30	3.336	7.363	10.77	11.3	0.069	22.6	100.0	3.17	0.25	60	Groundmas	NM-231C	1.005	0.001
	Integrated age ± 1σ			n=10		98.8	0.23	K2O=0.81%		5.025	0.071			NM-231C		
	Plateau ± 1σ	steps A-G		n=7	MSWD=1.67	65.4	0.29 ±0.07		66.2	5.466	0.048			NM-231C		

Notes:

Isotopic ratios corrected for blank, radioactive decay, and mass discrimination, not corrected for interfering reactions.
Errors quoted for individual analyses include analytical error only, without interfering reaction or J uncertainties.
Integrated age calculated by summing isotopic measurements of all steps.
Integrated age error calculated by quadratically combining errors of isotopic measurements of all steps.
Plateau age is inverse-variance-weighted mean of selected steps.
Plateau age error is inverse-variance-weighted mean error (Taylor, 1982) times root MSWD where MSWD>1.
Plateau error is weighted error of Taylor (1982).
Isotopic abundances after Steiger and Jäger (1977).
X preceding sample ID denotes analyses excluded from plateau age calculations.
Weight percent K_2O calculated from ^{39}Ar signal, sample weight, and instrument sensitivity.
Ages calculated relative to FC-2 Fish Canyon Tuff sanidine interlaboratory standard at 28.201 Ma (Kuiper et al. 2008).
D = ! AMU mass discrimination in favor of light isotope.
Decay Constant (LambdaK (total)) = 5.463e-10/a (Min et al., 2000).
Correction factors:
$(^{39}Ar/^{37}Ar)_{Ca}$ = 0.0007 ± 0.000005
$(^{36}Ar/^{37}Ar)_{Ca}$ = 0.00028 ± 0.00002
$(^{40}Ar/^{39}Ar)_K$ = 0.010 ± 0.002

Table DR-3.3. 40Ar/39Ar Sanidine analytical data

ID	$^{40}Ar/^{39}Ar$	$^{38}Ar/^{39}Ar$	$^{37}Ar/^{39}Ar$	$^{36}Ar/^{39}Ar$	$^{39}Ar_K$	K/Ca	$^{40}Ar^*$	Age	±1σ
				(x 10^{-3})	(x 10^{-15} mol)		(%)	(Ma)	(Ma)
Table of 40Ar/39? Sanidine analytical data									
Peach Springs Tuff									
CAF-2-35241, Sanidine, J=0.0038373±0.02%, D=1.02913±0.001574, NM-279A, Lab#=63972									
22	2.717	0.0118	0.0162	0.0798	5.063	31.6	99.2	18.761	0.006
01	2.703	0.0118	0.0177	0.0370	6.715	28.8	99.6	18.768	0.005
19	2.755	0.0121	0.0170	0.2014	6.232	30.0	97.9	18.775	0.007
04	2.760	0.0123	0.0174	0.2252	6.982	29.3	97.6	18.776	0.006
18	3.072	0.0223	0.0296	1.275	9.554	17.2	87.8	18.783	0.011
21	2.731	0.0120	0.0192	0.1158	8.166	26.6	98.8	18.787	0.005
23	3.235	0.0122	0.0207	1.823	4.671	24.7	83.4	18.787	0.019
05	2.761	0.0125	0.0178	0.2206	8.742	28.6	97.7	18.790	0.006
16	2.745	0.0120	0.0168	0.1596	3.292	30.4	98.3	18.791	0.010
07	2.744	0.0119	0.0222	0.1659	11.645	23.0	98.3	18.791	0.005
10	2.707	0.0118	0.0179	0.0400	6.622	28.5	99.6	18.791	0.005
15	2.702	0.0120	0.0169	0.0124	6.925	30.2	99.9	18.794	0.005
09	2.715	0.0119	0.0189	0.0625	10.135	27.0	99.4	18.796	0.005
14	2.763	0.0120	0.0183	0.2187	20.183	27.9	97.7	18.798	0.005
06	2.776	0.0124	0.0213	0.2678	3.347	24.0	97.2	18.799	0.011
20	2.779	0.0128	0.0182	0.2711	8.316	28.1	97.2	18.800	0.006
13	2.720	0.0118	0.0181	0.0660	9.988	28.2	99.3	18.814	0.004
12	2.719	0.0118	0.0178	0.0671	34.424	28.7	99.3	18.817	0.004
17	2.710	0.0117	0.0196	0.0283	11.004	26.1	99.7	18.818	0.004
11	2.710	0.0119	0.0207	0.0372	6.598	24.7	99.7	18.819	0.005
02	2.706	0.0117	0.0182	0.0212	8.300	28.1	99.8	18.820	0.004
24	2.722	0.0118	0.0218	0.0679	2.377	23.4	99.3	18.828	0.010
Mean age ± 1σ			n=22	MSWD=10.05		27.0 ±6.4		18.799	0.010
Apache Leap Tuff									
CAF-2-38005, Sanidine, J=0.003836±0.02%, D=1.02913±0.001574, NM-279A, Lab#=63973									
37	2.713	0.0119	0.0133	0.0717	4.705	38.3	99.3	18.756	0.007
21	2.719	0.0118	0.0143	0.0769	3.748	35.7	99.2	18.781	0.008
11	2.711	0.0117	0.0146	0.0538	2.974	34.9	99.5	18.781	0.008
39	2.712	0.0116	0.0124	0.0518	2.355	41.3	99.5	18.783	0.010
41	2.703	0.0119	0.0136	0.0228	1.441	37.6	99.8	18.783	0.015
34	2.714	0.0119	0.0157	0.0589	3.624	32.4	99.4	18.785	0.007
25	2.719	0.0118	0.0097	0.0748	2.978	52.6	99.2	18.785	0.008
42	2.714	0.0118	0.0119	0.0563	3.452	42.9	99.4	18.789	0.008
07	2.728	0.0118	0.0139	0.1053	4.802	36.8	98.9	18.790	0.007
40	2.711	0.0117	0.0135	0.0467	3.466	37.8	99.5	18.793	0.008
30	2.701	0.0116	0.0107	0.0107	2.460	47.6	99.9	18.793	0.009
08	2.721	0.0118	0.0122	0.0790	7.231	42.0	99.2	18.794	0.006
05	2.727	0.0118	0.0137	0.0986	6.763	37.3	99.0	18.795	0.006
12	2.777	0.0119	0.0149	0.2687	3.434	34.2	97.2	18.796	0.010
29	2.742	0.0118	0.0142	0.1492	2.869	36.0	98.4	18.799	0.010
03	2.726	0.0118	0.0145	0.0948	3.956	35.1	99.0	18.799	0.008
09	2.716	0.0118	0.0102	0.0593	3.379	50.2	99.4	18.799	0.008
17	2.707	0.0117	0.0116	0.0260	3.261	44.0	99.7	18.801	0.008
24	2.722	0.0117	0.0124	0.0741	2.521	41.3	99.2	18.807	0.010
15	2.706	0.0117	0.0149	0.0239	4.542	34.3	99.8	18.807	0.006
36	2.709	0.0119	0.0131	0.0314	2.570	38.9	99.7	18.807	0.009
28	2.709	0.0117	0.0135	0.0310	1.875	37.9	99.7	18.810	0.012
10	2.724	0.0118	0.0127	0.0831	2.058	40.0	99.1	18.810	0.012
13	2.827	0.0119	0.0144	0.4314	4.016	35.4	95.5	18.810	0.011
04	2.803	0.0122	0.0137	0.3505	1.195	37.2	96.3	18.812	0.023
26	2.716	0.0119	0.0132	0.0516	3.460	38.7	99.5	18.813	0.008
22	2.711	0.0117	0.0124	0.0314	3.595	41.2	99.7	18.818	0.007
06	2.706	0.0120	0.0097	0.0180	2.120	52.4	99.8	18.819	0.010
20	2.709	0.0117	0.0109	0.0215	2.667	46.8	99.8	18.823	0.009
31	2.717	0.0117	0.0135	0.0492	1.488	37.8	99.5	18.825	0.014
32	2.714	0.0118	0.0143	0.0408	3.188	35.8	99.6	18.826	0.008
27	2.793	0.0120	0.0130	0.3053	2.482	39.1	96.8	18.826	0.012
16	2.717	0.0117	0.0137	0.0498	1.478	37.3	99.5	18.826	0.014
33	2.726	0.0118	0.0112	0.0793	2.238	45.5	99.2	18.826	0.011
02	2.717	0.0120	0.0150	0.0455	2.398	33.9	99.5	18.837	0.010
35	2.859	0.0117	0.0135	0.5220	7.573	37.8	94.6	18.842	0.009
23	2.735	0.0119	0.0116	0.1018	1.237	44.1	98.9	18.845	0.017
18	2.825	0.0119	0.0131	0.4040	3.891	39.1	95.8	18.850	0.011
19	2.725	0.0118	0.0164	0.0637	1.773	31.0	99.4	18.856	0.013
38	2.718	0.0117	0.0131	0.0300	0.706	38.9	99.7	18.874	0.027
Mean age ± 1σ			n=40	MSWD=5.41		39.5 ±10.2		18.803	0.009

Notes:

Isotopic ratios corrected for blank, radioactive decay, and mass discrimination, not corrected for interfering reactions.
Errors quoted for individual analyses include analytical error only, without interfering reaction or J uncertainties.
Mean age is weighted mean age of Taylor (1982). Mean age error is weighted error
of the mean (Taylor, 1982), multiplied by the root of the MSWD where MSWD>1, and also
incorporates uncertainty in J factors and irradiation correction uncertainties.
Isotopic abundances after Steiger and Jäger (1977).
IC = Messured 40Ar/36Ar/295.5
Ages calculated relative to FC-2 Fish Canyon Tuff sanidine interlaboratory standard at 28.201 Ma
Decay Constant (LambdaK (total)) = 5.463e-10/a (Min et al., 2000)
Correction factors:
$(^{39}Ar/^{37}Ar)_{Ca}$ = 0.0007064 ± 0.000004
$(^{36}Ar/^{37}Ar)_{Ca}$ = 0.0002731 ± 0.000001
$(^{38}Ar/^{39}Ar)_{K}$ = 0.01261 ± 0.00002
$(^{40}Ar/^{39}Ar)_{K}$ = 0.00808 ± 0.00041

Table DR-4. U-Series ages from travertines from the Springerville area

sample#	sample ID	238U	error	232Th	error	[230Th/232Th]	error	230Th/238U	error	δ234Um	error	δ234Ui	error	uncorr age	+ error	- error	corr age	+ error	- error
T19	EE07-84A	309.49	0.76	41992.67	111.89	41.37	0.17	1.84	0.01	836.75	1.60	1645.62	13.69	240807	2784	2732	239306	2853	2797
T21#	EE07-81A#	263.88	0.70	586012.78	1384.04	2.54	0.01	1.85	0.01	706.34	2.71	1669.42	67.77	330998	7051	6755	304331	14019	12744
T23#	EE09-7#	269.13	0.65	712340.13	1724.58	2.15	0.01	1.86	0.01	734.04	1.31	1623.23	76.91	313890	6205	5945	280792	16368	14603
T26	K04-SPV-5C	175.75	0.58	3056.04	35.85	607.89	7.58	3.46	0.02	2359.12	4.49	4444.69	38.97	224210	3017	2960	224117	3015	2958
T28#	K04-SPV-2#	199.62	0.44	301960.87	932.59	5.62	0.03	2.78	0.01	1587.01	1.55	3258.42	57.68	265264	3481	3401	254534	6200	5944
T37#	EE07-75AR#	168.22	0.41	588289.29	1454.55	2.02	0.01	2.31	0.01	2010.46	2.72	2646.68	112.44	128375	932	926	97280	14713	13320
T38#	EE06LL-53B#	143.74	0.36	89725.10	212.35	11.19	0.05	2.28	0.01	2998.25	4.66	3739.07	21.81	82011	477	476	78126	1984	1957
T40	EE06LL-55D	101.01	0.25	302.82	46.41	2619.75	401.60	2.57	0.01	2871.65	6.26	3822.67	10.76	101232	630	628	101214	630	628

Powdered samples were drilled parallel to laminations with a 0.5 mm-diameter bit from the least porous laminae avoiding discolored and oolitic layers to minimize detritus. Sample powders were digested in 15N HNO3 and spiked with a 236U/229Th/233U mixed- spike, fluxed at low heat for one hour, dried down, and dissolved with 5-10 drops of 15N HNO3 and 2 drops of perchloric acid. After drying, the samples were dissolved in 500 µL of Bio-Rad AG® 1W-x8 200-400 mesh chloride form resin. Thorium fraction was collected with 6N HCl and uranium fraction was collected with 1N HBr. Samples were dried down and dissolved in 3% HNO3 for analysis on a Neptune MS-ICPMS.